Anti-migratory function of PMCA4b is mediated by p38 MAPK and actin cytoskeleton remodeling in BRAF mutant melanoma cells

Ph.D. Dissertation

Randa Naffa

Eötvös Loránd University

Faculty of Science

Doctoral School of Biology

Molecular Cell and Neurobiology program

Supervisor

Dr. Agnes Enyedi, Ph.D., DSc.

Co-supervisor

Dr. Peter Löw, Ph.D.

Head of the Doctoral School

Prof. László Nyitray, Ph.D., DSc.

Head of the Ph.D. program

Dr. Peter Löw, Ph.D.

Budapest
2021

Table of content

1. Acknowledgement

I would like to thank my committee members for their constructive comments and for their support.

Finally, I owe my deepest gratitude to my family for all their support and encouragements. They always kept me in their prayers and without them I was not able to accomplish my Ph.D.

2. Introduction

2.1. Skin Cancer - Melanoma

Cancer is a complex type of disease where cells acquire the ability to proliferate indefinitely and form a tumor. It starts to form as a result of re-modifying existing cellular processes involved in cell growth, cell death, polarity, differentiation, motility and migration [1].

Metastasis is responsible for 90% of cancer death where cells disseminate from their primary site to distal sites after invasion through the basement membrane (BM) and migrating through blood/lymphatic vessels (Figure 1) [2]. Therefore, understanding the mechanisms underlying this process and the genes involved will allow to control or even prevent cancer metastasis.
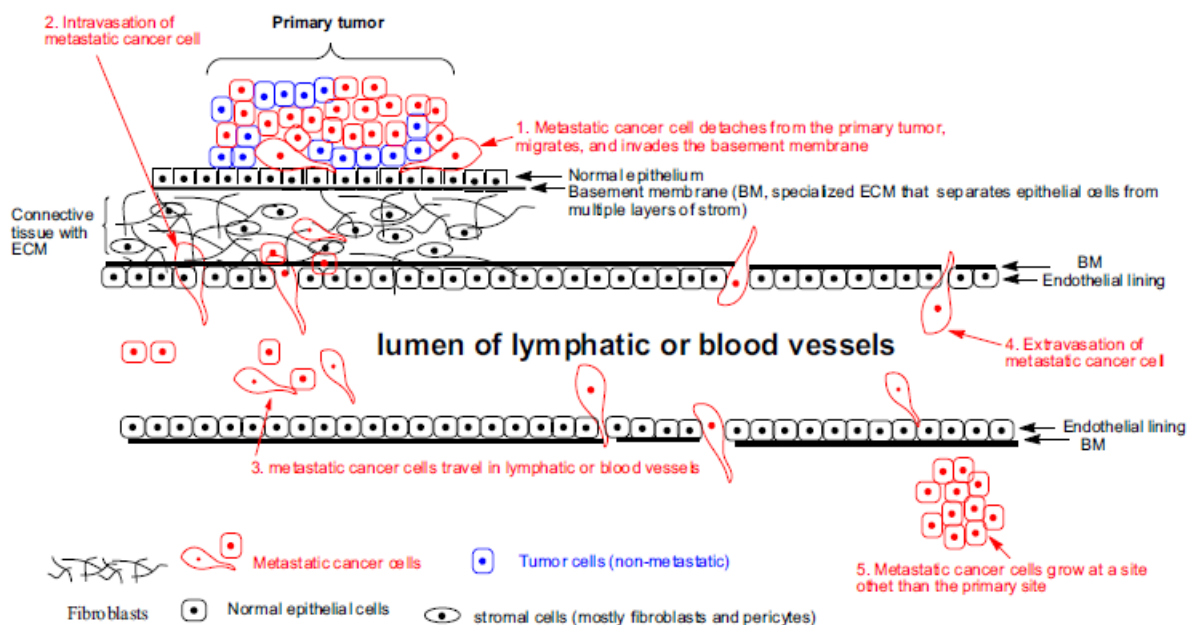
Figure 1. Overview of cancer metastasis [2]. Metastatic cancer cells detach from their primary site, invade the BM, intravasate and travel through the blood/lymphatic vessels, extravasate and finally settle down in a secondary site and self-proliferate.

Skin cancer is the most prevalent type of cancer in light-skinned population and regions of lower latitude as Australia, North America, North Europe and New Zealand. The incident rates vary with different ethnicity, geographical location, and even within the population according to age and gender. Around 20-30% of skin cancer are diagnosed in Caucasians and much less diagnosed in Asians (2–4%), blacks and Asian Indians (1–2%) [3].

Skin cancer is divided into melanoma and non-melanoma skin cancers (NMSCs). A benign and less aggressive type of skin cancer was observed with NMSCs compared to more aggressive and higher mortality rates in melanoma type of skin cancer [4]. Malignant melanoma contributes to >80% of skin cancer-related deaths although it accounts for only <1% of the cases [5]. In 2018, melanoma was reported as the 5th most common cancer in the United State with > 9000 melanoma-related deaths [6]. In many European countries, melanoma rates are found to double every decade and it may become the fourth most common cancer in the near future [7]. Generally, patients who are diagnosed with melanoma at a young age, are females, and have melanoma on their extremities have a better prognosis [8].

2.1.1. Pathological imbalance and melanoma development

Typically, skin is divided by a basement membrane into two layers, the epidermis and dermis. The upper epidermis layer constitutes multi-layered keratinocytes, which are constantly renewed by differentiation of basal cells and act as a primary barrier towards the outer environment. On another hand, the lower dermis layer constitutes fibroblast and blood vessels that are essential to provide the required mechanical and nutrient support. Pigment producing-neural crest-derived cells called melanocytes reside at the junction between the two layers are responsible for skin color. Each melanocyte contains melanin filled-melanosomes that are transferred through its dendrites to 36 adjacent keratinocytes for pigment induction. The darker the skin the more melanosomes are present. Melanin caps protect the nucleus of the keratinocyte from damage by ultraviolet radiation (UVR). Melanocyte proliferation, morphology and surface antigen expression are controlled by the undifferentiated keratinocytes. Normally, no melanoma proliferation is detected *in situ* [9], however, melanoma arise from malignant transformation of the melanocyte where it becomes no longer responsive to keratinocyte and this loss of homeostasis between melanocyte and keratinocyte results in a pathological imbalance in the skin. In contrast to normal melanocytes, melanoma cells start to lose their dendrites and contact with keratinocytes, proliferate rapidly and start to express melanoma-associated antigens (MAA) that are essential for invasion and metastasis [10]. Besides MAA, other tumor-associated antigens were discovered in melanoma cells that can be utilized as a therapeutic target.

For melanoma progression, malignant melanoma cells first start with the radial growth phase where cells proliferate and invade the dermis locally. The second phase includes vertical growth where cells grow vertically into subcutaneous tissue forming tumors. If this tumor is not resected the possibility of metastasis increases [11].

2.1.2. Melanoma etiology

The main environmental risk factor for the development of cutaneous melanoma is exposure to UVR resulting in induction of genetic mutations and DNA damage [4]. Sequencing the entire genome of melanomas showed nearly 80,000 bases mutated (mostly transition mutation: C>T) and around 100 structural rearrangements per one genome. Actually, melanoma has the highest mutational rate in all cancers [12]. The mutational landscape of melanoma showed that many of the oncogenic mutations are involved in the constitutive activation of mitogen-activated protein kinase (MAPK) pathway. Normally this pathway is stimulated by the binding of a ligand (e.g. epidermal growth factor (EGF), insulin-like growth factor (IGF)) to a receptor tyrosine kinase in the plasma membrane, which activates downstream proteins including small GTPase RAS proteins (HRAS, KRAS, NRAS), serine-threonine RAF kinases (ARAF, BRAF, CRAF), MEK kinases, ERK1 and ERK2. In the end, ERK protein enters the nucleus and activates the transcription factor ELK-1 that is responsible for cell growth and survival [13]. Activation of this pathway was also found to change the expression of several proteins involved in the migratory process [14]. In the case of cutaneous melanoma, nearly half of the mutations are in BRAF kinase at the codon 600 and 90% of them are substitution mutation from glutamic acid to valine (BRAF^{V600E}) [15]. Ras genes were also found mutated mainly at codons 12, 13 and 61 accounting for 15-20% of melanoma cases. Tumor suppressor genes were also reported to be affected in melanomas by either loss-of-function such as NF1, TP53, or CDKN2A or by inactivating mutations as in PTEN that lead to activation of the PI3K/Akt/mTOR pathway.

In other subtypes of melanoma other driver mutations were reported. For example, mucosal melanoma showed activation mutations or amplification of c-KIT tyrosine kinase receptor in about 25% of the cases [16] while mutations in the G-protein subunit were one of the driver mutations found in uveal melanoma [17].

Other signaling pathways were reported active in melanoma and found to interplay with MAPK pathways such as p38 MAPK [18], c-Jun N-terminal kinase (JNK) [19] and nuclear factor-kappa B (NF-κB) [20] leading to melanoma cell proliferation, migration and metastasis.

2.1.3. Melanoma treatment

Melanoma early diagnosis and treatment are essential for an increase in survival rate. At the early localized stage (0-II and resectable stage III), surgical removal of the lesion has a 5-year survival rate of 98%, however, once melanoma is developed and become regional or metastasize (unresectable stage III and IV), surgery treatment is not an option and the survival rate drops to 63% and 15%, respectively [21].

During the past decades, a significant advance in the treatments of melanoma has been developed especially for patients diagnosed with late-stage metastatic type of melanoma. Treatments included chemotherapy, immunotherapy, targeted therapy, or even combinations [22].

2.1.3.1. Chemotherapy treatment

The first standard care for treatment with metastatic melanoma was the administration of chemotherapeutic agent dacarbazine (DTIC) and a high dose of interleukin 2 (IL-2) that resulted in less than 10 months median overall survival [23]. Despite these treatments, late-stage melanoma still was associated with poor prognosis, therefore, in the last decade, many efforts have been made to understand the molecular background underlying melanoma development and metastasis to help identify new therapeutic targets.

2.1.3.2. Targeted therapy treatment

Several inhibitors have been developed or undergoing clinical trials against melanoma biomarkers (Table 1). As the main driving force of melanoma progression is the constitutive activation of the MAPK signaling pathway, specific inhibitors have been developed against BRAF and MEK kinases. FDA has approved three combinations of BRAF/MEK inhibitors for the treatment of an unresectable type of melanoma (dabrafenib and trametinib; vemurafenib and cobimetinib; encorafenib and binimetinib) [22]. These treatments showed high response and have increased the survival rate to around 16 months, however, although of this increased efficacy the treatment was limited by the development of drug-resistance in the melanoma patient after few months from treatments (relapse within 7 months) and nearly 10% did not respond at all (intrinsic resistance) [24,25].

Several molecular mechanisms have been suggested for the lack of response to these targeted inhibitors including mutational, non-mutational, or changes in the tumor microenvironment. For example, mutations in RAS, NF1, receptor tyrosine Kinases (RTKs), MEK1, changes in BRAF itself by having a splice variant that unable to bind to RAS, or reactivation of ERK by inhibiting the expression of the phosphatase DUSP6 (an inhibitor and regulator of ERK activity) in melanoma have resulted in resistance to inhibitors treatments and constitutive activation of MAPK pathway [7].

Other molecular alternatives driving resistance are the activation of parallel signaling pathways, such as the activation of the PI3K/AKT/mTOR pathway by deletion/inactivating mutations of the negative pathway regulator and tumor suppressor PTEN or the inactivation of the tumor suppressor retinoblastoma 1 (RB1) to decrease the requirement for BRAF/MEK signaling [26]. The discovery of these contributing signaling pathways provides new rationales

of second-line therapies, as demonstrated by the success of combinations of MAPK and PI3K/AKT/mTOR pathway inhibitors to overcome acquired resistance to monotherapy targeting BRAF alone [27].

Non-mutation mechanisms including up-regulation of RTKs or increasing its soluble ligands or growth factors were also described in acquiring resistance in melanoma. Increased hepatocyte growth factor (HGF) expression, for example, is a poor prognostic factor in melanoma [28]

As an example of environmental factors in inducing resistance in melanoma is the HGF secretion by the stromal cells as a result of an extrinsic non-cell autonomous signal ([28]).

In the case of NRAS mutant melanoma patients, the combination of MEK inhibitors with either PI3K-AKT or cyclin-dependent kinase 4/6 (CDK4/6) inhibitors were reported more efficient than MEK inhibitor monotherapy [29] while in the case of c-KIT mutant melanoma patients, C-KIT inhibitor (Imatinib) showed good response rates [30].

For patients with melanoma recurrence after surgery (unresectable cutaneous, subcutaneous and nodal lesions), FDA has approved local treatment with oncolytic herpes virus talimogene laherparepvec (T-VEC) [31].

Table 1. Biomarkers identified in melanoma as therapeutic targets [32].

Gene	Incidence	comments
BRAF	40-60%	Correlated with response to BRAF-targeted therapies. Has led to FDA approval of amplification and sequencing technologies, and multiple laboratory tests to assess BRAF mutation status
NRAS	20%	Correlated with response to MEK inhibitors
C-KIT	3% of melanoma; 20-30% melanomas arising from (CSD) skin, acral and mucosal sites	Kit-inhibitors have shown activity in patients with specific mutations
GNAQ	80% of uveal melanoma	MEK inhibitor failed to show efficacy in Phase III trials
NF1	46% of cases with BRAF and NRAS wild type	Early clinical trials
PTEN	25-30%	Implicated in mechanism of resistance to MAPK inhibition
CDK2	11%	Early clinical trials

Many new therapeutic targets were reported in the literature as a candidate to overcome the drug resistance developed in metastatic melanoma, however, still, clinical trials are needed to prove their efficacy [33,34].

2.1.3.3. Immunotherapy treatment

In the last few decades advancement in immunology and cancer biology research caused landmark change in treating patients with metastatic melanoma by identification novel therapeutic targets that elicit anti-tumor immunological response such as checkpoint inhibitors or T-cell programmed death receptor/ligand inhibitors [22].

Tumor cells are usually eradicated by immune cells through the recognition process between T-cell receptor (TCR) and the antigen presented by major histocompatibility complex (MHC) on the antigen-presenting cells (APC). However, this binding is influenced by many factors that determine T-cell activation or anergy [22]. The co-stimulatory signal induced by binding of B7 (CD80, CD86) on the APC with CD28 on the T-cell is required for T-cell activation, proliferation and production of growth cytokines IL-2, however, competitive binding of cytotoxic T-lymphocyte associated antigen 4 (CTLA-4) checkpoint molecule (which mimic CD28 and has a higher affinity toward B7) to B7, results in inhibition of this stimulatory signal. CTLA-4 can stop the autoreactive T-cell at the initial activation stage in lymph nodes [35]. However, at later stages in peripheral tissues, T-cell is regulated by T-cell receptor programmed death 1 (PD-1) receptor and the PD-1 ligand PD-L1 pathway. Similar to CTLA-4, PD-1 binding to its ligands (PD-L1 and PDL-2) expressed on cancer cells negatively regulate T-cells by preventing phosphorylation of TCR intermediates which results in inhibition of T-cell proliferation and production of IL-2 or tumor necrosis factor-alpha (T-cell dysfunction) [36]. These findings led to trials on antibodies developed against CTLA-1 (ipilimumab) and PD-1 (pembrolizumab and nivolumab) as therapeutic targets. In patients with cutaneous melanoma, trials showed promising results with a 5-year overall response as shown in Table 2 [22].

Table 2. Immunotherapeutic drugs for treating patients with cutaneous melanoma and their overall survival (OS) rates [22]**.**

	Approved drug or combination	5 year OS rate
Check point inhibitors	Pembrolizumab (first line)	43.3%
	Nivolumab (first line)	44%
	Ipilimumab (first-line)	26-33%
	Ipilimumab + nivolumab (first-line)	52%

Other immunotherapies were utilized including adoptive T cell therapy where tumor-specific T-cells are isolated, ex-vivo expanded and then infused back to the patient to target

cancer cells. However, variability in the response per patient and even in different cancer types and development of acquired resistance led to searching for new treatments.

2.2. Ca^{2+} signaling in health and disease

Calcium ion (Ca^{2+}) is a chemical element that is essential for the physiology and biochemistry of living organisms. It is involved in most biological functions and therefore its concentration is tightly controlled. At the level of organs, Ca^{2+} acts as the building block for bone formation (main mineral storage site) where it can be released under controlled conditions from bone into blood vessels as a dissolved ion or as bound to serum albumin. At the level of tissue, Ca^{2+} compartmentalization maintains the membrane potential in excitable tissues such as neuron and cardiac tissues. It is also reported to be involved in muscle contractions. While at the cellular level, Ca^{2+} acts as a second messenger that results in activating certain signaling pathways involved in several processes such as apoptosis, proliferation, cell division, differentiation, migration, or metastasis. Therefore, any alteration in Ca^{2+} signaling or homeostasis may trigger a wide range of diseases involved in neuron degeneration, fertility, metabolism, immunity and cancer formation [37,38]. Understanding how remodeling of Ca^{2+} ion can control such processes may allow a better understanding of the disease development, enable finding new potential therapeutic targets and identifying new biomarkers.

2.3. Molecular toolkit for maintaining cellular Ca^{2+} homeostasis

Ca^{2+} homeostasis is essential for proper cell functioning and it is tightly controlled through cell type specific toolkits. Normally, at resting state Ca^{2+} concentration is substantially different across the plasma membrane, its intracellular concentration is around 100 nM compared to its 10 thousand higher concentration (more than 1 mM) in the extracellular milieu (Figure 2) [39]. This large free Ca^{2+} concentration difference requires a lot of energy that is maintained by cells to prevent accumulation of cytotoxic calcium phosphates, and to allow only transient spatiotemporal increase in Ca^{2+} concentration for initiating signaling pathways or changing specific Ca^{2+} mediators for a specific function [40]. To control intracellular calcium concentration a specific composition of the toolkit is used by the cell that changes depending on the cell fate or in response to changes in the extracellular environment. This toolkit includes Ca^{2+} buffers, channels, pumps and exchangers. Ca^{2+} channels are known to allow entry of Ca^{2+} from the extracellular milieu into the cell (influx) or from the Ca^{2+} stores inside the cell such as the mitochondria and endoplasmic reticulum to the cytosol. Whereas, pumps and/or exchangers allow removal of Ca^{2+} out of the cell (outflux) or into the Ca^{2+} stores

for maintaining low cytosolic Ca^{2+} concentration level. The buffering system, where free intracellular Ca^{2+} ion is chelated by Ca^{2+} binding proteins or acidic lipids, is another tool to maintain low free intracellular Ca^{2+} concentration [41]. Ca^{2+} signaling toolkit proteins exist in many different isoforms, and their combination can generate distinct Ca^{2+} signaling patterns ranging from single spikes to high-frequency oscillations. The location, amplitude and frequency of the Ca^{2+} transients determine the type of Ca^{2+}-dependent proteins affected and hence the cellular process activated [42].

Any abnormalities in the expression, regulation, stability/subcellular localization and activity of toolkit proteins result in altered Ca^{2+} spatiotemporal and steady-state homeostasis, which can induce the hallmarks of tumorigenesis and metastasis. Ca^{2+} homeostasis might not be the driving cause of cancer formation but rather the consequence, nevertheless, they help to sustain cancer hallmarks [43].
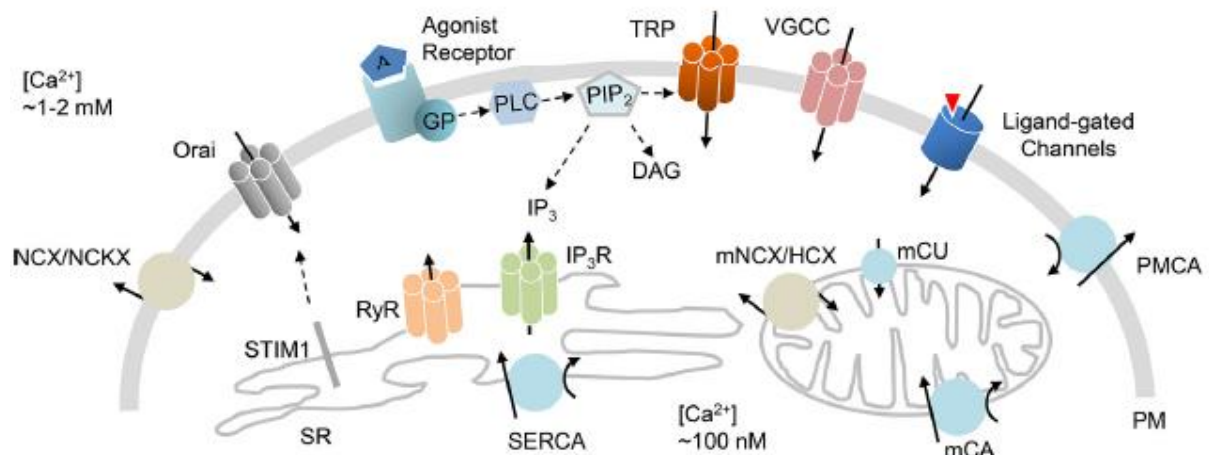
Figure 2. The molecular toolkit involved in Ca^{2+} homeostasis [39]. Schematic diagram showing Ca^{2+} channels responsible for Ca^{2+} entry (influx) from extracellular milieu or internal stores and transporters or exchangers responsible for Ca^{2+} removal (outflux) from the cytosol.

2.3.1. Intracellular calcium level increasing toolkit

In normal eukaryotic cells, several Ca^{2+} transport systems allow controlled increase in cytosolic Ca^{2+}. They are mainly channels that allow Ca^{2+} influx from the extracellular space of the cell by exploiting the electrochemical gradient across the plasma membrane or those that allow Ca^{2+} release from internal stores at specified space and time as a response to a particular stimulus. Ca^{2+} entry generate spikes/waves that last from microseconds to hours as in the case of exocytosis and fertilization of mammalian oocyte, respectively [44].

2.3.1.1. Plasma membrane Ca^{2+} entry channels

In literature, several types of Ca^{2+} channels have been identified that can be classified according to their gating property:

Voltage-operated channels (VOCs) are sensitive to any changes in the net electric charge produced across the plasma membrane. For example, it opens and allows Ca^{2+} influx upon depolarization. These are mainly found in excitable cells and involved in synaptic vesicle fusion or muscle contraction. This family consists of three groups: Cav1 (L-type channels), Cav2 (N-, P/Q and R-types) and Cav3 (T-type channels) [45].

Receptor-operated channels (ROCs) are ion channels that can be activated by binding specific ligand from the extracellular space, for example, glutamate, acetylcholine or ATP. This type includes the transient receptor potential (TRP) ion channel and P2X receptors. The former is mainly involved in sensory perception, cell growth and smooth muscle relaxation/contraction, while the later are gated by ATP and glutamate receptors [46,47].

Second-messenger-operated channels (SMOCs) can be activated by binding to second messengers in the cytosol, for example, arachidonic acid-regulated Ca^{2+} (ARC) channel, TRPC sensitive to diacylglycerol (DAG) and cyclic nucleotide-gated channels (CNGCs) [48].

Store-operated channels (SOCs) are sensitive to the intracellular Ca^{2+} store filling status of the sarco- or endoplasmic reticulum (ER), where they can sense Ca^{2+} depletion. Once the phosphoinositide pathway is activated Ca^{2+} is released from the ER through channels operated by inositol 1,4,5-trisphosphate (IP3) or ryanodine receptors. Most of the Ca^{2+} can re-enter the ER through the sarco-endoplasmic reticular Ca^{2+} ATPases (SERCAs), while some are extruded out of the cell through the plasma membrane Ca^{2+} ATPases (PMCAs). Therefore, to replenish Ca^{2+} depleted from the ER SOC activates the store-operated Ca^{2+} entry (SOCE) pathway that maintains intra ER free Ca^{2+} level at the micromolar concentration range. This pathway is considered one of the main pathways in both non-excitable and excitable cells for Ca^{2+} entry and it was first reported by James W. Putney in the 1980s [49].

One of the SOC protein members is called STIM protein (stromal interacting molecule) that act as a transmembrane Ca^{2+} sensor in the ER membrane through its EF-hand domain at the luminal side. These proteins can sense intraluminal Ca^{2+} depletion in the ER and move to ER-PM juxtaposition to activate SOC through oligomerization allowing Ca^{2+} entry from the extracellular milieu. The pore-forming ORAI protein family (e.g. ORAI1, ORAI2 and ORAI3) and some of the TRPC channels can act as SOCs. These two differ in the mode of STIM1-dependent gating. In the case of ORAI, STIM1 binds to ORAI1 directly through its calcium release-activated calcium (CRAC)-activating domain (CAD) and activates it while in the case

of TRPC, the polybasic domain in the C-terminus of STIM1 activates TRPC1 through electrostatic interactions leading to SOC channel activation [50].

2.3.1.2. Internal store Ca^{2+} release channels

The main Ca^{2+} stores in the cells are the endoplasmic reticulum ER/SR, mitochondria and Golgi apparatus. Once the cell surface receptors such as G-protein-coupled receptors (GPCRs) or receptor tyrosine kinase-linked receptors (RTKRs) are stimulated by binding to their ligands, hormones, growth factors or ATP, IP3 is produced from phosphatidylinositol 4,5-bisphosphate (PIP2) through phospholipase C (PLC) activation. IP3 acts as a second messenger and activates the inositol 1,4,5-trisphosphate receptors (IP3Rs) at the ER membrane in non-excitable cells. This activation results in quick release of Ca^{2+} from the stores to the cytoplasm. IP3R can also be activated by Ca^{2+} itself until it reaches 300 nM in the cytoplasm and causes receptor Ca^{2+} release inhibition [42]. In excitable cells, Ca^{2+} is released from the sarcoplasmic reticulum by ryanodine receptors (RYRs). RYRs can be activated by the L-type Ca^{2+} channel or through increasing Ca^{2+} concentration in the cytoplasm, and this mechanism is called Ca^{2+} induced Ca^{2+} release (CICR) [51].

Mitochondria also participate in intracellular Ca^{2+} homeostasis. They can be recruited to the newly formed CRAC channels and provide SOCE-regulatory activity. In addition, Ca^{2+} can be extruded from mitochondria lumen into the cytosol via the Na^+/Ca^{2+} exchange solute carrier family 8 member B1 (SLC8B1, known as NCLX) and the H^+/Ca^{2+} antiporter [52,53].

In the Golgi apparatus, maintaining luminal Ca^{2+} concentration is important for the regulation of Golgi function. The Ca^{2+} can be stored in the Golgi lumen up to 0.3 mM concentration in unstimulated cells forming a large gradient to that of the cytosol. Similarly, but independent of ER Ca^{2+} stores, Ca^{2+} can be released from Golgi through activation of IP3R located on their membrane by a high level of cytosolic IP3 [54].

Other channels were also found to be involved in adjusting cytosolic Ca^{2+} levels. An increase in cytosolic Ca^{2+} level occurs as a result of phosphatidylinositol 3,5-bisphosphate (PI(3,5)P2) and reactive oxygen species (ROS) production in the cell and consequent opening of the PI(3,5)P2 and ROS-sensitive lysosomal Ca^{2+} channel mucolipin 1 (MCOLN1, also known as TRPML1) and the two pore segment channel 2 (TPCN2). [55].

2.3.2. Intracellular calcium level decreasing toolkit

The lowering of Ca^{2+} in the cytosol to its basal level against its concentration gradient is an energy-consuming process and the main ATP-dependent Ca^{2+} extrusion systems are the plasma membrane Ca^{2+} ATPases (PMCAs), the sarco-endoplasmic reticular Ca^{2+} ATPases (SERCAs) and secretory pathway Ca^{2+} ATPases (SPCAs). PMCA can remove Ca^{2+} from

cytosol to the extracellular space while SERCA and SPCA reduce Ca^{2+} level in the cytoplasm by accumulating it in the ER and the Golgi lumen, respectively. These transporters have high Ca^{2+} affinity and low transport capacity. The other Ca^{2+} extrusion system is the plasma membrane Na^+/Ca^{2+} exchanger (NCX). Balancing Ca^{2+} in the cytosol relay also on mitochondria Ca^{2+} uniporters (MCUs) that allow Ca^{2+} entry into mitochondria. Both NCX and MCUs have high capacity for Ca^{2+} transport but low Ca^{2+} affinity [56]

Organelles such as lysosomes can act as Ca^{2+} stores, however, they are not compared to the Ca^{2+} stores in ER in terms of quantity. The source of Ca^{2+} can be either from vesicular trafficking/endocytosis of extracellular Ca^{2+} rich space or from those coming from Ca^{2+}/H^+ exchangers. [55].

2.3.2.1. Na$^+$/Ca^{2+} exchangers (NCX)

This type is mostly available in excitable cells such as the cardiac and skeletal muscle cells and cells of the nervous system. These transporters have high transport capacity to remove Ca^{2+} from the cytosol to the outside space that is needed for proper cell function such as cardiac excitation-contraction coupling, re-absorption of Ca^{2+} in the kidney and neuronal signaling. NCX can sense Ca^{2+} as it reaches micromolar concentration and they use the transmembrane electrochemical gradient of sodium across the cell to extrude Ca^{2+} to the extracellular space (one Ca^{2+}_{out} to three Na^+_{in}) [57]. The activity of these proteins can be affected by the concentration of Ca^{2+} and Na^+ in the cytoplasm. A high concentration of Ca^{2+} in the cytosol activates the exchanger whereas a high concentration of Na^+ de-activates it. NCX activity also can be regulated by interaction with other proteins through changing the NCX localization and recruiting it to a certain region in the plasma membrane to be part of the macromolecular complex [56].

NCX belongs to the family solute carrier 8 (SLC8) and it includes three proteins, NXC1, NCX2 and NCX3. NCX1 is cloned from the heart with the highest expression in the brain and kidney while NCX2 and NCX3 are expressed in skeletal muscles, brain and some neuronal populations [57].

2.3.2.2. Mitochondrial calcium uniporter (MCU)

Mitochondria Ca^{2+} uptake controls certain functions such as ATP production, however, Ca^{2+} overload may induce cell death, therefore, Ca^{2+} uptake is tightly controlled. Ca^{2+} entry to mitochondria lumen requires first Ca^{2+} to cross the outer mitochondrial membrane (OMM) via voltage-dependent anion channel (VDAC) family (VDAC1, VDAC2 and VDAC3) and then to enter the mitochondria matrix through MCU. The MCU itself is regulated positively by mitochondrial calcium uniporter regulator 1 (MCUR1) and negatively by mitochondrial

calcium uptake 1 (MICU1). The activity of the MCU increases when there is a high Ca^{2+} concentration in the entire cytosol or locally when it is in close proximity to the ER where Ca^{2+} is released by IP3R or RYR [58].

2.3.2.3. Ca^{2+} buffering system

Ca^{2+} buffering is another tool for controlling intracellular organelle Ca^{2+} stores available for Ca^{2+} signaling, protein folding, apoptosis and in the regulation of Ca^{2+} release pathways. Ca^{2+} buffers are variable calcium-binding proteins that have different affinities and capacities toward Ca^{2+} [59].

In ER, the total calcium is around 1 mM while the free Ca^{2+} is around 200 µM leaving the remaining Ca^{2+} in a bound form. Calreticulin is the Ca^{2+} binding protein in the ER that is responsible for 50% of the Ca^{2+} buffering capacity in non-muscle cells while calsequestrin is the main Ca^{2+} buffering protein available in the SER of muscle cells [60]. Calsequestrin was found to interact with RYR in SER depending on its luminal Ca^{2+} concentration. This interaction affects RYR by increasing or decreasing its activity in different tissues, e.g. when the Ca^{2+} level in the SR is at resting state, calsequestrin can inhibit RYR1 or activate the RYR1 and RYR2 in skeletal and cardiac muscle, respectively [61].

In the Golgi apparatus, Ca^{2+} is stored in the millimolar range and there are several proteins that act as Ca^{2+} buffers. The major buffer protein is nucleobindin (CALNUC) that has some homology to calreticulin [59].

In the mitochondria, Ca^{2+} was found precipitated out as $CaPO_4$. Mitochondria itself can act as a buffer as it takes the Ca^{2+} released from the ER lumen. The interaction between the ER and mitochondria was reported to be involved in cell death [62].

Ca^{2+} buffering was also have been reported to be available in the cytoplasm such as calretinin, calbindin-D9k, calbindin-D28k and parvalbumins. Some of these proteins showed Ca^{2+} sensor function [63].

2.3.2.4. Ca^{2+} transport ATPases

Three Ca^{2+} ATPases - SPCAs, SERCAs and PMCAs - are involved in removing Ca^{2+} from the cytosol and lowering it to its basal level. These pumps belong to a large family called P-type ATPase (E_1-E_2 ATPases). It is a large group of ion and lipid pumps and its name originated from their ability to auto-phosphorylate (P) a conserved aspartate residue intermediate within the pump during the enzymatic cycle by utilizing ATP to translocate ions across the plasma membrane against their concentration gradient. The activity of this type of pump is essential for many processes such as muscle contraction, generation of membrane potential and getting rid of toxic ions from the cells. P-type ATPases are phylogenetically

subdivided into five subfamilies based on conserved sequence kernels (P1-P5), the type of ligands transported and the way of regulation. This family shares a similar structure with ten transmembrane helices (M1-M10) and conserved regions between 2nd-3rd and 4th-5th domains at the cytoplasmic side [64].

2.3.2.4.1. Secretory pathway Ca²⁺ ATPases (SPCAs)

SPCA is a Ca^{2+} pump found in the Golgi apparatus that has a high affinity for Ca^{2+}. It is responsible for Ca^{2+} and Mn^+ homeostasis in both Golgi and distal parts of the secretory pathway, and this is important for the production and processing of proteins for secretion. There are two SPCA isoforms encoded by two genes *ATP2C1* (SPCA1) and *ATP2C2* (SPCA2). As a result of alternative splicing, SPCA1 has four variants (a, b, c, d). SPCA1 is more ubiquitously expressed while SPCA2 expression is more restricted to distinct tissues such as brain, salivary gland, gastrointestinal tract, thyroid gland, trachea, keratinocyte, prostate, testis, thyroid and mammary gland. It was shown that SPCA pumps are involved in providing Ca^{2+} in lactating mammary gland milk. It was reported that SPCAs are not involved in basal Ca^{2+} spiking but their loss reduce Ca^{2+} oscillation frequency [65,66].

2.3.2.4.2. Sarco-endoplasmic reticular Ca²⁺ ATPases (SERCAs)

The endoplasmic reticulum (ER) is a vital organelle for lipid and protein synthesis and for proper protein folding. ER is the main Ca^{2+} store of the cell and SERCA is the predominant pump responsible for its Ca^{2+} homeostasis. Any imbalance in Ca^{2+} homeostasis was found to result in improper protein folding leading to ER stress and Ca^{2+} uptake by mitochondria that eventually can lead to pro-apoptotic activation and cell death. Therefore, SERCA activity is tightly regulated in the cell to maintain 100-800 μM concentration of Ca^{2+} in the ER lumen compared to 100 nM concentration in the cytosol especially after Ca^{2+} transients. SERCA can be found in 12 different isoforms as a result of alternative splicing of three different genes ATP2A1, ATP2A2 and ATP2A3 giving rise to proteins named SERCA1(a-b), SERCA2(a-d), SERCA3(a-f), respectively. The expression of SERCA is tissue-dependent e.g. SERCA1a is mainly expressed in striated muscle while SERCA2a is prevalent in smooth muscle, cardiac muscle and non-muscle tissues. SERCA2b has a housekeeping function and is expressed ubiquitously, in many tissues together with SERCA3. SERCA3 differs from SERCA1 and 2 in that it has five-fold lower affinity for Ca^{2+} [67].

SERCA1 isolated from rabbit skeletal muscle was the first crystalized P-type ATPase. SERCA is a 110 kDa protein with 10 transmembrane helices and three cytosolic globular domains including the nucleotide-binding (N) domain for ATP binding, the phosphorylation (P) domain for aspartate residue phosphorylation and the actuator (A) domain to coordinate the

movement between the N and P domains. It has two Ca^{2+} binding sites between the M4-M5 and M6-M8 helices that allow entry of two Ca^{2+} to the ER lumen after ATP hydrolysis. Crystallographic studies showed that SERCA has two conformations E1 and E2. The enzymatic cycle includes activation of E1 state by binding of two Ca^{2+} followed by auto-phosphorylation utilizing ATP resulting in a conformational change and transition to the E2 state where Ca^{2+} is facing the ER luminal side. After the release of these two Ca^{2+} ions into the ER lumen and the phosphorylated intermediate becomes dephosphorylated, the pump returns to its E1 state. During this stage, 2-3 protons are transported in the opposite direction (Figure 3) [68].
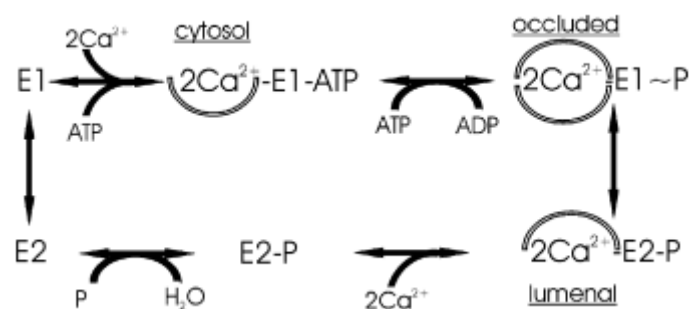
Figure 3. Schematic diagram of SERCA E1/E2 enzymatic cycle [68].

Endogenously SERCA is tightly regulated by controlling its expression or its activity level. SERCA can be inhibited by micropeptides such as phospholamban (PLN), myoregulin (MRLN), another-regulin (ALN), endoregulin (ELN) and sarcolipin (SLN) or it can be activated through long noncoding RNA called dwarf that can displace the micropeptide inhibitors. *In vitro* inhibition of SERCA is possible with thapsigargin [69].

2.3.2.4.3. Plasma membrane Ca^{2+} ATPases (PMCAs)

PMCAs are key transporter mechanisms for maintaining low basal free Ca^{2+} concentration in the cytoplasm by utilizing one ATP for each Ca^{2+} efflux. It was first discovered as an ATP-dependent active Ca^{2+} pump of the erythrocytes [70]. Later, using gel filtration chromatography, Wolf and his co-workers were able to partially purify a ~140 kDa protein from the erythrocyte membrane solubilized with detergent [71].

Mammals have four PMCA genes (*ATP2B1-4*) that are positioned on four different chromosomes (12, 3, X and 1) and encode for four protein isoforms PMCA1-4. As a result of alternative splicing at two splice sites named A and C, each gene has several transcript variants

(total over 30 variants), which are expressed in a tissue and developmental stage specific manner (Figure 4) [72].
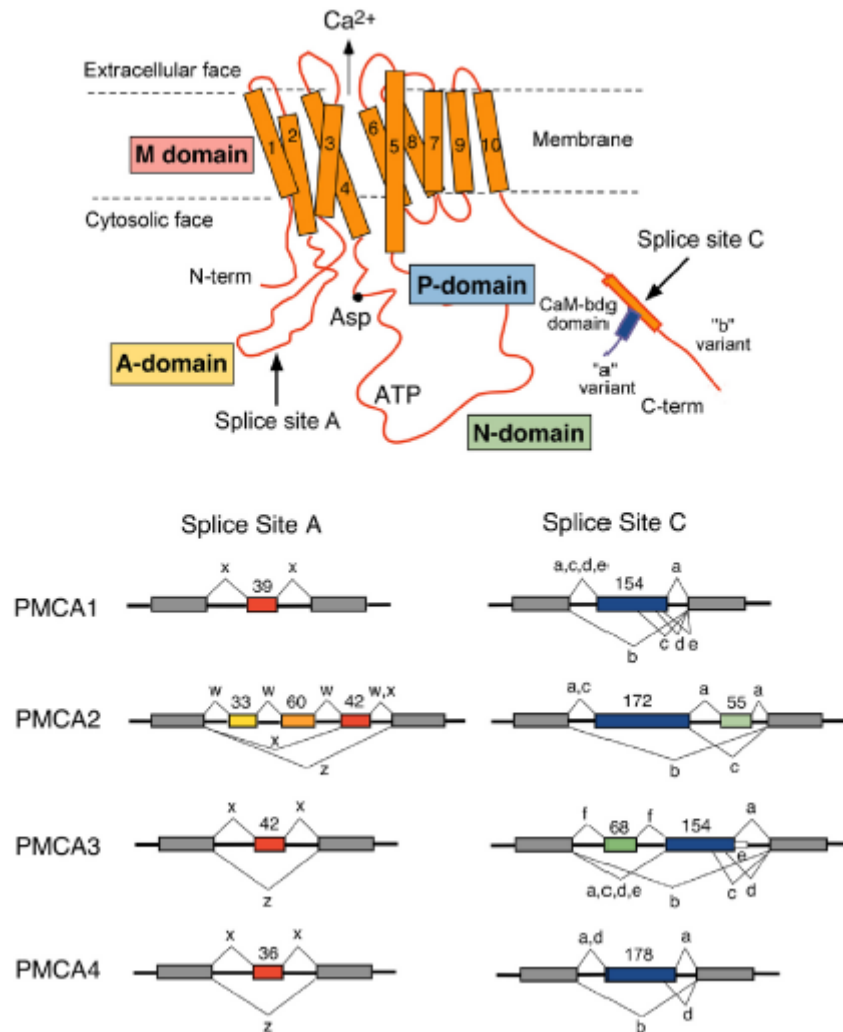
Figure 4. Schematic representation of PMCA structure (Top) and of the four PMCA genes with their splicing alternatives (bottom) [72]. The PMCA structure shown in the top consists of ten transmembrane domains (M domain) with amino (N) and carboxy (C) termini localized to the cytosolic side. It has two intracellular loops that contain three domains: A (actuator), N (nucleotide-binding) and P (phosphorylation). Arrows show the two splice sites A and C. ATP binding site (ATP) and aspartate (Asp) residue were labeled. At the C-terminus, both splice site C and CaM binding domain (CaM-bdg)-regulatory site are shown. Below represent the exons of all four PMCA genes showing the position of alternative splicing at A and C splice sites.

PMCA shares similar mechanical properties to SERCA including high affinity to Ca^{2+} (K_m range: 0.2-0.5 µM) and formation of an aspartyl phosphate intermediate during the enzyme

cycle. PMCA differs from SERCA in that it can transport one Ca^{2+} ion instead of two per one ATP hydrolyzed [73]. Structurally, similar to SERCA, PMCA contains 10 transmembrane domains (M domain), three cytosolic domains A, N and P, two intracellular loops and a C-terminal regulatory region (Figure 4). The N-terminus in PMCA protein composed of 90 residues and has a consensus binding site for 14-3-3 protein. The small loop between the second and third domains forms the A domain that contains a site for binding to acidic phospholipids, catalytic site for interaction with auto-inhibitory calmodulin (CaM)-binding motif and site A where an alternative splicing can occur generating several PMCA variants (x, w, z). The catalytic domain of this pump is located in the second loop between transmembrane helices 4 and 5 and it contains three sites: the ATP binding site (N-domain), a catalytic site with the aspartate residue for phosphorylation (P-domain) and another site for interaction with the auto-inhibitory CaM-binding sequence. The C-terminal regulatory region of the PMCA contains the following sites: a calmodulin-binding sequence motif (CBS), splice site C (PMCA variants a and b) that overlap with CBS, protein kinase A and C (PK) phosphorylation sites, an acidic phospholipid binding site, a caspase cleavage site and a PDZ binding motif [74].

2.3.2.4.3.1. PMCA isoforms and tissue distribution

The tissue distribution of PMCA isoforms and their variants produced by alternative splicing at both A and C sites is summarized in Table 3. PMCA1xb and PMCA4b are expressed ubiquitously. The other variants of PMCA1 are expressed in the brain and skeletal muscles while for PMCA4 heart and smooth muscle are the main expression sites. PMCA2 and PMCA3 are expressed in excitable cells. PMCA2 variant w/a is expressed in vestibular hair cells while PMCA2 variant w/b is expressed in the lactating mammary gland [72].

Table 3. PMCA isoforms and variants showing major sites of tissue expression [72].

Isoform	Alternative splice variants	Tissue distribution
PMCA1	x/a	Brain
	x/b	Ubiquitous; lung; small intestine; kidney
	x/c	Skeletal muscle, heart
	x/d	Skeletal muscle
	x/e	Brain
PMCA2	w/a	Brain; cochlear outer hair cells
	x/a	Brain; hippocampal presynaptic terminals
	z/a	Brain; excitable tissue
	w/b	Brain; lactating mammary epithelial cells; pancreas (β-cells)
	x/b	Brain; cerebellar Purkinje cells; spinal cord
	z/b	Brain; excitable tissue
	x/a	Brain; spinal cord

PMCA3	z/a	Brain; pancreatic (β-cells)
	x/b	Brain; adrenal gland; skeletal muscle
	z/b	Brain
PMCA4	x/a	Smooth muscle; bladder; uterus; heart
	z/a	Smooth muscle; heart
	x/b	Ubiquitous; heart; kidney
	z/b	Heart
	x/d	Heart
	z/d	Heart
	x/e	Brain; bladder
	z/e	Brain; bladder

2.3.2.4.3.2. Processes regulated by PMCA activity

As the expression of PMCA pumps is ubiquitous, their role was mainly associated with a housekeeping function controlling Ca^{2+} homeostasis in the cell, however, later it was found that different PMCA isoforms have more specialized functions in addition to their housekeeping role. Knockout mice experiments were utilized to understand their physiological role. PMCA1 knockout in embryo resulted in embryo death suggesting a housekeeping function. PMCA2 null mouse did not affect embryo viability, however, at day 10, imbalance and deafness were observed. Ataxia, reduced Ca^{2+} concentration in milk, and loss of motor neurons were also reported. In case of PMCA3, until now no knockout experiment was performed, however, since it is highly expressed in the choroid plexus of the brain, it was suggested that it may affect brain development and function. Isoform PMCA4, similarly to PMCA1, is ubiquitously distributed, therefore, it was expected to act as a housekeeping gene, however, the PMCA4 null mouse survived but caused male infertility as a result of a defect in sperm motility [75].

PMCA can modulate many other processes through its interaction with other proteins. For example, the specific variant PMCA4b was found to regulate cardiac contractility through the interaction of its C-terminal end with the PDZ domain of the neuronal nitric oxide synthase (nNOS) and this interaction resulted in decreased nNOS activity [76]. In another study on Jurkat cells, PMCA4 was found to interact with CD147 (basigin) and this interaction resulted in the reduction of IL-2 expression [77].

In addition, it was reported that PMCA can function as a signaling pathway modulator. One study showed that PMCA4b through interaction with its catalytic domain can act as a negative modulator to the Ca^{2+}-dependent phosphatase calcineurin. Calcineurin normally activates the nuclear factor of the activated T-cell (NFAT) signal transduction pathway, however, when PMCA4b interact with calcineurin its activity is reduced due to the low Ca^{2+}

environment produced by PMCA4b activity, and this results in the reduction of NFAT activity and inhibition of the downstream pathway [78]. Another study showed that co-expression of Ras-associated factor 1 (RASSF1) and PMCA4b resulted in inhibition of the EGF-mediated Ras signaling pathway after stimulation with EGF [79].

PMCA4b and the calcium/calmodulin-dependent serine protein kinase (CASK) was reported to co-precipitate in the brain and kidney. Luciferase functional assay in human embryonic kidney (HEK293) cells showed that the C-terminal end of PMCA4b can interact with the PDZ domain of CASK and this interaction results in inhibition of CASK activity [80].

PMCAs were also shown to interact with PIP2. Our laboratory has reported that this interaction helps in protecting PIP2 from hydrolysis to IP3 and DAG by PLC activity. Two predicted mechanisms for PIP2 protection have been suggested: one needs the activity of the PMCA where lowering Ca^{2+} level reduces PLC activity and hence PIP2 hydrolysis and the other one includes direct interaction between PIP2 and PMCA that makes PIP2 not accessible to PLC [81].

Many recent studies showed that alteration in PMCA expression is associated with tumorigenesis, however, their role is isoform dependent. For example, the particular isoform PMCA4b was found downregulated in many cancer cells and this contributed to cell transformation and malignancy. Our laboratory reported that PMCA4b was markedly downregulated in BRAF mutant melanoma cells and overexpression of PMCA4b resulted in a significant decrease in migration and metastasis with no effect on cell proliferation. Therefore, PMCA4b was suggested to act as a metastatic suppressor in these cell types [82].

It was shown that PMCA1 and PMCA2 expression in certain breast cancer cell lines are upregulated while PMCA4 was found downregulated when compared to normal breast epithelial cells [83–86]. Similarly, PMCA4 expression in colon cancer was downregulated especially in high-grade colon adenoma and in lymph node metastasis when compared to normal colon tissue where high PMCA4 is expressed [87,88]. Another study showed that PMCA1 mRNA and protein levels in primary oral squamous cell carcinomas (OSCCs), oral premalignant lesions (OPLs) and OSCC-derived cell lines were downregulated and PMCA1 gene inactivation could be as a result of epigenetic regulation [89].

2.3.2.4.3.3. Regulation of PMCA expression

PMCAs have certain transcription factor binding sites in the promoter and enhancer regions that may play role in regulating PMCA transcription but their proper function is still not well understood [90]. It was reported that the *ATP2B2* gene has four different transcription start sites where two of them are only expressed in neuronal tissue [91]. The transcription factor

c-myc can bind to the promoter region of the *PMCA4b* gene in differentiated B-lymphocyte that results in its reduced expression [92]. An erythroid-specific regulatory region in the intron 1 of the gene *ATP2b4* was reported to be important for its expression in erythroid cells but not required in non-erythroid cells [93].

Ca^{2+} itself was found to affect PMCA expression. A study on neuron cultures showed that an increase in Ca^{2+} concentration in cerebellar granule cells re-arranged the pattern of PMCA so that PMCA2 and 3 were upregulated, PMCA1 undergone truncation and PMCA4 degraded in a calcineurin-dependent manner [74].

Several studies reported from our laboratory showed that PMCA4b expression can be modulated by different mechanisms. In BRAF mutant melanoma, the BRAF/MEK/ERK pathway is active and inhibition of this pathway using BRAF (vemurafenib) or MEK (selumetinib) inhibitors increased PMCA4b expression. Similarly, it was shown that histone deacetylase (HDAC) inhibitors both in melanoma [94] and estrogen receptor (ER-α) positive breast cancer cells [86] upregulated PMCA4b expression. In MCF-7 cells, 17β-estradiol (E2) treatment was also found to upregulate PMCA4b expression indicating that PMCA4b expression is regulated by the ER-α pathway [86].

2.3.2.4.3.4. Regulation of PMCA activity

Ca^{2+}-calmodulin and alternative splicing. In the resting state, in the absence of calmodulin, the binding motif for calmodulin - located near the C-terminus of PMCAs - acts as an auto-inhibitor that binds to its receptors on both sites of the intracellular loops resulting in an inactive PMCA with a Kd for Ca^{2+} around 10-20 µM. An increase in intracellular Ca^{2+} concentration and binding of four Ca^{2+} ions to calmodulin allow this protein complex to bind to the CBS motif at the C-terminus and therefore frees the pump from the auto-inhibition and PMCA becomes active with a Kd < 1 µM [95].

The alternative splicing of PMCAs may affect their activity, regulation, localization and interaction with other proteins. As the splicing site at the C-terminus of PMCA overlaps with the calmodulin-binding site, any changes in this site as a result of alternative splicing will affect its binding to calmodulin and eventually the activity of the pump, for example, the "a" variant differs from "b" variant in having an insert in the site C and therefore this resulted in PMCA4a having a higher basal activity and faster activation with CaM than PMCA4b. In cell-free systems and at resting state, it was found that PMCA4b is the only inactive pump while the other pumps were found partially active [96].

Localization of PMCA was also different with different isoforms and different splice A variant, for example, PMCA2w/a was more localized to the apical region of the stereocilia in

cochlear hair cells of the inner ear while PMCA1xb localized mainly at its basolateral membrane [97].

The sequence of the catalytic region of the same variant may also determine the activity of the PMCA by affecting its interaction strength, for example, PMCA4b has a lower basal activity and slower activation with CaM than PMCA2b [95].

Phosphorylation by protein kinases. Another way of PMCA activity regulation is its phosphorylation by protein kinases (PK) A and C through interfering with calmodulin regulation or via de-inhibiting the pump. For example, PKC was found to increase PMCA4b activity, although not fully, and showed an additive effect to Ca^{2+}-calmodulin. However, the results were opposite when PKC phosphorylated PMCA2a and PMCA3a [98,99].

Acidic phospholipids. *In vitro* treatment of the pump with acidic phospholipids and their binding to the PMCA at specific sites showed an increase of PMCA affinity to Ca^{2+} and an increase in PMCA activity. This was explored using PMCA isoform 2 [100]. In addition, changes in the composition of the lipid content of the plasma membrane showed an effect on PMCA activity, for example, PMCAs in PIP2-rich lipid rafts are found more active [101].

Proteases. PMCA pumps also act as a substrate for certain enzymes such as Ca^{2+} dependent protease calpain and caspase 1 and 3. Calpain was found to activate the PMCA pump by cutting the calmodulin-binding sequence [102] while caspase 1 and 3 resulted in activation and inhibition of PMCA2 and 4, respectively [103].

PMCA localization and internalization. Localization of membrane proteins is essential for their proper function. Our laboratory showed that in low-density epithelial and endothelial cell cultures, PMCA4b is mostly localized to intercellular compartments and as the cells get more confluent the PMCA4b becomes more localized to the plasma membrane with higher extrusion Ca^{2+} capability. In addition, it was shown that a di-leucine-like motif (1167)LLL at the C-terminal region of PMCA4b was critical for internalization and L(1167-1169)A mutation was able to target PMCA4b to the plasma membrane. These results confirmed that PMCA4b internalization can mediate pump loss of function [104].

PMCA interaction with other proteins:

Protein 14-3-3. Binding of the regulatory protein 14-3-3ε to a region near the N-terminus of three out of four isoforms (PMCA1, 3 and 4) of PMCAs resulted in their inactivation [105,106].

PDZ domain interaction. All "b" splice variants of PMCA's C-terminal tail include a PDZ domain-binding motif to mediate interaction with proteins, harboring one or more PDZ domains. These are mostly scaffolding proteins that may link PMCAs to the actin cytoskeleton

or mediate their interaction with other proteins and affect their localization and/or activity [74,76,107]. PDZ domain-binding motif in PMCA 1, 2 and 3 of b variants have the same PDZ-binding sequence (-ETSL) while PMCA4b differ in one amino acid residue (-ETSV) therefore PMCA4b can interact with distinct scaffolding proteins [108,109].

As for localization, PDZ containing proteins such as the membrane associate guanylate kinase (MAGUK) family, Na+/H+ exchanger regulatory factor 2 (NHERF2), SAP-1 and PISP can interact with the PMCAs in an isoform-specific manner and this allows maintaining PMCAs to certain membrane domains for local regulation of Ca^{2+} signal [74].

Interaction of CASK PDZ domain with its binding motif in PMCA4b in mouse sperm resulted in inhibition of PMCA4b activity and an increase in cytosolic Ca^{2+} concentration that ultimately resulted in decreased sperm motility [110].

Neuroplastin (NPTN) and basigin (BSG). Neuroplastin and basigin/EMMPRIN/cd147 are Ig-domain containing proteins. Based on knockout studies on cells, tissue and virally transduced neurons, it was found that these proteins can serve as obligatory auxiliary subunits of the PMCA that allows them to regulate cytosolic Ca^{2+} concentration by increasing PMCA stability at the plasma membrane and hence Ca^{2+} extrusion capacity of the cell [111].

Cytoskeleton. A study in activated platelets showed that F-actin can interact with PMCAs and results in its inactivation [112]. Later, another study on purified erythrocyte PMCA proteins showed that interaction between monomeric G-actin and PMCA resulted in PMCA activation while filamentous F-actin interaction resulted in activity inhibition. These data were also confirmed in HEK cells expressing PMCA2 or PMCA4 [113].

The differences observed in PMCA isoforms and variants in term of expression, activity, kinetics, interacting proteins, localization and regulations results in functional diversity that is important to match cell or tissue-specific requirements and to respond to a variety of stimuli during growth and development. Other sources of PMCA variations include mutations and post-translational modifications are also reported [90].

2.4. Alteration in Ca^{2+} homeostasis and cancer development

Ca^{2+} is a key regulator of many physiological processes and its deregulation participates in the development of a variety of diseases ranging from hypertension to cancer. Cytosolic Ca^{2+} acts as a second messenger in the cell and any intracellular increase in its concentration may alter a variety of processes through its effect on many Ca^{2+}-dependent proteins or effectors involved in key signaling pathways regulating cell proliferation, migration and apoptosis [114].

Therefore, in normal cells, the intracellular Ca^{2+} concentration is under tight control using a toolkit of Ca^{2+} channels, pumps and exchangers. For cells to transform to malignancy they should acquire characteristics of cancer - called cancer hallmarks - including continuous proliferation, angiogenesis induction, avoiding apoptosis, allowing cells to migrate, invade and then metastasize [115]. Ca^{2+} is involved in all these processes therefore any alteration in spatiotemporal cytosolic Ca^{2+} concentration or Ca^{2+} signal kinetics may result in cancer development [116].

Cancer cells use the same Ca^{2+} signaling toolkit as normal cells, however, changes in the expression, cellular localization and/or activity of these tools in response to gene mutations or post-translational modifications may result in changes in Ca^{2+} fluxes and cytosolic Ca^{2+} concentration [117]. Examples of altered Ca^{2+} toolkit protein expression levels in a variety of human cancers are presented in Table 4 [118].

Table 4. Ca^{2+} channels and pumps mRNA and protein levels in several types of cancer [118].

Channel/transporter	Cancer type	Changes
IP3R		
IP3R1	Glioma	Decreased
IP3R2	Lymphocytic leukemia	Increased
IP3R3	Glioma, gastric, colon, head and neck cancer	Increased/mutation
Ca^{2+}-ATPases		
SERCA2	Colon cancer	Increased
SERCA3	Gastric, lung, choroid plexus tumor, and in myeloid leukaemia	Decreased
SPCA1	Breast cancer	Increased
SPCA2	Breast cancer	Increased
PMCA1	Oral cancer	Decreased
PMCA2	Breast cancer	mRNA elevated
PMCA4	Colon cancer	Decreased
VGCC		
$Ca_v1.2$	Colon and oesophageal cancer	Increased
$Ca_v2.3$	Glioma	Increased
$Ca_v3.1$	Glioma	Increased
$Ca_v3.2$	Prostate, ovarian, glioma, breast, oesophageal, hepatoma, melanoma, and colon cancer	Increased
TRP		
TRPC1	Breast cancer	Increased
TRPC3	Ovarian and breast cancer	Increased
TRPC6	Oesophageal, glioma, and breast cancer	Increased
TRPM1	Melanoma	Decreased
TRPM7	Pancreatic and breast cancer	Increased

TRPM8	Pancreatic, prostate, bladder, breast, melanoma, colon, and lung cancer	Increased
TRPV1	Bladder and prostate cancer	Decreased/Increased
TRPV2	Bladder and prostate cancer, hepatocarcinoma	Decreased/Increased
TRPV4	Non-melanoma skin cancer, tumor endothelial cell derived prostate and breast cancer	Decreased
TRPV6	Breast, prostate, lung, thyroid, colon and ovarian cancer	Increased
Orai & STIM		
Orai1	Pancreatic adenocarcinoma, glioma, melanoma, breast, oesophageal, renal, and NSCLC	Increased/constitutive activated
Orai3	Breast, prostate, and lung	Increased
STIM1	Hepatoma, melanoma, cervical, colorectal, breast, and pancreatic adenocarcinoma	Increased
STIM2	Breast, colorectal cancer, and melanoma	Increased/Decreased
Purinergic receptor		Increased
P2X3	Hepatoma	
P2X5	Melanoma, colorectal, brain, breast, and renal cancer	Increased
P2X7	Neuroblastoma, melanoma, leukaemia, breast, prostate, papillary thyroid, pancreatic, colon, renal, cervical, and B-chronic cancer	Increased
P2Y2	High metastatic breast cancer, hepatoma and colon cancer	Increased
P2Y4	Colon cancer	Increased
MCU	Breast, colon, and prostate cancer	Decreased/Increased

2.4.1. Role of Ca^{2+} in cell proliferation

Cells to increase in number, undergo proliferative cell cycles of four phases: G1, first growth; S, DNA synthesis; G2, second growth; M, mitosis. The whole process is tightly controlled and there are checkpoints for cells to complete the cycle. Ca^{2+} is essential for cell proliferation and division where checkpoints and cell cycle progression are dependent on Ca^{2+} especially in early stages G1, G1/S and G2/M. [119]. For cells to enter the G1 phase, transcription factors such as AP1 (FOS and JUN), NFAT and cAMP responsive element-binding (CREB) should be activated first to regulate the expression of cell cycle regulator cyclin-dependent kinases CDK2 and 4 and cyclin D and E. Ca^{2+} is required to promote activity of proteins involved in cell cycle progression. In the S phase, Ca^{2+} is needed for CDK2 and 4 assembly and activation to allow phosphorylation of retinoblastoma (RB1) and hence its inactivation for cells to progress and enter the S phase. Ca^{2+} and CaM were also required for centrosome duplication during G1/S phase transition. The Ca^{2+}/Calcineurin pathway regulates

Cyclin A, D and E, and activates the NFAT pathway. In addition, Ca^{2+} oscillation during G2/M transition was found to regulate the separation of the centrosome via CaMKII (Ca^{2+}/calmodulin-dependent protein kinase II) activity [116].

Studies showed that an increase in basal Ca^{2+} level may induce cell cycle progression and hence cell proliferation. In cancer, many Ca^{2+} channels were found overexpressed and contribute to increased cell proliferation. For example, changes in expression of transient receptor potential cation channels, including TRPV1, TRPV2, TRPV6, TRPM8, TRPM2 and TRPC6 have been demonstrated in prostate cancer (PC) [116]. Increased expression of both TRPC6 and TRPV6 were able to induce NFAT signaling and as a consequence increase prostate cell proliferation and malignancy. TRPV6 is considered as a prognostic factor for PC [120]. Similar to PC, TRP channels (TRPV6, TRPC6, TRPM7) have been reported to control breast cancer cell proliferation, as well [121].

Calcium Orai channels and STIM expression were also reported to be elevated in various types of cancers. An increase in cytosolic Ca^{2+} concentration mediated by SPCA2 and Orai1 in breast cancer cells was found to activate the Ras signaling pathway through ERK activation and to promote downstream expression of Cyclin D1 [122]. Another study in non-small cell lung carcinoma (NSCLC) demonstrated the contribution of Orai3 in controlling cell proliferation and cell cycle through the AKT pathway where Orai3 was found overexpressed [123]. Similar overexpression of Orai3 was observed in breast, lung, and prostate cancer [124].

2.4.2. Role of Ca^{2+} in cell motility, migration and metastasis

One of the hallmarks of cancer is the ability of cells to migrate from the primary site, invade, disseminate to the secondary site and develop metastasis. Several steps involved in cell metastasis including cell deformation, detachment/adhesion, invasion and migration are Ca^{2+}-dependent processes. In normal migrating cells, a gradient increase of Ca^{2+} across the cell from front-to-rear helps in the formation of leading edge/protrusions at the front and trailing edge detachment at the rear. Studies showed that voltage-gated calcium channels, TRP and PLC/IP3R signaling pathways are involved in such processes. However, other local spatiotemporal increases of Ca^{2+} were detected in restricted micro-domains in different regions of migrating cells. For example, a transient increase in Ca^{2+} levels "calcium flickers" at the lamellipodia are generated by TRPM7 stretch-activated channel [125]. These flickers have been involved in directional migration and without them cells can move faster but cannot respond to any directional cues.

A similar Ca^{2+} gradient was observed when migrating human umbilical vein endothelial cells (HUVECs) was studied. They related the low Ca^{2+} level at the cell front to the presence of PMCA and its enhanced ability to extrude Ca^{2+}. In addition, they reported that localization of STIM1 toward the front of the cell helped in decreasing Ca^{2+} concentration in the ER lumen. Tyrosine kinase signaling is also increased at the cell front where a polarized activation of PLC generates IP3 and DAG. IP3R activity results in the formation of local Ca^{2+} pulses that induce Ca^{2+}-dependent modulators such as myosin light chain kinase (MLCK) activity [126].

Cell migration involves changes in cytoskeleton dynamics, focal adhesion (FA) (disassembly at the rear and assembly at the front) and directional sensing. Local increase of Ca^{2+} by IP3R at the ER was essential for activation of certain Ca^{2+}-dependent modulators such as calmodulin kinase II (CaMKII) or calpain that are important for focal adhesion and cytoskeleton organization. These can activate effectors and signaling pathways including focal adhesion kinase (FAK) (calpain 2 can regulate its activity by proteolysis), PI3K, and MLCK. TRPM7 channel is suggested to be involved in FA disassembly, cell detachment and migration [125,127]. In solid tumors, motility and migration are mainly of mesenchymal type and recent studies showed the involvement of voltage in-dependent Ca^{2+} channels such as Orai and TRP in such processes [116].

Increased migration and metastasis of several types of cancer have been connected to increased intracellular Ca^{2+} concentration through overexpression of Ca^{2+} channels. For example, in metastatic prostate cancer, overexpression of both Orai and TRP calcium channels was involved in the regulation of prostate cancer (PC) cell migration. Inhibition of SOCE (Orai1) resulted in reduced migration of both androgen-independent and androgen-dependent prostate cancer cells [128]. In addition, TRPM7 channel also regulates cell migration in PC. A high cholesterol level increases TRPM7 activity that leads to an increase in cytosolic Ca^{2+} concentration and calpain activation. In turn, calpain reduces E-cadherin expression and increases PC cell migration [129].

In NSCLC, TRPM7 channel expression is induced by EGF. Knockdown experiments and pharmacological inhibitor treatment with or without EGF resulted in decreased cell migration [130]. In glioblastoma, IP3R3 expression was shown to be elevated and its inhibition by caffeine resulted in reduced cell motility using *in vitro* and *in vivo* models [131].

2.4.3. Role of Ca^{2+} signaling in melanoma development and metastasis.

As discussed earlier, an increase in intracellular Ca^{2+} concentration in several types of cancers as a result of changes in expression of Ca^{2+} channels or pumps has led to enhancement of tumor cell proliferation and metastasis. In melanoma, the expression of several Ca^{2+}

channels was found to be upregulated and was found to be involved in melanoma development and metastasis (Figure 5).
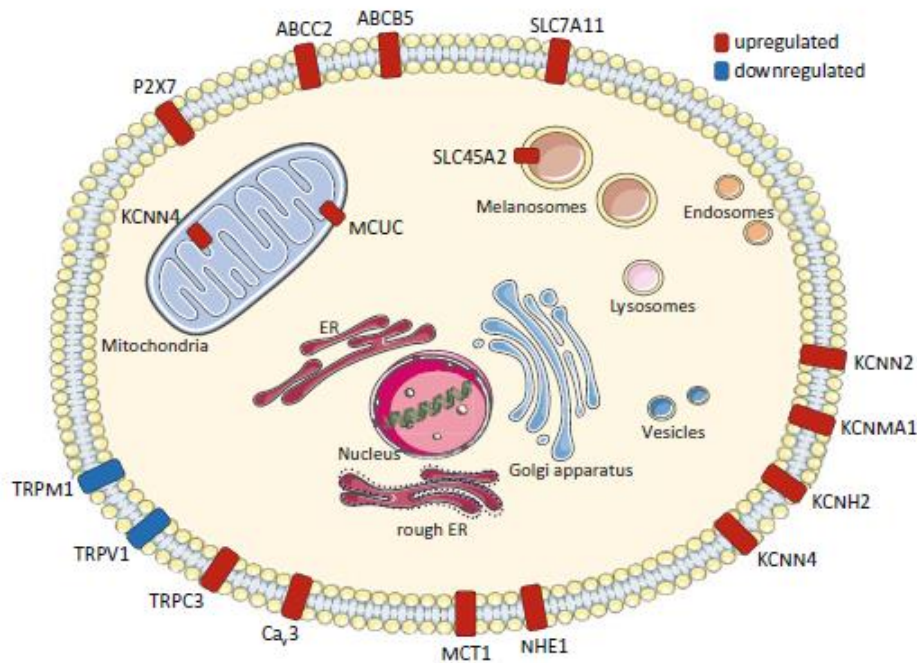
Figure 5. Schematic illustration of channels and transporter proteins in melanoma cell [132]. Red: up-regulated, blue: down-regulated.

Transient receptor potential melastatin (TRPM) is involved in the regulation of melanocyte behavior and it was reported that an increase in expression of TRPM2, TRPM7 and TRPM8 in melanoma cells contributed to increased cell proliferation and metastatic capacity [133].

T-type calcium channels (TTCCs) are overexpressed in melanoma and this contributed to an increase in cell proliferation, migration and metastasis. Fast activation of TTCCs by weak depolarization allows a transient increase in intracellular Ca^{2+} concentration and this allows direct binding of Ca^{2+} to CaM in the favour of mitotic and cell cycle progression. TTCCs knockdown (especially $Ca_v3.1$ and $Ca_v3.2$ isoforms) reduced cell viability by inducing cell cycle arrest at G1 and S phases. In addition, $Ca_v3.2$ expression was found to be associated with the expression of Glut1 (hypoxia marker), cyclin D1 and Ki-67 (proliferation markers). TTCK blockers were reported to be effective in reducing migration and invasion of BRAF mutant melanoma cells by inhibiting its autophagy [134]. Similarly, voltage-gated Ca^{2+} channels (VGCSs) upregulation in melanoma was found to enhance cancer proliferation by providing Ca^{2+} wave oscillations that favor cell cycle progression [135].

The major source of Ca^{2+} in non-excitable cells is the store-operated Ca^{2+} entry (SOCE). The depletion of Ca^{2+} from the endoplasmic reticulum (ER) is sensed by the STIM protein, which then activates the Orai Ca^{2+} channel at the plasma membrane. Two studies showed that SOCE expression is upregulated in melanoma cells independent of the BRAF mutational status and when SOCE is inhibited by either knocking down or by using synthetic inhibitors it resulted in reduced melanoma cell proliferation, migration and metastasis. The first study showed that induction of SOCE is associated with activation of the CaMKII/Taf-1/ERK pathway and SOCE inhibition will result in inhibition of melanoma progression [136]. The second study found that STIM1 and ORAI1 generated Ca^{2+} oscillations resulted in enhanced melanoma invasion by inducing invadopodia precursor formation through Src activity and by enhancing extracellular matrix (ECM) degradation through increased matrix metalloproteases (MMPs) production [137].

Calcium-activated chloride channel regulator-2 (CCLA2) was found to enhance melanoma metastasis by facilitating cell adhesion through interaction with β4 integrin at the cell surface [138].

Ryanodine receptors (RyR1, RyR2, RyR3) are involved in the regulation of intracellular Ca^{2+} concentration in excitable tissues such as muscles and neurons and it was found upregulated in melanoma [139].

In BRAF mutant melanoma cells, high concentration of vemurafenib induced increase in cytosolic Ca^{2+} that resulted in ER stress and apoptosis. Combination of vemurafenib with thapsigargin, an inhibitor of SERCA pumps, was found to reduce the effective concentration of vemurafenib and overcome resistance acquired by vemurafenib treatment alone [140].

Our laboratory demonstrated that the PMCA4b Ca^{2+} pump was down-regulated in BRAF mutant melanoma cells, and its overexpression resulted in inhibition of cell migration *in vitro* and metastasis *in vivo*. We also found that the RAS-BRAF-MEK-ERK pathway was involved in PMCA4b down-regulation since BRAF inhibition with vemurafenib up-regulated PMCA4b at both the mRNA and protein levels [82].

All these data show that Ca^{2+} homeostasis is essential for normal cell functioning and changes in its level may produce many types of diseases. Remodeling of the Ca^{2+} signaling toolkit in different types of cancers could be the direct driving force for cancer development, and could help in sustaining cancer hallmarks. Many Ca^{2+} channel inhibitors have been suggested as a promising candidate for therapeutic targeting, however, the ubiquitous role of Ca^{2+} in different signaling pathways, and the presence of some of these channels in several types of tissues, may exhibit difficulty in finding a promising selective drug. Those Ca^{2+}

channels that are significantly elevated in restricted tissues may provide a better target for drug selection [116].

2.5. Mitogen-activated protein kinases-MAPK superfamily

MAPK signaling pathway is one of the key pathways identified in eukaryotic cells. It regulates a variety of cellular processes such as proliferation, apoptosis, differentiation, stress response, gene expression and motility. The MAPK cascades consist of three evolutional conserved serine-threonine kinases that can be activated by growth factors, mitogen, environmental stress and inflammatory cytokines. Upon stimulation, MAP Kinase-kinase-kinase (MAPKKK/MAP3K) becomes active by interaction with GTPases or by phosphorylation via protein kinases downstream of the receptor. Active MAP3K selectively phosphorylates and activates downstream MAP2K, which in turn activates MAPK by phosphorylation at two conserved sites (Thr/Tyr) in the activation loop.

In mammal cells, there are three main MAPK subfamilies: extracellular signal-regulated kinases (ERKs) 1 and 2 (ERK1/ERK2); c-Jun N-terminal kinase/stress-activated protein kinase (JNK/SAP) 1, 2 and 3; and p38 kinases α, β, γ and δ. Other MAPK subfamilies have been reported as ERK 3, ERK4, ERK5, ERK7 and ERK8, however, their exact role is not fully understood. The activity of MAPK results in phosphorylation of a large variety of substrates such as transcription factors, cytoskeleton proteins, phospholipases and other protein kinases named MAPK-activated protein kinases (MKs) (Figure 6) [141].
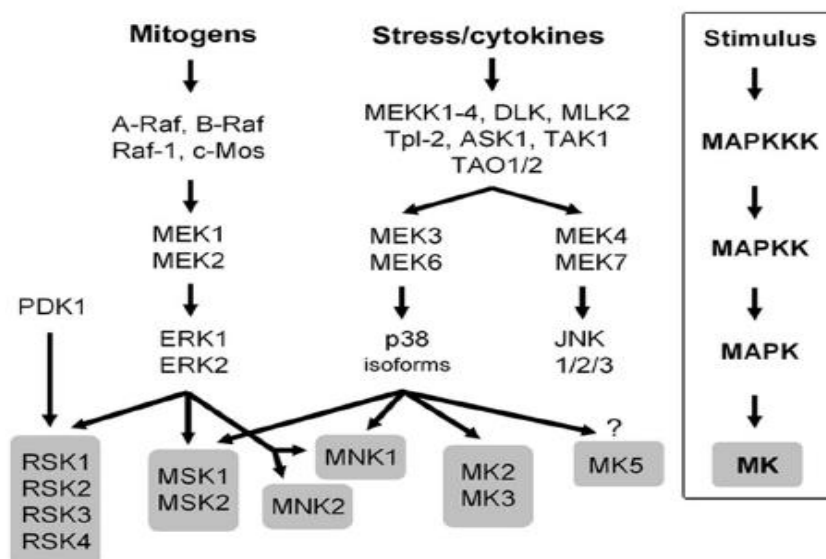
Figure 6. Schematic diagram of MAPK signaling pathway. A stimulus such as a mitogen or cellular stress can activate ERK and p38 pathways leading to activation of other MKs.

In a previous section, we discussed the role of BRAF point mutation in constitutive activation of the MAPK pathway and the development of melanoma. In the literature, other active MAPK-signaling pathways - p38 MAPK and JNK - and the NF-κB pathway were also found to contribute to melanoma progression and metastasis [18–20].

2.5.1. The p38 MAPK family

P38 is a proline-directed serine/threonine protein kinase initially identified as a 38 KDa protein that can be tyrosine phosphorylated upon treatment with endotoxin or hyperosmolarity shock. It is the mammalian homolog of the *Saccharomyces cerevisiae* Hog1p MAP kinase which is involved in the signaling pathway controlling response to stress and cytokines [142]. P38 MAPK can phosphorylate several substrates in response to a variety of stimuli such as oxidative stress, UV light, growth factors (CSF-1, GM-CSF, VEGF and PDGF), DNA damage, osmotic shock and pro-inflammatory cytokines (TNF-α and IL-1). Therefore, p38 MAPKs are also known as stress-activated protein kinases (SAPKs). Their activation is not only stimuli specific but also cell type-specific, for example, insulin treatment of adipocytes 3T3-L1 activates p38 MAPK while the same treatment in check forebrain neuron cells results in its inactivation [143]. P38 MAPK activity is involved in the regulation of several processes such as proliferation, metabolism, differentiation, migration and apoptosis (Figure 7).
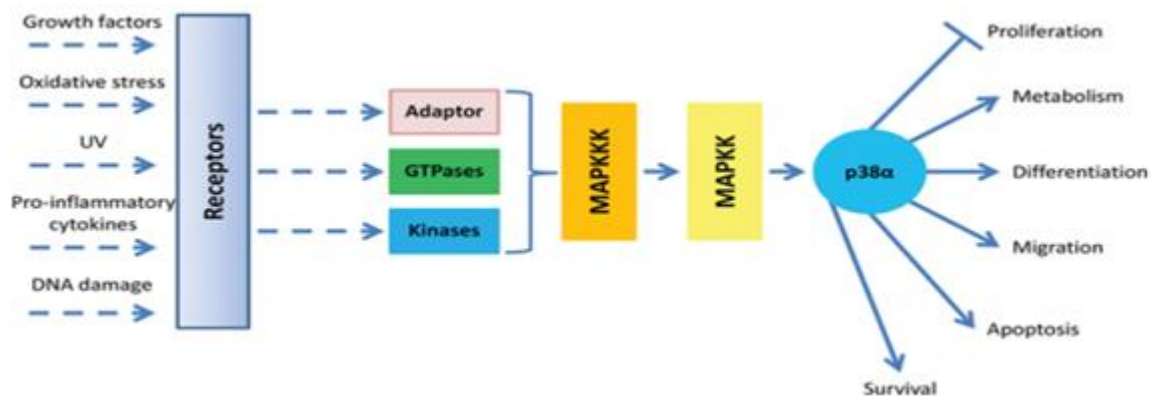
Figure 7. Schematic diagram showing p38α upstream activators and its effect on downstream processes. → stimulation, ⊣ inhibition**.**

In mammals, four splice variants encoded by four different genes with different tissue expression patterns have been identified: α (MAPK14), β (MAPK11), γ (ERK6/MAPK12/SAPK3) and δ (MAPK13/SAPK4). All four isoforms share 60% amino acid sequence similarity but only 40-45% to other MAPK family including JNKs and ERKs. Despite their similarities, they differ in their tissue expression, downstream effectors, upstream

activators, and chemical inhibitor sensitivity. P38α and p38β are ubiquitously expressed, however, p38α is more abundant in most cell types than p38β. The p38γ and δ are differentially expressed in skeletal muscle and endocrine gland, respectively [144]. P38α knock out experiments in mouse embryo were shown to be lethal while mouse deficient of p38 MAPK isoforms β, γ or δ showed no effect on embryo viability.

2.5.2. Regulation of the p38 MAPK signaling pathway

Many physiological processes are regulated by the p38 MAPK pathway and any de-regulation may lead to several pathological developments. Therefore, in normal cells p38 MAPK activity is regulated by four different mechanisms:

P38 dual phosphorylation: External stimuli such as environmental stress, inflammatory cytokines, or growth factors can activate MAP3K (MLKs, ASK1, TAK1 and some members of the MEKK family) through activation of low MWT GTP-binding proteins of the Rho sub-family (Rac1, CD242, Rit and Rho) or activation of hetero-trimeric G-protein coupled receptors. Once MAP3K is activated it activates downstream MAPK kinases named MKK3 or MKK6 (SKK3). Both are highly selective and can activate p38 MAPKs through dual phosphorylation at Thr-180 and Tyr-182 in the Thr–Gly–Tyr motif of the activation loop present between the kinase domains. Phosphorylation of p38 MAPK results in conformational changes and alteration in the alignment of two kinase halves (N- and C- terminal domains), which allows easier access to the p38 substrates and hence increases p38 MAPK activity [145]. Experiments on MKK3 and MKK6 dual knockdown resulted in non-viable-mouse at a mid-gestation stage with defects in the placenta and embryonic vasculature development. However, knocking down either one of them showed no effect on mouse viability indicating potential redundancy [146].

P38 auto-phosphorylation: Two MKK-independent mechanisms were proposed to activate p38 MAPK. The first one was identified using a yeast two-hybrid screen. The authors found an adaptor protein called TAB1 (Transforming growth factor-β-activated protein 1 (TAK1)- binding protein 1) that can bind to p38α MAPK (but not the other isoforms) and activate it through p38 MAPK auto-phosphorylation, and this was implicated mostly in the ischemic heart and immunological processes. However, a study showed that TAB1 induced autophosphorylation and enhanced activity resulted in different downstream p38α targets. This was explained by the ability of TAB1 to sequester p38α in the cytosol independent of the MKK-activated p38α functions [147].

The other MKK-independent mechanism was identified in a study using T-cells. Stimulation of T-cell antigen receptor (TCR) resulted in activation of proximal tyrosine kinases that in turn phosphorylated p38α at a non-canonical tyrosine residue Tyr323 [148].

P38 binding proteins and scaffolds: Protein kinases in the MAPK signaling pathway may interact with other protein kinases in the cascade or interact through scaffold proteins. For example, a scaffold protein called osmosensing scaffold for MEKK3 (OSM) was found to activate p38α through its complexing with MKK3, MEKK3 and Rac [149].

The TAB1 protein itself, mentioned above, was also found to be a substrate of p38α that can be phosphorylated at Ser423, Thr431 and Ser438 although these serine residues are not followed by proline. Transforming growth factor-β (TGF-β)-activated kinase-1 (TAK1) is a kinase that lies upstream of p38α, JNK and IκB kinase (IKK) usually activated by inflammatory stimuli and found to interact with TAB1. Phosphorylation of TAB1 by p38α terminates its ability to activate TAK1 and hence p38α activity itself. Therefore, it was suggested that TAB1 can mediate a negative feedback loop following its phosphorylation [150].

Downregulation of the P38 MAPK signaling pathway: In mammals, many protein phosphatases contribute to the inactivation of p38 MAPK including the Tyr phosphatase PTP and the Ser/Thr phosphatase PP2C [151].

2.5.3. P38 MAPK substrates

P38 MAPK has more than 100 protein substrates in the cell that can be directly phosphorylated to regulate different processes such as protein degradation/localization, endocytosis, cell cycle, metabolism, mRNA stability and translation, chromatin remodeling and cytoskeleton dynamics [152]. P38 MAPK downstream targets were identified using pyridinyl imidazole inhibitors such as SB203580 and SB202190 that can inhibit both p38α and β. The use of a new potent p38 pan-inhibitor diaryl urea BIRD796 that can inhibit all four p38 MAPK isoforms at different concentrations and the use of specific knockout mice approach helped in identifying new substrates and the physiological role of the other two isoforms γ and δ [153].

Some of the p38 MAPK substrates and their function are demonstrated in Figure 8. Activated p38 MAP kinase has been shown to phosphorylate and activate protein kinases such as MAPKAP kinase 2, transcription regulating factors such as activating transcription factor (ATF1), transcription factors such as NFAT, myocyte enhancing factor (MEF), serum response factor accessory protein-1 (SAP-1) and other proteins such as TAB1-3 and Heat shock protein 27 (Hsp27) [147].

P38 γ and δ MAPK isoforms can also phosphorylate similar substrates of p38 MAPK α and β including some of the transcription factors (SAP1, Elk-1, or ATF2), however, they cannot phosphorylate protein kinases MAPKAP-K2 or MAPKAP-K3 [154].
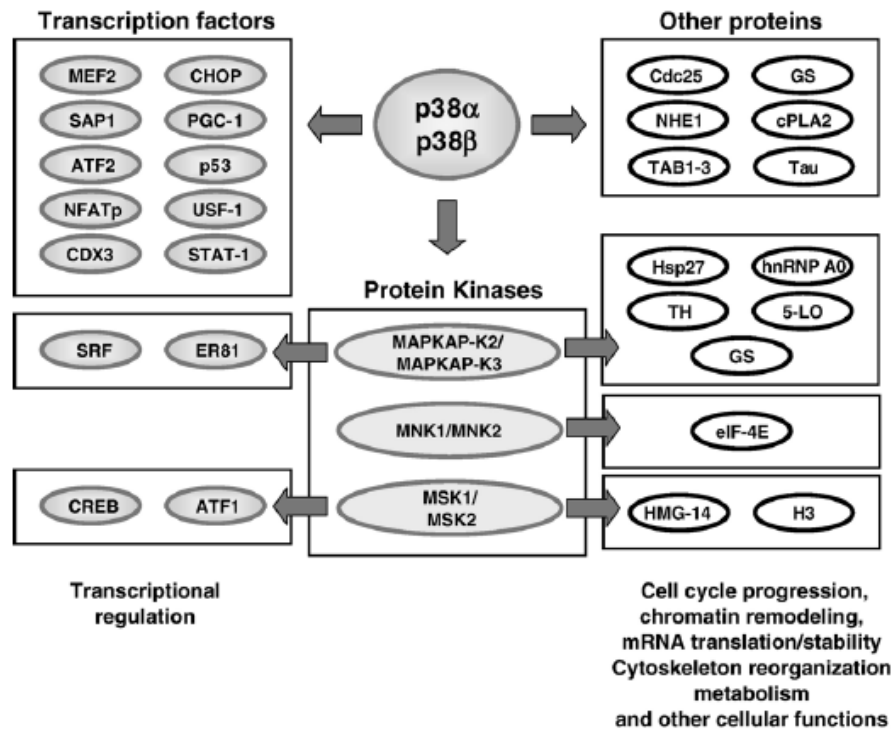
Figure 8. Some of the P38 α/β MAPK downstream substrates and their function [147]. P38 MAPK can regulate the activity of several proteins such as protein kinases, transcription factors and other proteins involved in a variety of physiological functions.

2.5.4. Role of p38α in tumorigenesis

Several studies showed the contribution of the p38 MAPKs subfamily in physiology alteration and transformation of cells. P38 MAPK activity has been shown to affect several processes including angiogenesis, apoptosis, differentiation, cell cycle, tissue invasion and metastasis. Dual functions of p38 MAPKs have been reported in several types of cancer [155]. Classically, p38α has been considered as a tumor suppressor that can suppress tumor initiation and induce differentiation. For example, it has been reported that loss of MKK3 and MKK6 and hence p38 MAPK activity *in vivo* results in increased proliferation and tumorigenesis after treatment with TNF [156]. However, other studies reported that p38α during tumor progression can act as a tumor promoter where inhibition of p38α decreases tumor survival and dissemination [155].

2.5.4.1. Role of p38α in tumor initiation

In breast cancer, one study showed that p38 MAPK activity can inhibit tumor initiation. Wip1 knockout mice showed reduced mammary tumorigeneses through the activation of p38 MAPK and p16 and p19 pathways [157]. However, many other studies supported the role of p38α in tumor progression in breast cancer. For example, an *in vivo* study showed that the use of the p38 MAPK inhibitor PH797804 in mice after treatment with polyoma middle T (PyMT) impaired breast tumor growth [158]. In addition, high levels of active p38 MAPK in breast cancer patients were correlated with poor prognosis, tamoxifen resistance and lymph node metastasis [159].

In colon cancer, p38α normally regulates colon epithelial integrity and intestinal homeostasis. Knocking out of p38α in intestinal epithelial cells of mice showed increased colitis correlated with colon tumorigenesis initiation by altering assembly of tight junction although at the same time p38 MAPK activity was found to be required for cancer cell survival [160]. In another study, p38 MAPK activity inhibition by SB202190 in a xenograft model showed a reduction in tumor growth [161].

In vivo xenograft models for non-small cell lung cancer, glioma, melanoma, breast, ovarian and myeloma showed a significant delay in tumor growth as a result of p38 MAPK activity inhibition by LY2228820 inhibitor [162].

Available data concerning the role of p38 MAPK suggest that it could act as a tumor suppressor in the early stages of oncogene induced-cancer initiation by inducing cell apoptosis, however, as the tumor progresses, changes in gene expression and signaling pathways - inducing cell transformation that might be driven by other stimuli in the surrounding microenvironment - may alter p38α function to favor tumor progression [155].

2.5.4.2. Role of p38 MAPK in cell cycle regulation

Several studies have reported the involvement of the p38 MAPK pathway in the regulation of cell cycle checkpoint transitions between G1/S and G2/M phases in response to a variety of stimuli including UV/DNA damage, reactive oxygen species (ROS) and treatment with chemotherapeutic agents. Based on cell type, p38 MAPK activity can result in progression or inhibition of cell cycle at G1/S phase through regulation of cyclin levels (Cyclin A or D1), CDC42, p21 and phosphorylation status of either retinoblastoma (pRb) or p53 tumor suppressors [163]. For example, micro-injection of Cdc42 into NIH3T3 cells caused G1 arrest in a p38α dependent mechanism [164]. A requirement for p38 MAPK activity was reported in case of M phase arrest in somatic cells as a result of spindle fibers disruption after nocodazole treatment, and in case of G2 phase arrest as a result of exposure to UV light/DNA damage and CDC25B phosphorylation [147].

2.5.4.3. Role of p38 MAPK in cell invasion and migration

A study on endothelial cells showed the role of p38α MAPK activity in mediating actin re-organization and endothelial cell migration after treatment with vascular endothelial growth factor (VEGF). p38 MAPK inhibition by SB203580 resulted in reduced endothelial cell migration [165]. Many other studies reported the involvement of p38α in transducing chemotactic signals. A study in human breast epithelial cells showed that H-Ras activation induced cell motility and invasion through activation of p38 and ERKs while N-Ras activation and its downstream activation of ERKs was not sufficient [166]. Studies on cells derived from mice deficient in different isoforms showed that only p38α was involved in relaying the chemotactic signal [167].

In literature, the role of p38α MAPK in cell migration has been focused more on the actin cytoskeleton rather than changes in gene expression. Initial studies showed that inhibition of p38α and therefore, subsequent downstream phosphorylation of HSP27 by MAPKAP-K2 resulted in inhibition of actin cytoskeleton re-organization that are essential for cell migration. *In vitro*, when HSP27 is not phosphorylated it acts as a cap-binding protein that blocks actin polymerization whereas its phosphorylation increases actin dynamics [165,168,169].

Other investigations showed that the p38α pathway can regulate cell invasion, motility, and angiogenesis through the regulation of MMPs. In human squamous cell carcinoma, inhibition of p38α MAPK activity by SB203580 resulted in reduced MMP-9 expression and secretion after treatment with phorbol myristate acetate (PMA) and hence reduced cell invasion [170].

The ability of p38α in transducing chemotactic signals is essential for certain physiological functions such as angiogenesis and neutrophil cell migration, however, this increase in p38α activity is transient. Therefore, in the case of diseases such as cancer, where high and persistent p38α and downstream substrate activity increases cell motility, tumor growth (via angiogenesis), migration, invasion and metastasis, p38α can be considered as a possible therapeutic target.

2.5.5. Other active signaling pathways in melanoma

2.5.5.1. JNK signaling pathways

JNK is one of the major MAPK pathway subgroups. It can be activated by environmental stress and cytokines similar to that of the p38 MAPK pathway. Upon stimulation, MKK4 and MKK7 are activated that subsequently induce activation of JNK by phosphorylation at THr183 and Tyr185. Active JNK in turn phosphorylate c-Jun enabling it to cooperate with c-Fos and ATF2. These factors allow the activation of a wide spread of factors

involved in cell proliferation, cell cycle, apoptosis and differentiation [171]. In melanoma, the MAPK pathway is constitutively active, and a study showed that the activation of this pathway results in the activation of the JNK pathway and the c-Jun oncogene that subsequently lead to activation of Rack1 and cyclin D1. They also reported that an ERK-independent mechanism is important for JNK activity and the high protein kinase C (PKC) activity in melanoma is the possible activator of JNK. PKC was found essential for melanoma growth and metastasis [19].

2.5.5.2. NF-κB signaling pathway

NF-κB is a transcription factor that has a v-Rel homology domain at its N-terminus that is structurally similar to that of the retroviral oncoprotein v-Rel. NF-κB is composed of an inducible heterodimer: RelA (p65) and NF-κB1 (p50) subunits and are usually retained in the cytoplasm by the inhibitor IkB proteins [172]. Several stimuli such as stress, UV irradiation, cytokines, free radicles, bacterial or viral antigens cause phosphorylation of IκB and subsequent degradation by the ubiquitin-proteasome pathway. This results in the activation of NF-κB and translocation to the nucleus. This is mainly through the phosphorylation of IκB. Studies showed that NF-κB plays role in a variety of physiological processes including apoptosis, proliferation, regulation of pro-angiogenic factors such as IL-8 and MMP-9. Therefore, high expression of NF-κB was demonstrated in several types of cancers. In melanoma, an *in vivo* study showed that high activity of NF-κB contributed to melanoma development and tumorigenesis through enhancing angiogenesis and metastasis [20].

2.6. Role of the actin cytoskeleton in cell migration and metastasis.

Cell motility and the ability to migrate is an important cellular process for many physiological activities such as angiogenesis, embryo development, defense against a pathogen and immune response. Migration is also vital in many pathological conditions, such as wound healing, tissue repair, immunodeficiency, and cancer metastasis [37].

Several types of cues act as an attractant for directional cell movement and migration including, chemical or ligand cues (chemotaxis), substrate-bound chemoattractant cues (haptotaxis) and mechanical cues (mechanotaxis). Both single and leader cells of collectively moving cells respond to these cues in a similar way, however, follower cells that are behind the leader cells respond to cues from their neighboring cells [126].

Cells forward movement and ability to turn results in cell shape changes that require spatiotemporal coordination between structural components that generate forces such as F-actin, focal adhesion, myosin, and regulatory components as Rac1, RhoA and CDC42. This

type of coordination allows cells to modulate migratory processes such as adhesion, polarization, protrusion and retraction [173].

2.6.1. Cell migration mechanisms

As cells migrate in response to chemo-attractant gradient, they transduce signals through their cell surface receptors and provoke many intracellular responses to allow cells to migrate such as vesicular transport, polarization and cytoskeleton reorganization [173].

Cell migration consists of four progressive processes (Figure 9). 1) Protrusion: upon extracellular stimulation, cells start to polarize and form protrusions such as filopodia and lamellipodia and this is accomplished by *de novo* polymerization of actin at the leading edge. 2) Adhesion: for cells to contact the substrate, protruded membrane form and stabilize a new adhesion complex (integrin-dependent) that eventually mature into focal adhesions. 3) Translocation: by the contractile forces of actin and myosin, the cell body with its nucleus are translocated. 4) Retraction: the adhesive complex at the back edge are disassembled and the trailing edge starts to retract. All these steps require actin re-organization under the control of Rho protein family GTPases and inhibition of any of these proteins showed to reduce cell invasion and migration [174]. Therefore, controlling cell migration through actin cytoskeleton remodeling may allow controlling cancer cell invasion and metastasis.
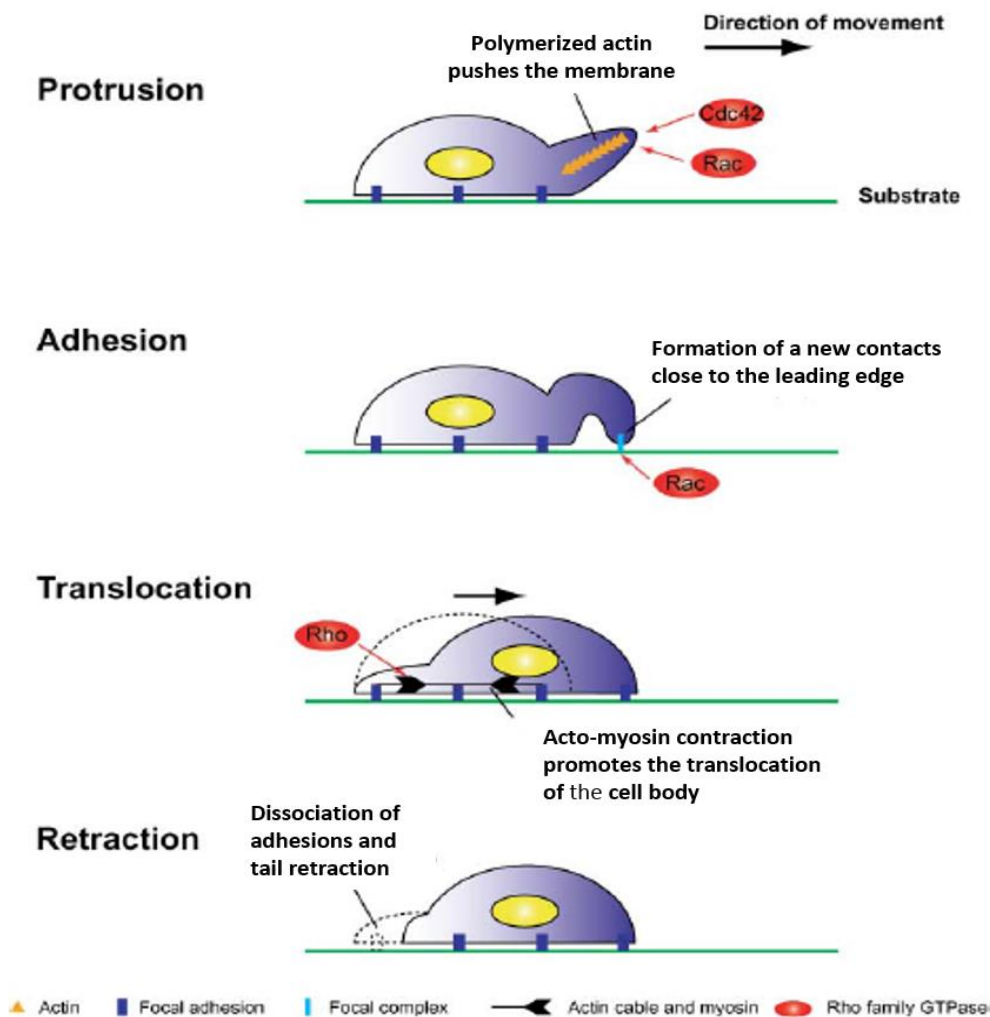
Figure 9. Four steps for cell migration on a substrate [174]. The migration steps include membrane protrusion toward the chemoattractant, adherent to the substrate, translocation of the whole cell, and finally retracting the trailing edge. This process is regulated by the Rho family and GTPases and requires actin cytoskeleton remodeling.

2.6.2. Modes of cell migration in cancer

There are three modes for cell migration in cancer; 1) collective migration, 2) mesenchymal migration and 3) amoeboid migration. In collective migration mode, cells are usually moving together in sheet-like structures to maintain cell-cell junctions already present between cells. Both endothelial cell migration during angiogenesis and epithelial cell migration during wound healing are examples of collective migration [175,176]. As epithelial cells start to de-differentiate the cell-cell junction proteins are lost and cadherin function is suppressed, therefore, cells start to move separately (individual migration) rather than collectively using mesenchymal migration mode. This type of transition is called epithelial-mesenchymal

transition (EMT) that primarily indicate tumor progression. During this process protrusions formed at the front adhere to the substrate in an integrin-dependent manner and ECM enzymes are secreted to form a path [177]. These types of cells usually have more elongated morphology and these fibroblast-like cells show similar migration mechanisms [178]. However, when cell-cell junction and cell-substrate adhesion both are inhibited at the same time the type of migration changes from collective to amoeboid type. In the case of mesenchymal to amoeboid transition (MAT), inhibition of both cell-substrate adhesions (become integrin-independent and making cells more rounded) and the ECM degradation are reported and the cells start to move relying on actomyosin contractility forces to squeeze the cell body within the ECM gaps [179]. The cancer cells have the ability to alternate between mesenchymal and amoeboid modes of migration, therefore, both should be repressed to reduce cancer cell invasion and migration [174].

2.6.3. Regulation of actin turnover

The actin cytoskeleton is composed mostly of actin filaments. Actin filaments are cytoplasmic actin monomers forming a polar linear polymer with two ends; the barbed end (plus end) and the pointed end (minus end). The structural polarity produced by actin polymerization determines the pushing force directionality. At the barbed end, actin monomers are added in the form of ATP-actin-profilin complexes for actin elongation and as a result ATP is hydrolyzed to ADP and profilin dissociates back to the cytosol. This makes actin-ADP more susceptible to dissociation. The main site for actin depolymerization is at the pointed end where ADP-actin monomers bind the severing protein actin-depolymerizing factor (ADF/cofilin) with high affinity. The released actin subunits in the cytosol bind again to profilin and competing with cofilin allow nucleotide exchange of ADP to ATP (Figure 10) [180]. The process of actin turnover includes three steps: nucleation, elongation, and disassembly. Many regulatory and actin-binding proteins are involved in these processes in addition to their role in the formation of actin networks or bundles (Table 5) [181].
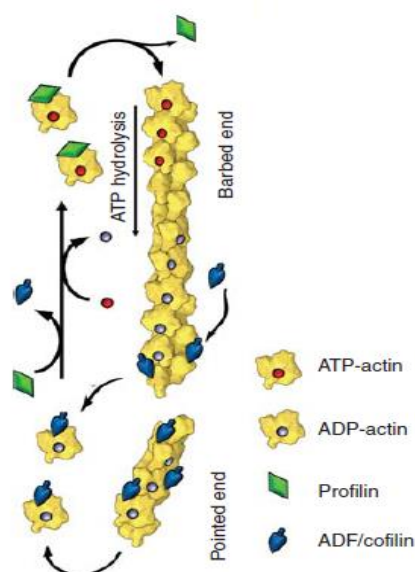
Figure 10. Actin turnover dynamics [180]. For actin polymerization, more and faster ATP-actin subunits are added to the barbed end with the help of profilin compared to the pointed end. For actin depolymerization, more ADP-actin subunits are released with the help of ADF/cofilin at the pointed end for recycling.

Table 5. Actin regulatory protein and their function [181]

Protein name	Function(s)
Arp2/3 complex	Actin nucleation and branching
N-WASP	Strong nucleation promoting factor that binds to Arp2/3 complex to nucleate branched actin filaments
WAVE-2	Regulators of *de novo* actin polymeriztion
Alpha-actinin-4	Actin filament cross-linking protein, bind actin to the cortical cytoskeleton and its associated proteins
Gelsolin	Actin capping and severing protein
Tropomodulin 3	Actin capping protein, negative regulator of cell migration
Cofilin	Actin severing protein, membrane protrusion, and cell motility
Cortactin	Binds F-actin to prompt nucleation of new filaments

2.6.4. Ca^{2+} and actin cytoskeleton remodeling

As Ca^{2+} signaling can be tightly controlled by the cell in a spatiotemporal manner through their molecular toolkits, it should be a good candidate to regulate cell polarity, motility, chemotaxis and migration [182–184]. In turn, all these processes require changes in actin dynamics. Interestingly, several studies showed the involvement of Ca^{2+} signaling in actin re-arrangements, invadopodia and lamellipodia formation and focal adhesion turnover [37,185].

During cell migration, small Ca^{2+} oscillatory pulses were reported at the cell leading edge in the front as a result of polarized receptor tyrosine kinase signaling and its interaction

with pulsatile stretch, and TRP channel activity for releasing Ca^{2+} from the ER. A study in bone marrow-derived mast cells (BMMCs) showed the involvement of Ca^{2+} channel TRPM4 in migration through regulation of Ca^{2+}-dependent actin cytoskeleton re-organization [186]. Another study in breast cancer cells showed the involvement of TRPV4 in increased migration as a result of its effect on actin dynamics through Ca^{2+}-dependent activation of AKT [187].

In addition, it was shown that an increasing front-to-rear Ca^{2+} gradient is necessary for cells to move. A very low level of Ca^{2+} is usually kept at the cell front so that any small change in Ca^{2+} concentration can be sensed by migratory responsive proteins including actin, actin-binding proteins, myosin and focal adhesions. PMCA but not SERCA was reported to be essential for a similar Ca^{2+} gradient across the cells [126].

PMCA interaction with F-actin was first demonstrated in activated platelets [188]. After that, it was reported that purified PMCA protein-bound both G-actin and F- actin and these interactions affected PMCA activity, which in turn altered the cytoskeleton polymerization status. It was suggested that active PMCA lower cytosolic Ca^{2+} concentration and this promotes actin polymerization. While as F-actin binds to PMCA this results in its inactivation and an increase in Ca^{2+} level and hence actin depolymerization [189].

Although, there is no reported direct interaction between Ca^{2+} and actin many actin regulators are affected by Ca^{2+}. For example, Ca^{2+} was found to regulate several Ca^{2+}-dependent proteins involved in actin cytoskeleton re-modelling, focal adhesion turnover, filopodia and lamellipodia formation such as protein kinase C, calmodulin-dependent kinases, Rho GTPases, myosin and cofilin.

2.6.5. Ca^{2+} and Cofilin

Changes in free cytoplasmic Ca^{2+} concentration can affect actin dynamics via its effect on many actin-binding proteins including the actin severing protein cofilin. It is a 19 KDa protein available in three isoforms, cofilin 1 (ubiquitously expressed), cofilin 2 (in muscles), and ADF. Cofilin activity regulates actin dynamics during cell motility by its ability to depolymerize actin by removing ADP-actin subunits from the actin filaments. However, cofilin was also suggested as a polymerization factor via its ability to produce actin monomers for recycling [190].

Cofilin activity showed to be essential for cell polarity/directionality, chemotaxis and protrusion formation. Directionality of cells toward chemotactic signals is facilitated by the ability of cofilin to produce actin filament-free barbed ends to initiate and define the location of protrusions at specific compartments such as the lamellipodia and invadopodia during their movement. Therefore, cofilin activity is tightly regulated by the cell via three mechanisms: 1)

Phosphorylation: LIM or TES kinases induce cofilin inactivation by phosphorylation at serine residue 3 while its dephosphorylation through chronophin (CIN), slingshot (SSH), or any other phosphatases results in its re-activation, 2) PIP2: PIP2 binding to cofilin at the plasma membrane blocks its activity while PIP2 hydrolysis through PLCγ1 activity restores cofilin activity, 3) Cortactin: cofilin binding to dephosphorylated cortactin at invadopodia blocks its activity while cortactin tyrosine phosphorylation by Abl or Src kinases restores cofilin activity [191]. Any misregulation of cofilin activity and localization may result in disease development such as cancer metastasis. Dysregulation of cytosolic Ca^{2+} concentration affects cofilin activity, for example, a study showed that high cytosolic free Ca^{2+} concentration can increase cofilin activity via its dephosphorylation by the calcium-dependent phosphatase calcineurin [192].

Since many studies showed the involvement of Ca^{2+} in modulating actin cytoskeleton dynamics and PMCA as a pump helps in maintaining low cytosolic Ca^{2+} levels, we investigated the role of PMCA in actin cytoskeleton remodeling and its contribution to the reduced migratory effect observed in melanoma cells overexpressing PMCA4b.

3. Objectives

Plasma membrane Ca^{2+} pump (PMCA4b) is a key regulator of intracellular Ca^{2+} homeostasis. Previously, our laboratory identified PMCA4b as a putative metastatic suppressor in BRAF mutant melanoma cells. Loss of tumor suppressors have been identified in many types of cancers due to the increased degradation of these proteins. In melanoma, we reported downregulation of PMCA4b at both the mRNA and protein levels. Identifying the regulators involved in PMCA4b degradation and targeting the corresponding pathways could provide new strategies for cancer metastasis treatment and/or for overcoming cancer resistance.

As cells start to metastasize, they move from the primary tumor site, invade and form tumors at other sites in the body. For such activities actin remodeling was reported to be essential as many proteins and factors regulate cell metastasis through their effect on actin dynamics directly or indirectly. One of these factors is intracellular free Ca^{2+} concentration.

Therefore, the following objectives were addressed:

1. To identify the pathways involved in the regulation of PMCA4b expression and stability in BRAF mutant melanoma cells.

2. To identify pathways involved in PMCA4b degradation.

3. To identify the role of PMCA4b stability on the migratory, metastastatic, colony and spheroid forming activities of BRAF mutant melanoma cells.

4. To identify the role of PMCA4b expression and trafficking on the morphology and migratory behavior of BRAF mutant melanoma cells.

5. To identify the role of PMCA4b activity and trafficking on the distribution of cytosolic Ca^{2+} levels and controlling near-actin Ca^{2+} concentration essential for actin remodeling and integrity.

4. Materials and Methods

4.1. Cell culture

In our study, we used the following cell lines: BRAF/NRAS wild-type melanoma cells (MEWO), two BRAF (V600E) mutant melanoma cells (A375 and SK-MEL-28), HeLa cervix adenocarcinoma cells (HeLa), breast cancer cells (MCF-7). All cell lines were purchased from ATCC except the HeLa cell line was from ECACC. For cell culture, we used Dulbecco's modified Eagle's medium (DMEM) (Lonza, USA) supplemented with 10% FBS (Thermo Fisher Scientific, USA), 2 mM L-glutamine (Lonza) and 1% penicillin-streptomycin (Lonza). Cells were incubated in a humidified 5% CO_2 incubator at 37°C.

4.2. DNA constructs for transient transfections

For transient transfection of the cells, the following DNA plasmids were used: pEGFP-actin and pmCherry-C1 were purchased from Clontech Laboratories Inc., USA. The mCherry-PMCA4b plasmid, the pEGFP-PMCA4b-L$^{1167-1169}$A trafficking mutant [104], the mCherry- or GFP-PMCA4b-DE non-functional mutants (D672E), the SB-CAG-GFP-PMCA4b-CAG-Puro and SB-CAG-GFP-PMCA4b-LA-Puro constructs were generated previously [81,82]. pCAGGS-GCaMP2-actin, Cofilin-pmCherryC1 and CMV-R-GECO1 plasmids were gifts from Karel Svoboda (Addgene plasmid # 18928; http://n2t.net/addgene:18928; RRID:Addgene_18928) [193], Christien Merrifield (Addgene plasmid # 27687; http://n2t.net/addgene:27687; RRID: Addgene_27687) [194] and from Robert Campbell (Addgene plasmid # 32444; http://n2t.net/addgene:32444; RRID: Addgene_32444), respectively [195].

Cells were cultured in 8-well Lab-Tek II chambered coverglass (Nunc, USA) overnight. Then, cells were transiently transfected with one plasmid or combination as indicated in the experiment using FuGENE HD transfection reagent (Promega, USA) according to the manufacturer's instructions. After 24 hours, medium was changed and the appropriate drugs at a certain concentration and at a specific time were used as indicated.

4.3. Stable cell lines generation

Cell lines prepared by our laboratory: SB-CAG-GFP-PMCA4b-CAG-Puromycin construct was used to prepare A375-GFP-PMCA4b, HeLa-GFP-PMCA4b and MCF-7-GFP-PMCA4b stable cell lines while SB-CAG-GFP-PMCA4b-LA-CAG-Puromycin construct was used to prepare the A375-GFP-PMCA4b-LA stable cell line. The protocol for their stable transfection is as described previously [82]. For PMCA4b Knockdown and generation of MCF-7-Sh-4b cell line, MCF-7 cells were transfected with the PMCA4b shRNA plasmid (sc-42602-

SH, Santa Cruz Biotechnology, USA) using the FuGENE HD transfection reagent (Promega). After 48 hours, fresh medium was changed and Puromycin dihydrochloride (1µg/ml) (sc-108071, Santa Cruz Biotechnology) was added for the selection. The medium with Puromycin was changed every 2-3 days for two weeks. Western blot was used to determine PMCA4b protein level after silencing.

SB-GCAMP6 construct kindly provided by Prof. Orban laboratory (MTA-TTK, Budapest, Hungary) was used to generate A375-GCAMP6 stable cell line for Ca^{2+} measurement study as described previously [196].

The HEK-mCherry-MKK6EE-Dox cell line used as a model for p38 activation was kindly provided by the Reményi laboratory (MTA-TTK, Budapest, Hungary). For preparation, pEBDTet vector with a constitutively active mCherry-MKK6 fusion construct with phospho-mimicking activation loop residues (MKK6EE) was transfected in HEK293T cells [197]. For selection, puromycin was added and refreshed every two days for more than a week. For constitutive activation of the FLAG-tagged MKK6EE doxycycline, doxycycline (Dox) (2 µg/mL) in DMEM containing 10% FBS treatment was used and activation was confirmed by Western blots. Western blot was used to confirm selective activation of p38 and not that of ERK1/2, ERK5, or JNK using MAPK phosphorylation specific antibodies.

4.4. Chemical Reagents

BRAF V600E inhibitor vemurafenib (PLX4032), NF-κB inhibitor (BAY11-7082), JNK inhibitor (SP600125) and p38 MAPK inhibitors (SB203580 or SB202190) were purchased from Selleck Chemicals (Munich, Germany). For storage, inhibitors were dissolved in DMSO and stored at -80 ℃. The proteasome inhibitor (MG132), anisomycin, calcium ionophore (A23187), Cytochalasin D (cytD) and Phalloidin-TRITC for F-actin staining all were dissolved in DMSO. Chloroquine (CQ) and doxycycline hydrochloride (Dox) were dissolved in pure water. All these reagents were purchased from Sigma-Aldrich (St. Louis, USA) and stored at - 20 ℃. The DMSO final concentration in all experiments performed is < 0.01%

4.5. Cell treatments

For cell treatments, cells were first cultured overnight in 8-well Nunc Lab-Tek II chambered coverglass (Nunc, USA) or 6-well plate for immunostaining or protein extraction-western blot experiments, respectively. Then the fresh medium was added together with the drug as appropriate and incubation continued as indicated in each experiment. Briefly, cells were treated with 0.5 µM vemurafenib, 10 µM of p38, JNK, or NF-κB inhibitor, or 10 µM

CQ/48 hours or 50 µM CQ treatment and/or starvation were applied in the last 3 hours of the 48 hours incubation period.

For the HeLa-GFP-PMCA4b cells experiment, cells were treated with 10 µM p38 inhibitor for 48 hours and in the last one hour, 2.6 µg/ml of anisomycin was added.

For the HEK-mCherry-MKK6EE-Dox cells experiment, cells were transfected with SB-CAG-GFP-PMCA4b-CAG-Puro, as described in the previous section. After 24 hours, the medium was replaced with a fresh medium containing 10 µM p38 inhibitor for an additional 25 hours. Then, for activation, a 2 µg/ml doxycycline was added alone or in combination with the p38 inhibitor for 24 hours.

4.6. Quantitative real-time polymerase chain reaction

To measure PMCA4b mRNA level in A375, MEWO and SK-MEL-28 cells after treatment for 48 hours with increasing p38 inhibitor (SB202190) concentrations 1, 3, 6, 10, 30 µM. Total RNA was first extracted from cells then cDNA was synthesized and quantified using Trizol reagent (Life Technologies), RevertAid Reverse Transcriptase kit (Thermo Scientific), and PCR-TaqMan assays (Thermo Scientific): TaqMan assays Hs00608066_m1 (PMCA4b), Hs99999905_m1 (GAPDH), respectively, as described previously [82]. This was done in Prof. Michael Grusch laboratory at the Medical University of Vienna, Vienna, Austria.

4.7. Western blot analysis

To measure protein level, cells were cultured in 6-well plates for 48 or 72 hours as indicated in the experiment. After that, cells were washed with PBS and then incubated with 6% TCA at 4 ℃ for at least one hour. Total extract was centrifuged and precipitated proteins were dissolved in a modified Laemmli sample buffer (62.5 mM Tris-HCl, pH 6.8, 10% glycerol, 2% SDS, 5 mM EDTA, 125 mg/ml urea, 100 mM DTT and 0.28 mg/ml bromophenol blue). For protein concentration determination, the modified Lowry method was used. Samples were run in 10% or 15% acrylamide gel for protein separation and then electroblotted onto PVDF membranes (Bio-Rad, USA) as described previously [82]. The membrane was blocked with 5% milk and incubated with the appropriate primary antibody listed in Table 6. For detection, a horseradish peroxidase (HRP) - conjugated anti-rabbit, anti-mouse, or anti-chicken secondary antibodies were applied on the membrane (Jackson ImmunoResearch, dilution 1: 10,000) and then visualized with Pierce ECL Western Blotting Substrate (Thermo Scientific). For densitometry analysis, ImageJ software (National Institutes of Health, USA), v1.42q was used.

4.8. Immunofluorescence microscopy

For PMCA4b/Ja3, EEA1, Rab7, Rab11, LAMP1, LC3A/B and vinculin immunostaining, cells were washed with PBS-2x then fixed with 4% paraformaldehyde (PFA) for 10 minutes at room temperature (R.T). Cells were washed with PBS-5x and then were permeabilized with ice-cold methanol for 1 min (except vinculin) and washed again with PBS-4x. For blocking, cells were incubated in a blocking buffer (PBS containing 2 mg/ml bovine serum albumin, 0.1% Triton-X 100, 1% fish gelatin, 5% goat serum) for 1 hour at R.T. For immunostaining, the primary antibody against the protein of interest (Table 6) was applied for 1 hour at R.T and after that cells were washed with PBS-3x. As a secondary antibody, AlexaFlour-594 conjugated anti-rabbit IgG (Invitrogen, USA), AlexaFlour-488 conjugated anti-mouse IgG (Invitrogen), or AlexaFlour-647 conjugated anti-rabbit IgG (Invitrogen) were used as appropriate and were incubated for 1 hour at R.T. Cells were washed 3x and kept in PBS at 4ºC. In the case of vinculin immunostaining, cells were stained after that with Phalloidin-TRITC for 30 min at R.T then washed with PBS. For nuclei staining, DAPI (1μM) was applied for 10 min and then washed with PBS.

For HeLa-GFP-PMCA4b, HEK-mCherry-MKK6EE-Dox/transiently transfected with SB-CAG-GFP-PMCA4b-CAG-Puro cells, A375 cells or A375-GFP-PMCA4b cells/ transiently transfected with Cofilin-pmCherryC1 or co-transfected with PMCA4b-DE in A375 cells, the cells were first washed with PBS and then fixed with 4% PFA for 10 min at R.T, washed again and kept in PBS.

For F-actin staining, cells were fixed and permeabilized similarly and then incubated with Phalloidin-TRIC for 20 minutes. Cells were washed and kept in PBS.

To investigate the effect of Ca^{2+} influx on actin cytoskeleton integrity. A375-GFP-PMCA4b cells and A375 cells with or without GFP-PMCA4b-DE expressed plasmid were cultured in 8-well Lab-Tek II chambered coverglass (Nunc) for 48 hours. To initiate Ca^{2+} influx, 2 μM A23187 in HBSS buffer containing 2 mM Ca^{2+} (20 mM HEPES, pH 7.4, 0.9 mM $MgCl_2$ and 2 mM $CaCl_2$) was added and incubated for 10 min at 37°C. As for positive and negative controls, treatments with 2.5 μM cytD or 2 μM A23187 in HBSS buffer without Ca^{2+} (in the presence of 100 μM EGTA) were used, respectively. Phalloidin-TRITC staining was used as described previously. Area and circularity parameters were determined using ImageJ software, v1.42q.

In all experiments, images were taken by confocal laser microscopes Zeiss LSM710, or LSM800 using a Plan-Apochromat 40x or 63x oil immersion objectives as indicated (Zeiss,

Germany). Excitation wavelengths 405, 488, 543 and 633 nm were used for the acquisition of blue, green, red and far-red fluorescent images, respectively.

4.9. siRNA transfection

A375 or A375-GFP-PMCA4b melanoma cells were cultured in a 6-well plate or 8-well Lab-Tek II chambered coverglass (Nunc) for western blot or immunostaining experiments. Next day, cells were transfected with ON-Target plus SMARTpool PMCA4b (ATP2B4) siRNA (50 nM, Dharmacon research, Inc, cat. # L-006118-00-005), SignalSilence® p38 MAPK siRNA I (100 nM, Cell Signaling Technology, cat. #65645), for knocking down PMCA4b and p38 MAPK, respectively. As a negative control, SignalSilence® control siRNA (50 nM, Cell Signaling Technology, cat. #65685) was used. The transfections were performed with DharmaFECT 1 transfection reagent (Dharmacon research, Inc, UK) according to the manufacturer's recommendations. Next day, the medium was changed and 10 µM p38 inhibitor was added as indicated in the experiment for an additional 48 hours. A 30 µg protein from total cell lysate was analyzed by Western blot using an anti-PMCA4 (JA9) antibody. As a loading control, the anti-β-tubulin antibody was used. ImageJ software v1.42q was utilized for densitometry analysis of the Western blots.

4.10. Transmission Electron microscopy (TEM)

After 48 hours of cell culture, cells were treated with 50 µM CQ for the last 3 hours, harvested and washed with DMEM free serum. After centrifugation, cells were fixed with 0.2 M Na-Cacodylate, 8% glutaraldehyde, 16% formaldehyde, 29.2 mM sucrose and 1 M CaCl$_2$ for 1 hour. Cells were washed with 0.1 M cacodylate buffer and then 1% uranyl-acetate was added for contrast. Samples were embedded into LR Gold resin and then subjected to ultrathin sectioning. Sections were treated with 5% H$_2$O$_2$ for 5 minutes, washed, treated with 0.3% Na-borohydride, 50 mM NH4Cl, 50 mM glycine and 0.05 M TBS, washed and then blocked in 3% milk for 30 min. For immunostaining, samples were incubated overnight with anti-GFP antibody (chicken, 1:100) (Invitrogen, A10262) and then secondary antibody 12 nm anti-Chicken gold (1:40) (Jackson, 703-205-155) was applied for 4 hours. For contrast staining, Pb-citrate was used. TEM images were taken by JEM-1011 transmission electron microscope (Jeol) equipped with a Morada digital camera (Olympus) using iTEM software (Olympus).

4.11. Proliferation assay

Sulforhodamine B (SRB) assay was used to assess cell proliferation. A375 and A375-GFP-PMCA4b melanoma cells were seeded in triplicate in 96-well plates at 5 x 10^3 cells/well. Next day, p38 inhibitor or vemurafenib treatments were added at the indicated concentrations and incubated for 48 hours. For cell fixation, 10% (w/v) trichloroacetic acid was applied for 1

hour at 4°C then washed with water and left to dry. For staining, 0.4% (w/v) SRB was applied for 15 minutes at R.T. After that, cells were washed with 1% (v/v) acetic acid solution and the bound SRB dye was solubilized in 10 mM Tris base solution for 10 min at R.T with agitation. A microplate reader (EL800, BioTec Instruments, Winooski, VT) was used for O.D measurement at 570 nm.

4.12. Cell cycle analysis

The ratio of cells in each cell cycle phase after treatments was determined based on its DNA content as described previously [82]. Briefly, A375, A375-GFP-PMCA4b and MEWO cells were cultured in a 6-well plate. Next day, cells were treated with 10 μM p38 inhibitor (SB202190) or 0.5 μM vemurafenib for 48 hours. After that, cells were trypsinized, lysed with lysis buffer mixed with 10 μg/ml DAPI and incubated for 5 min at 37°C. To stop the reaction a stabilization buffer was added and 10 μl of each sample was loaded on 8-well NC slide. For fluorescent quantification, the NucleoCounter NC-3000™ system (Chemometec) was used.

4.13. Colony-forming assay

A375 and A375-GFP-PMCA4b cells were seeded in 6-well plates at 1×10^3 cells/well in triplicates. Next day, treatments with 0.5 μM vemurafenib or 10 μM p38 inhibitor (SB202190) were added on A375 cells and incubated for an additional 7 days. Every fourth day treatments were refreshed. For colony fixation, (3:1) methanol:acetic acid was applied for 30 minutes then washed with PBS. For colony staining, 0.5% crystal violet was applied for 30 minutes then solubilized by 2% SDS with agitation. For O.D measurement at λ570 nm, a microplate reader (EL800, BioTec Instruments, Winooski, VT) was used.

4.14. Spheroid-forming assay

To prepare spheroids from A375 and A375-GFP-PMCA4b melanoma cells, a rounded bottom 96-well plate coated with 5 mg/ml poly-HEMA (2-Hydroxyethyl methacrylate, Sigma-Aldrich) was used. A total of 150 cells/well were seeded in triplicates and incubated at 37°C in a 5% CO_2 incubator. On the third day, treatments with 0.5 μM vemurafenib or 10 μM P38 inhibitor (SB202190) were added and incubated for an additional 6 days. The formed spheroids were photographed on days 0, 3 and 6 using a phase contrast microscope. For analysis, ImageJ software v1.42q was used to measure spheroid area and radius. From these data, volume was calculated as described previously [198].

For spheroid fixation, treated or control A375-GFP-PMCA4b spheroids was transferred to an 8-well Lab-Tek II chambered coverglass (Nunc, USA) and then fixed with 4% PFA for 15 min at R.T. After that spheroids were washed with PBS-3x and then covered with

VECTASHIED anti-fade mounting media (BioMarker). Images with Z-stack were taken using Zeiss, ApoTome microscope, 10x objective.

4.15. Reversal of multicellular spheroid (MCS) formation

First, Spheroids were formed from A375 and A375-GFP-4b cells similar to the previous section. After four days, spheroids were transferred to a regular 24-well plate for them to re-attach and induce MCS reversal as described previously [199]. Next day, treatments with 10 µM p38 inhibitor (SB202190) or 0.5 µM vemurafenib were added as indicated for an additional 48 hours. During the incubation time, cells migrate from the spheroid into the plate surface. For cell fixation, (3:1) methanol:acetic acid solution was applied for 30 minutes and then washed with PBS-2x. For staining, cells were incubated with 0.5% crystal violet for 30 minutes. To determine the extent of the migrated MCS, images were taken for the whole plate and the surface area for MCS was calculated by ImageJ software v1.42q. As for confocal microscope imaging, cells were fixed with 4% PFA then treated with 0.1% Triton X-100 (Sigma-Aldrich) for permeabilization. For staining, Phalloidin-TRITC (Sigma-Aldrich) (0.1 µg/ml) and DAPI (1 µM) were used to stain F-actin and nucleus, respectively. Images were taken by confocal laser microscopes (Zeiss, LSM800, 40x objective).

4.16. Cell morphology analysis

Morphological parameters (circularity and surface area) of individual cells or cultured cells were determined by ImageJ software, v1.42q after applying a black mask for displaying cell contour on images taken by phase-contrast microscope using 4x and 10x objectives, respectively.

4.17. Nearest neighbor distance analysis

After 48 hours cell culture in 6-well plates, phase contrast images were taken for A375-GFP, A375-GFP-PMCA4b, A375-GFP-PMCA4b-LA, MCF-7, MCF-7-GFP-PMCA4b and MCF-7-Sh-PMCA4b cells. Binary images of cell centers determined by the "Particle analysis" function of ImageJ software, v1.42q was used to calculate the nearest neighbor distance using the graph plugin of ImageJ, v1.42q

4.18. Non-directional cell motility assay

To follow the random cell motility, A375, A375-GFP-PMCA4b and A375-GFP-PMCA4b-LA cells were seeded in 96-well plates. Next day, for nucleus staining, cells were treated with 0.1 µM Hoechst 33342 for 1 hour. Images were taken automatically every 30 min for 24 hours and the fluorescence signals for Hoechst and GFP were recorded. In all experiments, cells were kept at 37°C and 5% CO_2. The software, microscope and motility

analysis used were as described previously [94]. Single cell motility time-lapse movies were created from the several images taken during the experiment.

4.19. Directional cell migration assay

A375, A375-GFP-PMCA4b, A375-GFP-PMCA4b-LA cells were cultured in a 6-well plate. Next day, A375 and A375-GFP-PMCA4b cells were treated as described in the experiment and cultured for 48/72 hours as indicated. After that cells were harvested and directional migration was assessed using the modified Boyden chamber assay [94]. Briefly, cells were seeded into the upper 48-well Boyden chamber (Neuro probe, USA) and the attractant 100 µg/ml fibronectin (Merck KGaA, Germany) prepared in serum-free medium was added to the lower chamber. In between, an uncoated Nucleopore membrane (Whatman, Germany) with 8 µm pore diameter was used. After 3 hours of incubation at 37 ºC and 5% CO_2, the cells at the upper side of the membrane were removed by scraping while migrated cells at the lower side were fixed with methanol and then stained with Toluidine blue. Light microscopic images were taken using a 10x objective lens and the number of migrated cells/field was counted.

4.20. Ca^{2+} signal measurements

In all experiments where Ca^{2+} signal measurement is needed, cells were seeded in 8-well Lab-Tek II chambered coverglass (Nunc, USA). Next day or after treatments, to initiate Ca^{2+} influx, a 2 µM Ca^{2+} ionophore A23187 (Sigma-Aldrich) was added to the cells in HBSS buffer (20 mM HEPES, pH7.4, 0.9 mM $MgCl_2$, 2 mM $CaCl_2$ and 10% FBS) after washing cells 2x with the same buffer. For fluorescent detection, live-cell imaging or images were taken using Olympus IX-81/Zeiss LSM710 confocal laser microscope or Carl Zeiss Z1 microscope equipped with a Yokogawa CSU-X1 spinning-disk confocal module (Zeiss, Germany) every 0.3 seconds or 15 seconds using 60x or 100x oil objective, respectively. The relative fluorescence intensities were calculated as F/F0 (where F0 was the average initial fluorescence) using Fluoview FV500 software v4.1. or ImageJ software, v1.42q as indicated and data were analyzed using a GraphPad Prism software v5.01. Cells were kept at 37 ºC and 5% CO_2 during the whole experiment.

In the case of the A375-GCAMP6 cells experiment, treatments with 0.5 µM vemurafenib or 10 µM P38 inhibitor (SB202190) were applied for 48 hours before ionophore addition. During live-cell imaging, a GCAMP6 fluorescent signal was detected.

For near actin Ca^{2+} signal measurement, A375 cells were co-transfected with pCAGGS-GCAMP2-actin and one of the following plasmids: mCherry-PMCA4b or mCherry-PMCA4b-

DE and cultured for 48 hours before ionophore addition. During live-cell imaging, both GCAMP2 and mCherry signals were detected. Images were captured before, during (peak), and after the addition of A23187 by 7 min. The software ZEN 2.3 (blue edition) was used to create videos.

For determining the distribution of basal cytosolic Ca^{2+} concentration, A375, A375-GFP-PMCA4b and A375-GFP-PMCA4b-LA cells were transfected with CMV-R-GECO1 plasmid for 48 hours before ionophore addition. A line plot was drawn across the cells and R-GECO fluorescent signal was analyzed using ImageJ software, v1.42q.

4.21. Live-cell imaging

For live-cell imaging of actin in cells, we cultured A375 cells in 8-well Lab-Tek II chambered coverglass (Nunc, USA). Next day, the cells were co-transfected with GFP-actin and one of the following plasmids: pmCherry-C1, mCherry-PMCA4b, or mcherry-PMCA4b-DE for 48 hours. HBSS buffer (20 mM HEPES, pH7.4, 2 mM $CaCl_2$, 0.9 mM $MgCl_2$ and 10% FBS) was used for cell washing and as a live-cell imaging medium. To initiate Ca^{2+} influx, a 2 µM A23187 in was added. As positive and negative controls, 2 µM A23187 in HBSS buffer without Ca^{2+} (in presence of 100 µM EGTA) and 2.5 µM cytD were used, respectively. All treatments were done at 37 ºC for 10 min. Live-cell imaging for GFP and mCherry fluorescence signals were acquired after excitation at 488 and 5561 nm, respectively. Z-stack images were taken every 15 seconds using Carl Zeiss Cell observer SD microscope equipped with a Yokogawa CSU-X1 spinning-disk confocal module (Zeiss, Germany), 100x 1.4 N.A., oil immersion objective. Data were presented as 3D images at zero, 5 and 10 min time intervals. Movies were created from a single Z-stack using ZEN 2.3 (blue edition) software. Morphological parameters (circularity and surface area) and Kymographs were analyzed by ImageJ software v1.42q.

4.22. Fluorescence recovery after photobleaching (FRAP)

The type of cells and DNA plasmid combination used were as described in the previous section. Phenol-free complete DMEM medium containing 25 mM HEPES (Gibco) were used as a live cell imaging medium and cells were kept at 37ºC in all FRAP experiments. Both GFP and mCherry fluorescent signals were detected simultaneously using solid-state lasers (488 nm and 546 nm) of a Carl Zeiss Cell Observer SD microscope equipped with a Yoko-gawa CSU-X1 spinning-disk confocal module. At the end of the experiment, differential interference contrast (DIC) images were taken. Three regions of interest (ROI) were determined for GFP-actin photobleaching: cell-free edge, cell connections and ruffles (lamellipodia). A 488 nm bleaching

laser with 40x 1.4 N.A. oil immersion objective was used at 20-40% intensity (RAPP UGA-42 Firefly 2L system) for photobleaching. Images were acquired every 0.2 s over 120 s time interval. Mean fluorescence intensity of a non-bleached region, background and ROI were analyzed using ImageJ software, v1.42q. Relative GFP-actin fluorescent intensity was calculated from data imported into Microsoft excel software 2016 (Microsoft Corporation by Impressa systems, USA) as follows: background intensity was removed from each ROI and at every time point, then the calculated ROI intensities were divided by a reference area intensity measured from a surrounding un-bleached cell. For normalization, the post-bleach intensities were normalized to the first 10 pre-bleach time points mean. For FRAP data analysis, post-bleach data of the first 90 seconds was introduced into GraphPad Prism software v5.01 (GraphPad Software Inc., USA) and non-linear regression analysis was performed on the post-bleach sections to calculate both half time of FRAP recovery curve ($t_{1/2}$) and the mobile fraction. Carl Zeiss Z1 microscope equipped with a Yokogawa CSU-X1 spinning-disk confocal module (Zeiss, Germany), 40x, oil objective was used.

4.23. Statistical analysis

All data were presented as the mean ± standard deviation or error (SD, SEM) from two to three independent experiments as indicated. For comparison of two groups, an unpaired t-test was used. Chi-square test was used to test relationships between two categorical variables (stress fibers or lamellipodia count). For comparisons between control and experimental groups, we used one-way analysis of variance (ANOVA) with Dunnett's multiple comparison post-hoc test. In the case of an experiment with different doses vs days or morphological data vs time, a two-way ANOVA was used followed by Bonferroni post-hoc test. Data with $p < 0.05$ is considered significant. P-values donated with $< 0.05, < 0.005$ and < 0.001 represent asterisks *, **, and ***. All statistical analysis described were performed by GraphPad Prism software (v5.01).

5. Results

5.1. p38 MAPK modulates PMCA4b stability.

5.1.1. Inhibition of p38 MAPK increased PMCA4b abundance in BRAF mutant melanoma cells but that of the JNK and NF-κB pathways did not.

Previously, we reported that PMCA4b is downregulated in BRAF mutant cells and inhibition of the MAPK pathway upregulated its expression at both the mRNA and protein levels [82]. In order to identify additional regulators of PMCA4b in BRAF mutant melanoma cells, we investigated the p38 MAPK, JNK and NF-κB pathways, which have been reported to be active in these cells [18–20]. Using specific inhibitors of JNK (SP600125), NF-κB (BAY11-7082) and p38 (SB203580, P38i-1 and SB202190, p38i-2), we found that inhibition of the p38 MAPK pathway resulted in PMCA4b protein level enhancement in BRAF mutant (A375) but not in BRAF wild type (MEWO) melanoma cells (Figure 11). p38 inhibition reduced p-ERK level in A375 cells, however, less effectively than vemurafenib did. This effect may indicate cross-talk between BRAF and p38 MAPK pathways or could be a result of limited inhibitor specificity.
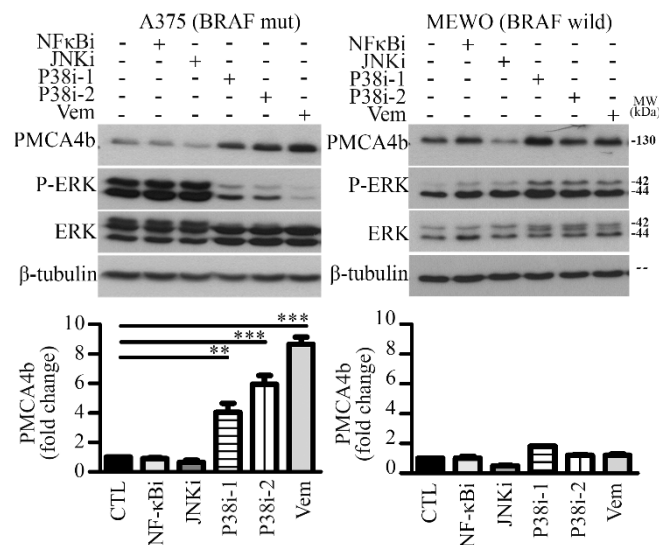
Figure 11. BRAF and p38 MAPK but not JNK or NF-κb are involved in the regulation of PMCA4b abundance in BRAF mutant melanoma cells. BRAF mutant (A375) and BRAF wild (MEWO) type cells were cultured in 6-well plates and 10 μM of each inhibitor were applied for 48 hours as indicated. Vemurafenib with 0.5 μM treatment was used as a positive control. The protein expression level of PMCA4b, P-ERK and ERK was analyzed by Western blots. Data were normalized to β-tubulin. Bars indicate means ± SE from three independent experiments.

Similarly, in BRAF mutant melanoma cells (A375 and SK-MEL-28) treatment with the p38 MAPK inhibitor (p38i-2) for 48 hours showed a significant increase in PMCA4b protein level in a dose dependent manner. In contrast, no PMCA4b upregulation was observed at the mRNA level with the exception at a high p38i-1 concentration (30 μM). No additive effect could be detected when p38i and vemurafenib were combined (Figure 12). Using the p38 inhibitor at the effective dose (10 μm) and at different time points showed that an increase in protein but not mRNA level is significant at 48 hours (Figure 13). These data suggest that the p38 MAPK pathway regulates PMCA4b steady-state level post-translationally. In the following experiments we used 10 μM p38i-2 and 48 hours incubation time as an optimal treatment option.
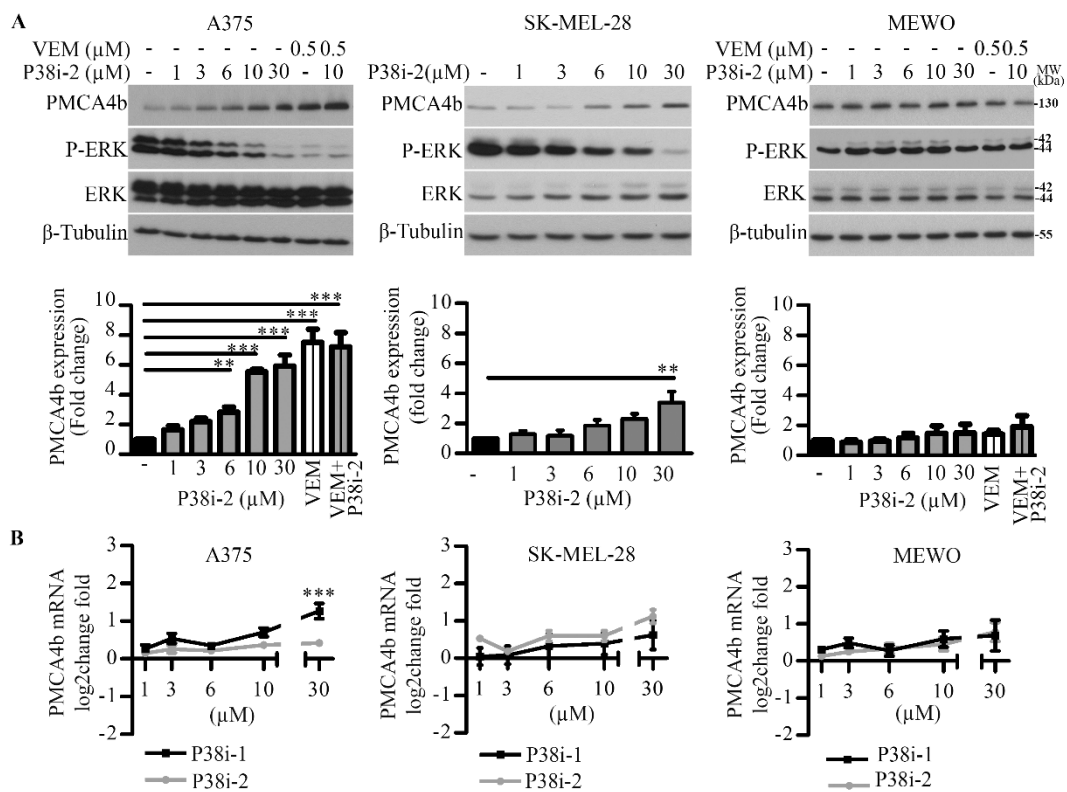
Figure 12. Inhibition of P38 MAPK increases PMCA4b abundance at the protein level without affecting its expression at the mRNA level. A dose-response curve. (A) Concentration dependent treatment of BRAF mutant (A375 and SK-MEL-28) and BRAF wild (MEWO) type cells with p38i-2 inhibitor for 48 hours. A combination of vemurafenib and p38i-2 was tested in A375 and MEWO cells. Protein expression level of PMCA4b, P-ERK and ERK was determined by western blot. Data were normalized to β-tubulin. The graph represents the densitometry analysis of Western blot using the ImageJ software. Bars indicate means ± SE from three independent experiments. **(B)** Same experiment in (A) with p38i-1 and p38i-2

treatments for 48 hours. Total RNA was extracted and qPCR was performed to analyze PMCA4b mRNA level. Data indicate means ± SE from three independent experiments.
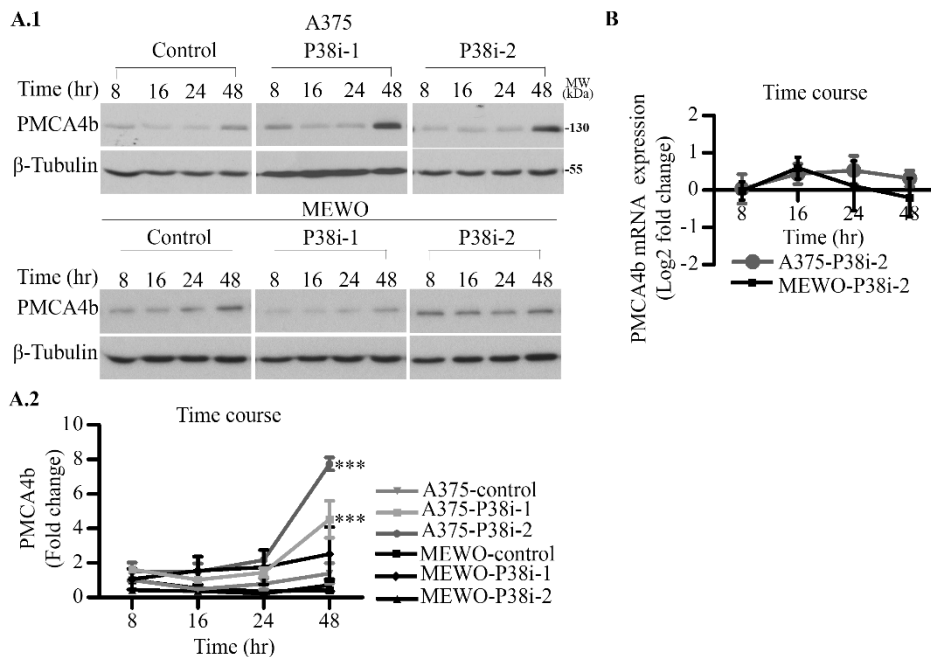
Figure 13. A relatively long exposure to the p38 inhibitor is needed to reach a new PMCA4b steady-state protein level. (A1+A2) A 10 μM of p38i-1or p38i-2 inhibitor was added to A375 and MEWO cells at different timing as indicated. The protein levels of PMCA4b was determined by Western blot. Data were normalized to β-tubulin. The graph represents the densitometry analysis of Western blot using the ImageJ software. Data indicate means ± SE from three independent experiments. (**B**) Using the same experiment condition in (A1), total RNA was extracted and qPCR was performed to analyze PMCA4b mRNA level. Data indicate means ± SD from three independent experiments.

According to the literature, the p38 MAPK pathway is activated in A375 BRAF mutant melanoma cells, therefore, we tested the effect of p38i-2 on its substrate HSP27. In good accordance with previous findings [18,200], high levels of phosphorylated HSP27 (p-HSP27) could be detected in the control cells confirming that p38 MAPK was active in BRAF mutant cells. Treatment of the cells with p38i-2 induced dephosphorylation of p-HSP27 and the level of p-HSP27 decreased (Figure 14). Since the p38 MAPK pathway is already activated in BRAF mutant melanoma cells the p38 MAPK activator anisomycin increased the p-HSP27 level slightly but not significantly. Treatment of the cells with p38i-2 alone or in combination with anisomycin induced dephosphorylation of p-HSP27 and the level p-HSP27 decreased. This experiment also provides confirmation on the specificity of the p38 inhibitor used in this study.
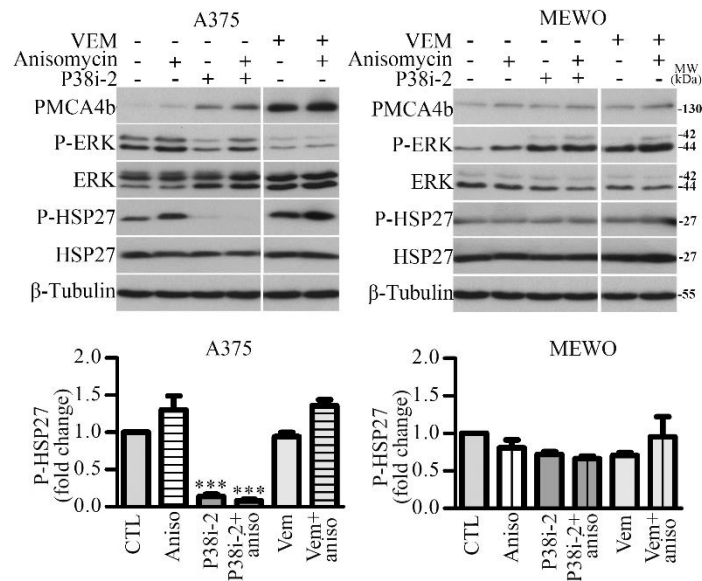
Figure 14. P38 inhibitor reduces phosphorylation of HSP27 in BRAF mutant but not in BRAF wild type melanoma cells. Cells were treated with 0.5 μM vemurafenib, 10 μM p38i-2 or 2.6 μg/ml anisomycin (positive activator of p38) alone or in combination as indicated in the figure for 48 hours. Protein expression level of PMCA4b, P-ERK, ERK, P-HSP27 and HSP was determined by Western blot. Data were normalized to β-tubulin. Bars indicate means ± SE from three (A375) and two (MEWO) independent experiments.

5.1.2. The enhanced PMCA4b abundance increased Ca^{2+} clearance from BRAF mutant melanoma cells.

Previously, we showed that vemurafenib treatment enhanced the abundance of PMCA4b in the plasma membrane that resulted in increased Ca^{2+} extrusion capacity of the cells [82]. Similarly, we show here that p38 inhibition increased the endogenous PMCA4b steady-state protein level in the plasma membrane using confocal microscopy (Figure 15A). To examine if the increased PMCA4b abundance in response to p38i-2 affected Ca^{2+} clearance capacity of the cells, we used A375 melanoma cells stably transfected with the genetically encoded green fluorescent Ca^{2+} sensor GCAMP6f [196]. Cells were treated with p38i-2 and 48 hours after treatment changes in fluorescence of GCAMP6f was monitored after the addition of 2 μM Ca^{2+} ionophore A23187. A23187 was used to allow Ca^{2+} entry into the cells independent of the plasma membrane Ca^{2+} channels. Analysis of the fluorescence signal showed nearly doubled cytosolic Ca^{2+} clearance rate after the peak in response to p38i-2 treatment ($T_{1/2}= 74.6 \pm$ s) compared to the control, not treated A375 melanoma cells ($T_{1/2}= 181.1 \pm$ s) (Figure 15B). These results indicate that - similarly to vemurafenib ($T_{1/2}= 81.8 \pm$ s)

- p38i-2 treatment can increase Ca^{2+} clearance from A375 cells by increasing the abundance of PMCA4b at the plasma membrane.
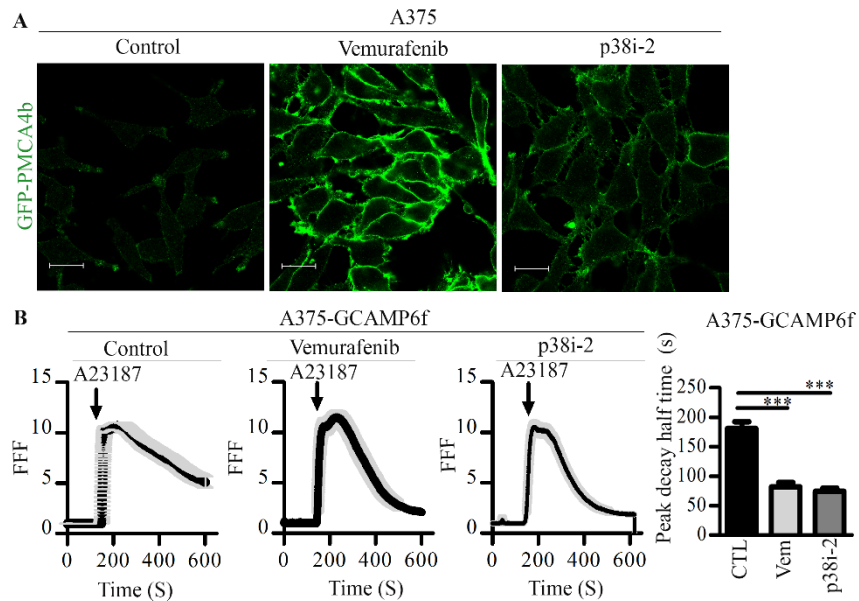
Figure 15. P38 inhibitor enhances Ca^{2+} clearance from A375 cells by increasing PMCA4b at the plasma membrane. (**A**) Confocal microscopy images of A375 cells immunostained with anti-PMCA4b antibody (JA3) after treatment with 0.5 µM vemurafenib and 10 µM p38i-2 for 48 hours. Scale bar, 20µm. (**B**) For intracellular Ca^{2+} signal measurement, a 2 µM A23187 (arrow) was added to initiate Ca^{2+} entrance in A375-GCAMP6f cells after treatment with 0.5 µM vemurafenib and 10 µM p38i-2 for 48 hours. Live cell imaging of GCAMP6 signal was detected for 10 minutes. A total of 14-15 cells were analyzed and data were represented as fluorescent intensity values (F/F0) ± SE of two independent experiments. Bars represent half peak decay time mean ± SE.

5.1.3. Inhibition of P38 MAPK pathway increased PMCA4b stability

Treatment of BRAF mutant melanoma A375 cells with p38i-2 markedly increased PMCA4b abundance at the protein level without having significant effect at its mRNA level, therefore, we assumed that p38 MAPK affected PMCA4b stability. To test this hypothesis, we treated A375 cells with vemurafenib for 48 hours. During this treatment the expression of PMCA4b is increased as shown in Figure 16. Then we removed vemurafenib and tested PMCA4b expression after an additional 24 and 48 hours by Western blotting. As shown in figure 16A, after vemurafenib removal high p-ERK levels were quickly restored and the PMCA4b abundance decreased to its low basal steady-state level within 48 hours. The addition of either p38i-2 or the lysosome inhibitor CQ prevented PMCA4b protein degradation, and

pERK was also reduced slightly by p38i-2 suggesting cross-talk between the pathways (Figure 16A).

To investigate further the effects of p38i-2 and CQ we used a stable A375 cell line expressing GFP-PMCA4b and examined the subcellular localization of the pump by confocal microscopy. As shown in Figure 16B, GFP-PMCA4b positive perinuclear vesicles were observed in control cells and their number further increased with CQ treatments. This indicated that CQ inhibited PMCA4b degradation at the lysosomal level. Importantly, p38 MAPK inhibition reduced the number of the GFP-PMCA4b positive vesicles almost completely even in the presence of CQ suggesting that p38 MAPK mediated internalization and subsequent degradation was responsible for the low steady-state PMCA4b abundance in BRAF mutant melanoma cells. Similarly, vemurafenib was able to block PMCA4b internalization suggesting that the BRAF pathway was also involved in PMCA4b degradation – at least partly through the activation of p38 MAPK - that may explain the lack of additivity of the corresponding inhibitors.
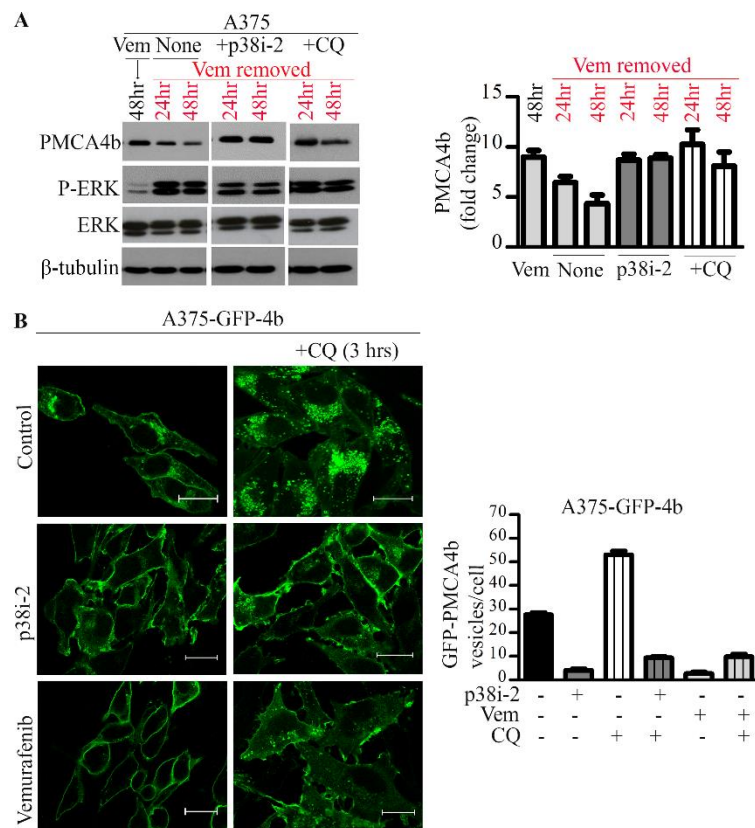
Figure 16. Both p38 inhibitor and chloroquine protect PMCA4b from degradation, however, while chloroquine (CQ) trapes PMCA4b in intracellular vesicles p38 inhibitor holds it in the plasma membrane. (**A**) A375 cells were incubated with vemurafenib for 48 hours and then removed for additional 24 or 48 hours. As vemurafenib removed 10 μM p38i-

2 inhibitor or 10 µM CQ was added to the medium. The protein expression level of PMCA4b, P-ERK and ERK was determined by Western blot. Data were normalized to β-tubulin. Bars indicate means ± SE. (**B**) A375-GFP-PMCA4b cells were treated with 10 µM p38i-2 inhibitor or 0.5 µM vemurafenib for 48 hours and 50 µM CQ for 3 hours alone or in combination as indicated. GFP signal was detected using confocal microscopy, 40x objective. Scale bar, 20 µm. The number of GFP-PMCA4b positive perinuclear vesicles/cell were counted (eight cells/group) and represented as a means ± SE.

5.1.4. Activation of p38 MAPK enhanced PMCA4b degradation through the endolysosomal system

To investigate the degradation pathway of PMCA4b we immunostained A375-GFP-PMAC4b cells with specific endolysosomal and autophagic markers including the early endosomal marker EEA1 (early endosomal antigen 1), the late endosomal marker Rab7 (Ras-related protein-7), the lysosomal marker LAMP1 (lysosomal-associated membrane protein 1), the recycling endosomal marker Rab11 (Ras-related protein-11) and the autophagosome marker LC3 (microtubule-associated protein 1A/1B-light chain 3) (Figure 17A and B). In control cells, 9.3% of the total GFP-PMCA4b vesicles were EEA1 positive. Starvation increased the proportion of EEA1 positive vesicles to 23.5%. Treatment of the cells with the p38 MAPK inhibitor p38i-2 the formation of EEA1 positive GFP-PMCA4b vesicles were nearly fully diminished even after starvation indicating that p38 MAPK activity induced PMCA4b internalization and degradation at the early endosomal level (Figure 17A). Further analysis of GFP-PMCA4b trafficking showed that most of the GFP-PMCA4b vesicles co-localized with Rab7 (28.8%) and LAMP1 (43.4%) and less Rab11 (8.3%) markers. Only 4.6% of the vesicles co-localized with the autophagic marker LC3. Similarly, a transmission electron microscopy experiment showed GFP-PMCA4b positive puncta in an autolysosome of A375-GFP-PMCA4b cells (Figure 17C). No contribution of the proteasome system could be detected in PMCA4b degradation since the proteasome inhibitor MG132 did not show any effect on PMCA4b protein level (Figure 17D). In conclusion, we found, for the first time, that PMCA4b is degraded through the endolysosomal system and that the p38 MAPK pathway was involved (Figure 17E).
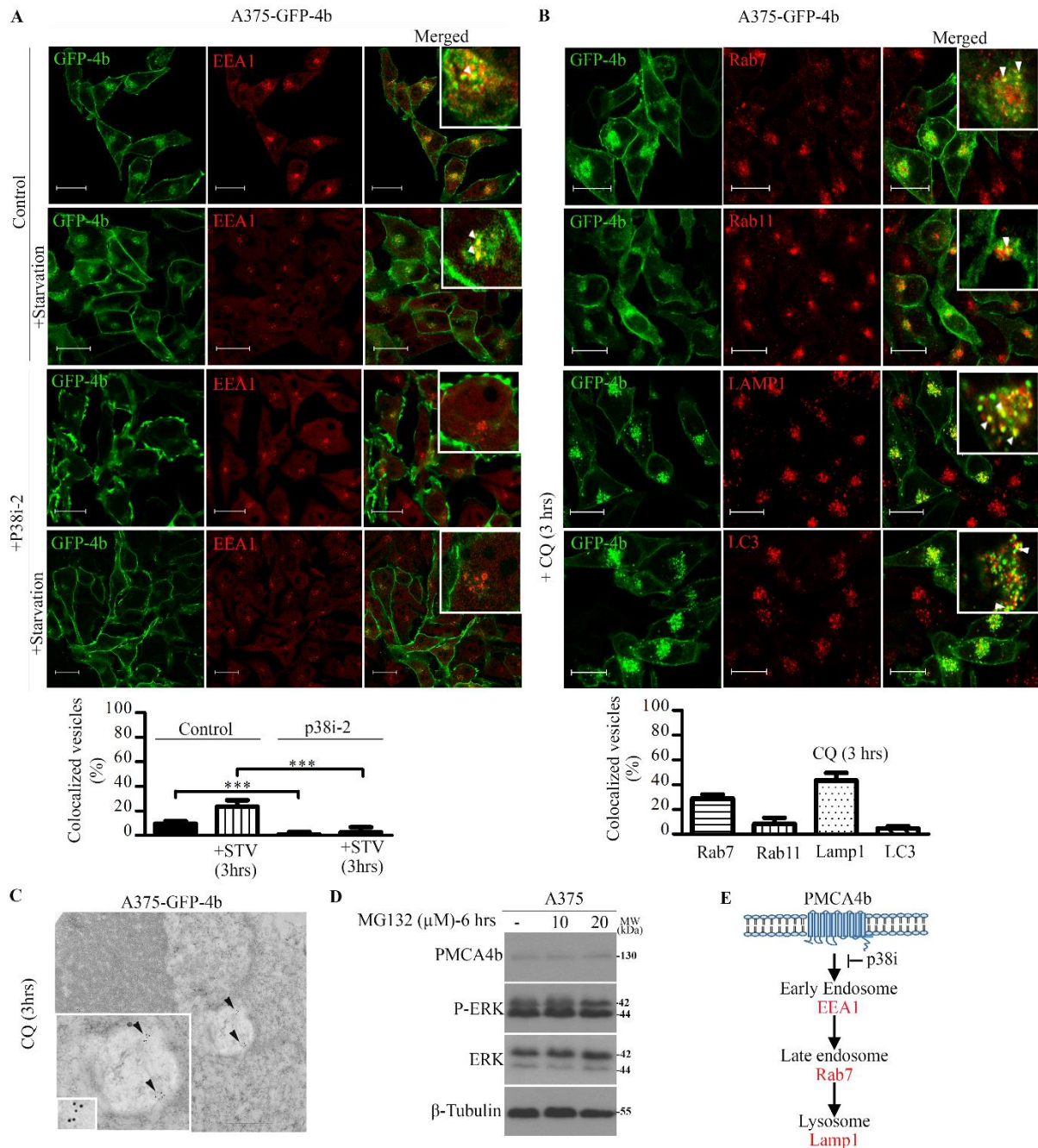
Figure 17. p38 inhibitor prevents PMCA4b internalization and subsequent degradation through the endolysosomal system. (**A**) A375-GFP-PMCA4b cells were treated with 10 μM p38i-2 for 48 hours with or without starvation (3 hours). Images were taken with confocal microscopy after EEA1 immunostaining. Co-localized GFP-PMCA4b and EEA1 vesicles (yellow) from 6 cells/group were counted. Bars represent % of co-localized vesicles means ± SE. Scale bar, 20 μm. (**B**) A375-GFP-PMCA4b cells were cultured for 48 hours and CQ was added in the last 3 hours as indicated. Cells immunostained for Rab7, Rab11, LAMP1 and LC3 were analyzed under a confocal microscope. The numbers of co-localized vesicles with GFP-PMCA4b for 7-9 cells/group were counted. Bars represent % of co-localized vesicles means ±

SE. Scale bar, 20 µm. (**A+B**) Insets show magnified part of a cell, Scale bar, 10 µm. Arrowheads indicate co-localization of GFP-PMCA4b with marker tested. (**C**) A375-GFP-PMCA4b cells were fixed and then immunostained with anti-GFP antibody after treatment with CQ for 3 hours. Then cells were processed and imaged by JEM-1011 transmission electron microscope (Jeol). Arrowheads represent positive PMCA4b protein. (**D**) A375 cells were cultured in a 6-well plate and treated with MG132 at 10 and 20 µM for 6 hours. The protein expression level of PMCA4b, P-ERK and ERK was analyzed with Western blot. β-tubulin was used as a loading control. The experiment was run three times. (**E**) The chart shows PMCA4b degradation through the endolysosomal system.

5.1.5. p38 MAPK modulates PMCA4b internalization in HeLa and HEK cell model systems.

To confirm that p38 MAPK acts as a modulator of PMCA4b trafficking we used two additional human cell models. Previously, it was reported that HeLa cells have low basal p38 MAPK activity [201], therefore, we used a HeLa cell line stably expressing GFP-PMCA4b and induced p38 MAPK activation with anisomycin. A strong increase in the number of GFP-PMCA4b positive intracellular vesicles was detected after 1 hour of anisomycin treatment that was blocked nearly completely by the addition of p38i-2. On the contrary, p38i-2 treatment alone – without ionomycin - did not show any effect on PMCA4b localization in correlation with the low basal p38 activity of these cells (Figure 18).
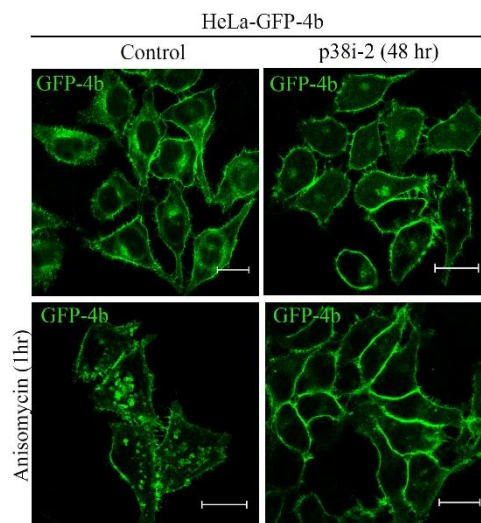
Figure 18. p38 MAPK acts as a modulator of PMCA4b internalization in HeLa cells. HeLa-GFP-PMCA4b cells were treated with 10 µM of p38i-2 (48 hours) or 2.7 µg/ml anisomycin (1 hour) alone or in combination. Images were taken using confocal microscopy, 40x objective. Scale bar, 20 µm.

To confirm that p38 MAPK was responsible for the increased internalization of PMCA4b, we used a HEK-mCherry-MKK6-Dox cell line in which doxycycline treatment induced p38 MAPK activation. Western blot analysis showed that p38 MAPK activity is increased within 24 hours of doxycycline treatment as supported by the high levels of both p-P38 and its substrate P-HSP27. p38i-2 treatment inhibited phosphorylation of the p38 MAPK substrate HSP27 confirming proper functioning of the model system (Figure 19A). Then we transfected HEK-mCherry-MKK6-Dox cells with GFP-PMCA4b and tested its localization by confocal microscopy. As shown in Figure 19B, p38i-2 treatment did not affect the localization of GFP-PMCA4b in the control cells without doxycycline, whereas it was able to block doxycycline treatment induced GFP-PMCA4b internalization. All these data confirm that p38 MAPK can act as a modulator of PMCA4b stability in different cell types by enhancing its internalization and subsequent degradation through the endolysosomal pathway.
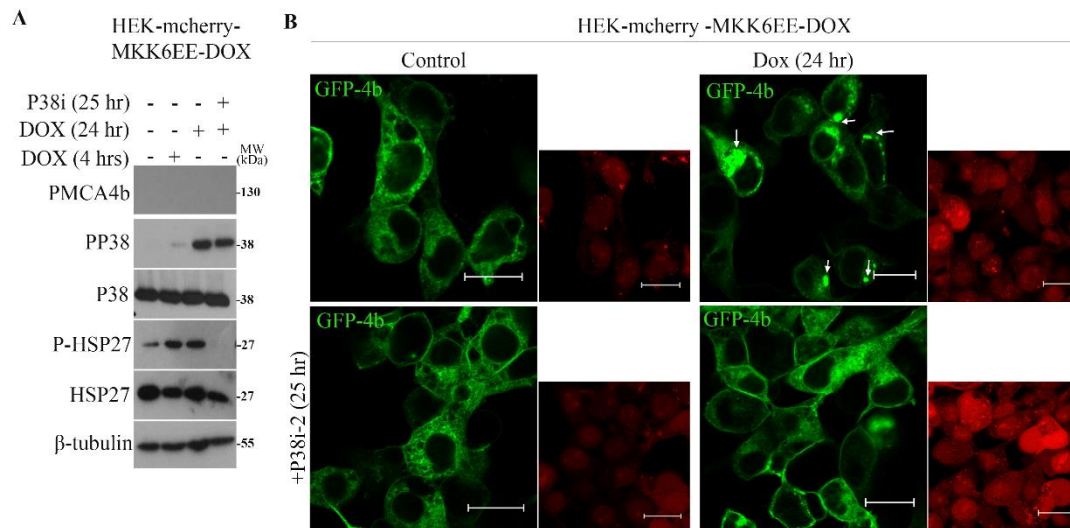
Figure 19. p38 MAPK acts as a modulator of PMCA4b internalization in doxycyclin inducible HEK-mCherry-MKK6 cells. (**A**) HEK-mCherry-MKK6EE-Dox inducible cells were treated with 10 µM p38i-2 for 25 hours and in the last 4 or 24 hours incubation 2 µg/ml doxycycline was added to the medium for MKK6 induction. The protein expression level of PMCA4b, PP38, P38, P-HSP27 and HSP-27 was analyzed with Western blot. β-tubulin was used as a loading control. (**B**) After 24 hours transfection of HEK-mCherry-MKK6EE-Dox cells with SB-CAG-GFP-PMCA4b-CAG-Puro construct, cells were treated with 10 µM p38i-2 for an additional 25 hours. During the last 24 hours of p38i-2 treatment, 2 µg/ml doxycycline was added to induce MKK6. Images were taken using confocal microscopy, 40x objective. Scale bar, 20 µm. Arrowheads indicate GFP-PMCA4b positive vesicles. Images shown next to each picture represents the mCherry signal for the same cells. Scale bar, 20 µm.

5.2. Inhibition of p38 MAPK reduced melanoma cell migration, metastatic activity, colony and spheroid formation without affecting cell viability.

5.2.1. Changes in cell cycle progression and cell viability after p38 inhibitor treatment.

It was reported that inhibition of p38 MAPK may affect cell viability and cell cycle progression in cancer cells, therefore, we examined the effect of p38i-2 on these processes in A375, A375-GFP-PMCA4b and MEWO cells. As shown in Figure 20A, p38i-2 treatment reduced cell viability of both A375 and A375-GFP-PMCA4b cells at high inhibitor concentrations (IC_{50} = 31.17 µM) with no significant differences between the cell types. It is important to note that at the p38i-2 effective dose (10 µM), 75.3% of cells were viable. No effect of p38i-2 on cell viability in BRAF wild type cells (MEWO) could be detected (Figure 20A). In contrast, vemurafenib reduced significantly cell viability at low inhibitor concentration (IC_{50} = 0.19 µM) in BRAF mutant A375 cells. As expected, no effect of vemurafenib on viability of BRAF wild type MEWO cells could be detected.

Cell cycle analysis after p38i-2 treatment showed a significantly reduced number of cells in both S and G2/M phase that in turn significantly increased the number of cells in the Go/G1 phase in both A375 and A375-GFP-PMCA4b cells. However, in contrast to the vemurafenib treatment that showed significant cytotoxicity, p38i-2 treatment displayed low cytotoxicity as cells did not accumulate in the Sub-G1 phase. Neither cell proliferation nor cell death was affected by p38i-2 or vemurafenib treatment in BRAF wild type cells (MEWO) (Figure 20B). In addition, PMCA4b over-expression in A375 cells did not affect any of the cell cycle phases and hence cell proliferation in agreement with the results of the BrdU incorporation assay reported previously [82].
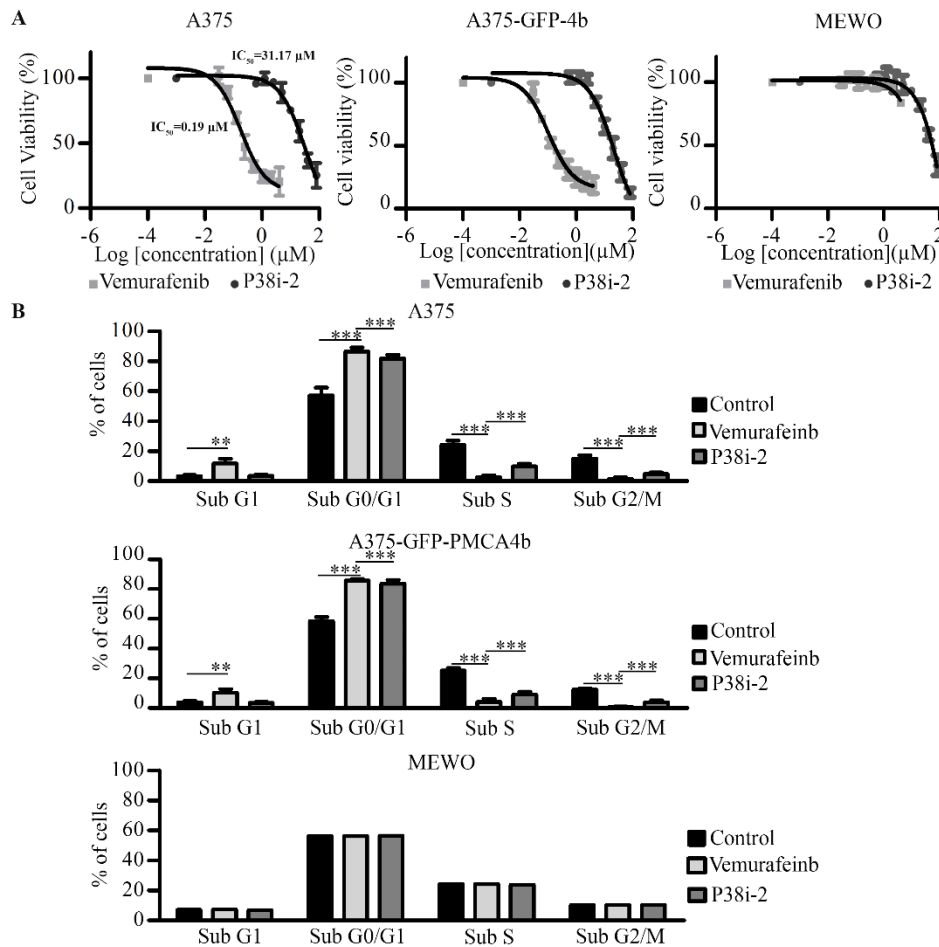
Figure 20. P38 inhibitor displays low cytotoxicity while induces cell cycle arrest in BRAF mutant but not in BRAF wild type cells. (A) A375, A375-GFP-PMCA4b and MEWO cells were cultured in a 96-well plate. Next day, cells were treated with eight increasing concentrations of p38i-2 and vemurafenib and incubated for 48 hours. Viability was assessed by SRB assay. Data represent the % of viable cells ± SE of three independent experiments. **(B)** The same cells in (A) were treated with 0.5 μM vemurafenib or 10 μM p38i-2 for 48 hours. Then cell cycle was analyzed based on DNA content and the ratio of cells in each sub-phase was determined. Data indicate means ± SE of three independent experiments.

5.2.2. The effect of p38 inhibitor on colony formation

Next we investigated the effect of p38i-2 on colony formation. As shown in Figure 21, similar to vemurafenib, p38i-2 significantly reduced colony formation in A375 cells. PMC4b over-expression, on the other hand, induced significant changes in colony morphology rather than a reduction in cell density. In the case of A375 cells, the cells grew over each other and formed aggregates while A375-GFP-PMCA4b cells formed flat monolayer. Interestingly, p38i-2 treated A375 cells showed similar monolayer formation as seen in the case of the

PMCA4b over-expressing cells underlining the importance of PMCA4b in cell morphology changes.
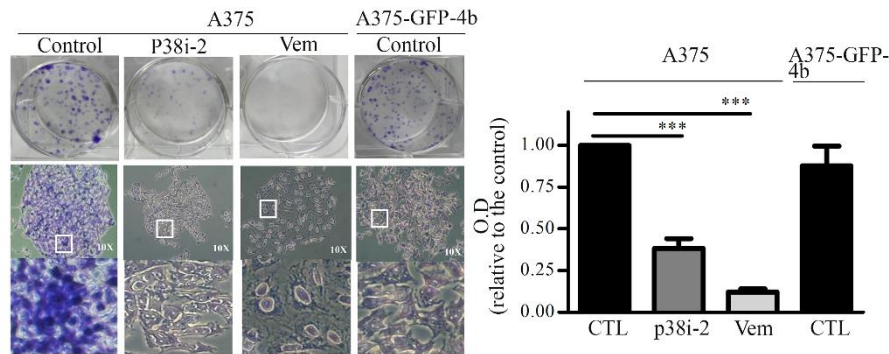
Figure 21. P38 inhibitor reduces colony formation in A375 melanoma cells. A375 cells were cultured in 6-well plates. Next day, cells were treated with 0.5 μM vemurafenib or 10 μM p38i-2 for 6 days. A375-GFP-PMCA4b cells were cultured in parallel. Treatments were refreshed on the fourth day. Cells were fixed and stained with 0.5% crystal violet. Bars represent normalized O.D mean ± SD of three independent experiments.

5.2.3. Spheroid formation is moderately affected by p38 inhibitor treatment and/or PMCA4b over-expression in A375 melanoma cells.

Spheroid formation is a very useful tool to test new compounds on cancer cell proliferation and viability [202]. To study the effect of p38i-2 and vemurafenib on spheroid formation, A375 cells were grown for 3 days on poly-HEMA coated 96-well plates to allow spheroids to form and after that treatments were added at the effective doses for additional 6 days. A375-GFP-PMCA4b spheroids were grown for the same total of 9 days. As shown in Figure 22A1, p38i-2 treatment reduced A375 spheroid volume although less effectively than vemurafenib. A375-GFP-PMCA4b spheroids showed significant volume reduction compared to the parental cells. The reduced spheroid size of the PMCA4b expressing cells could be a result of a delay in compact spheroid formation. (Figure 22A2). Interestingly, no spheroids were formed from the BRAF wild type cells (MEWO) using the same culture conditions (Figure 22B).

Integrins are a family of proteins that link the extracellular matrix with the actin cytoskeleton, and some are involved in spheroid formation [203]. A study showed that β4-integrin is involved in epithelial cell migration and cancer cell invasion [204]. Therefore, we investigated if β4-integrin expression is affected by p38i-2 treatment or by PMCA4b over-expression in melanoma cells. As shown in Figure 22C1, β4-integrin is highly expressed in A375 cells while no β4-integrin could be detected in the BRAF wild type MEWO cells. Both

p38i-2 treatment and PMCA4b over-expression reduced β4-integrin expression in A375 cells suggesting that increasing PMCA4b abundance could result in reduced β4-integrin expression and hence in a delay in spheroid formation and reduced spheroid size (Figure 22C2).
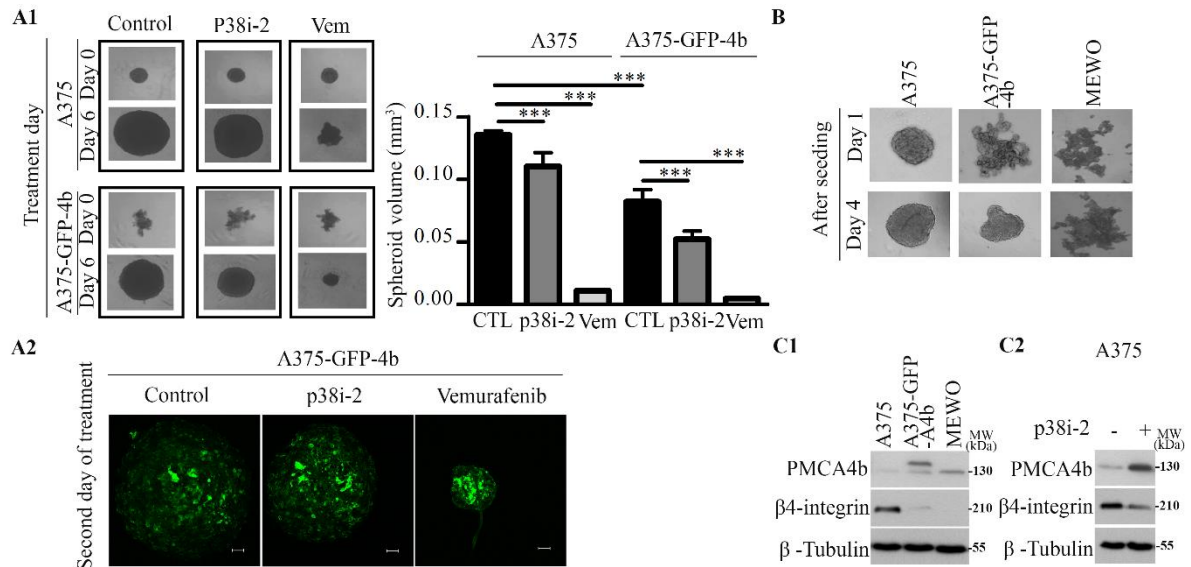
Figure 22. Spheroid growth is reduced with PMCA4b expression and/or p38i-2 treatment in A375 melanoma but not in MEWO cells. (A1) For spheroid formation, A375 and A375-GFP-PMCA4b cells were cultured in POLY-HEMA treated 96-well plate for 9 days. On third day, (Day 0) 0.5 μM vemurafenib or 10 μM p.38i-2 treatments were added. Images were taken on days 0 and 6 by phase contrast microscope, 4x objective. Spheroid volume was calculated based on area and radius determination. Data represent means ± SD of three independent experiments. **(A2)** Confocal microscopy images of A375-GFP-PMCA4b spheroid formed similar to the previous section; however, on the third day 0.5 μM vemurafenib or 10 μM p38i-2 treatments were added for 48 hours. Z-stack images were taken for spheroids after fixation using Axio Imager.M2 microscope (ZEISS) with an ApoTome2 grid confocal unit (ZEISS), 20x objective. Scale bar, 100 μm. **(B)** A375, A375-GFP-PMCA4b and MEWO spheroids were formed for 4 days. Phase-contrast microscope images were acquired on days 1 and 4. **(C1+C2)** same cells were cultured for 48 hours and A375 cells were treated with 10 μM p38i-2. Proteins level of PMCA4b and β4-integrin were determined by Western blot. β-tubulin was used as a loading control. Experiment was repeated three times.

5.2.4 A375 melanoma cell migration and metastatic activity is reduced by p38 inhibitor treatment in a PMCA4b dependent manner.

Previously we reported that PMCA4b can act as a metastatic suppressor through its ability to reduce cell migration [82]. To assess if p38i-2 can affect melanoma cell migration, we used a Boyden chamber assay where cells migrate towards fibronectin as attractant. As shown in Figure 23, p38i-2 decreased migration of A375 cells by 63%. Knocking down PMCA4b expression with siRNA (Figure 23B1 and B2) increased the number of migrated cells and reversed the effect of p38i-2 by 33.6% (Figure 23A, B1 and B2) suggesting that PMCA4b played a role. The cells treated with the negative siRNA did not show any of these effects. Further, we tested if p38 MAPK inhibition was indeed responsible for the reduced migratory character of the cells, cells were treated with p38 MAPK siRNA that reduced p38 MAPK expression by 60%. As shown in Figure 23A1 and B3, the decrease in p38 MAPK expression resulted in a significant 54.5% decrease in cell migration suggesting that p38 MAPK is essentially involved in the regulation of migration activity of BRAF mutant cells.
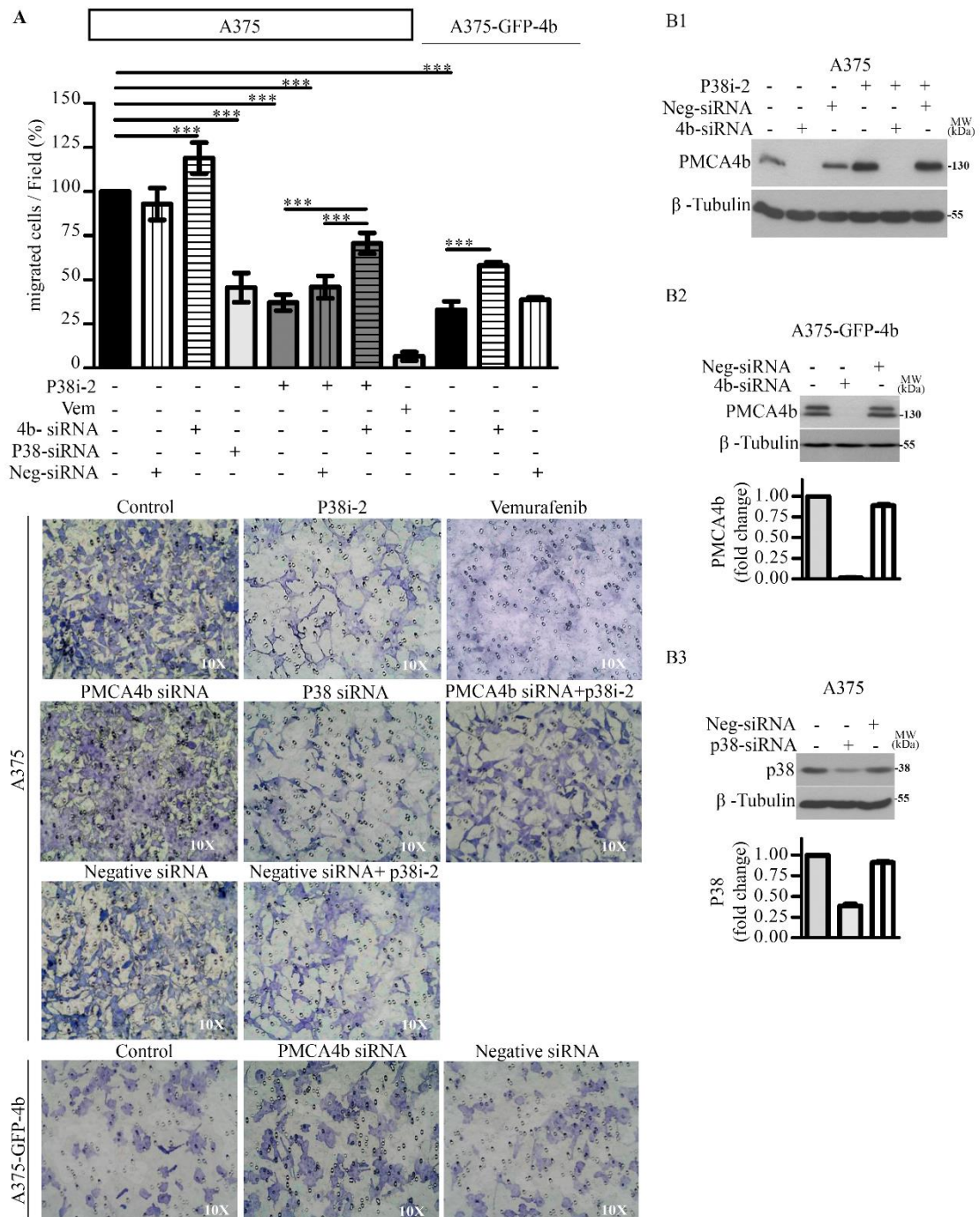
Figure 23. P38 MAPK inhibition or knockdown strongly decreased A375 melanoma cell migration in a PMCA4b dependent manner. (A) Directional migration of A375 and A375-GFP-PMCA4b cells was assessed using Boyden chamber assay after treatment with 10 µM p38i-2 or 0.5 µM vemurafenib for 48 hours +/- siRNA as indicated. Images (n=4) were captured for the lower membrane side and cells were counted. Bars represent the average number of migrated cells/field means ± SD of two independent experiments. **(B1, B2, B3)** Cells were transfected with siRNAs for 72 hours or p38i-2 for 48 hours alone or in combination as

indicated. Protein expression level of PMCA4b and p38 was determined by Western blot. β-tubulin was used as a loading control. The experiment was repeated three times.

Next, we used an *in vitro* model - reversal growth of anchorage-independent multicellular spheroid (MCS) into monolayer [199] - to test the metastatic activity of A375 cells. To study the effect of p38i-2 on the metastatic activity of A375 and A375-GFP-PMCA4b cells, we prepared spheroids as described in the previous section. On the fourth day of growth spheroids were transferred to a 24-well plate and treated with p38i-2 and vemurafenib for 48 hours (Figure 24A). The surface area for each metastatic MCS generated by the outgrowth of cells into monolayer was calculated. A significant reduction in surface area of metadtatic MCS was observed in response to p38i-2 (54.6%) and vemurafenib (28.9%) treatments. As expected, GFP-PMCA4b expression itself caused a dramatic reduction in MSC metastasis compared to the parental A375 cells (Figure 24B). Moreover, confocal microscopy images of A375-GFP-PMCA4b spheroids showed lower GFP-PMCA4b signal at the outer layer of the monolayer where cells start to migrate (Figure 24C) in agreement with the notion that cells migrate faster when PMCA4b abundance is low. All these data highlight the importance of the p38 MAPK pathway and PMCA4b in A375 melanoma cell migration and metastasis.
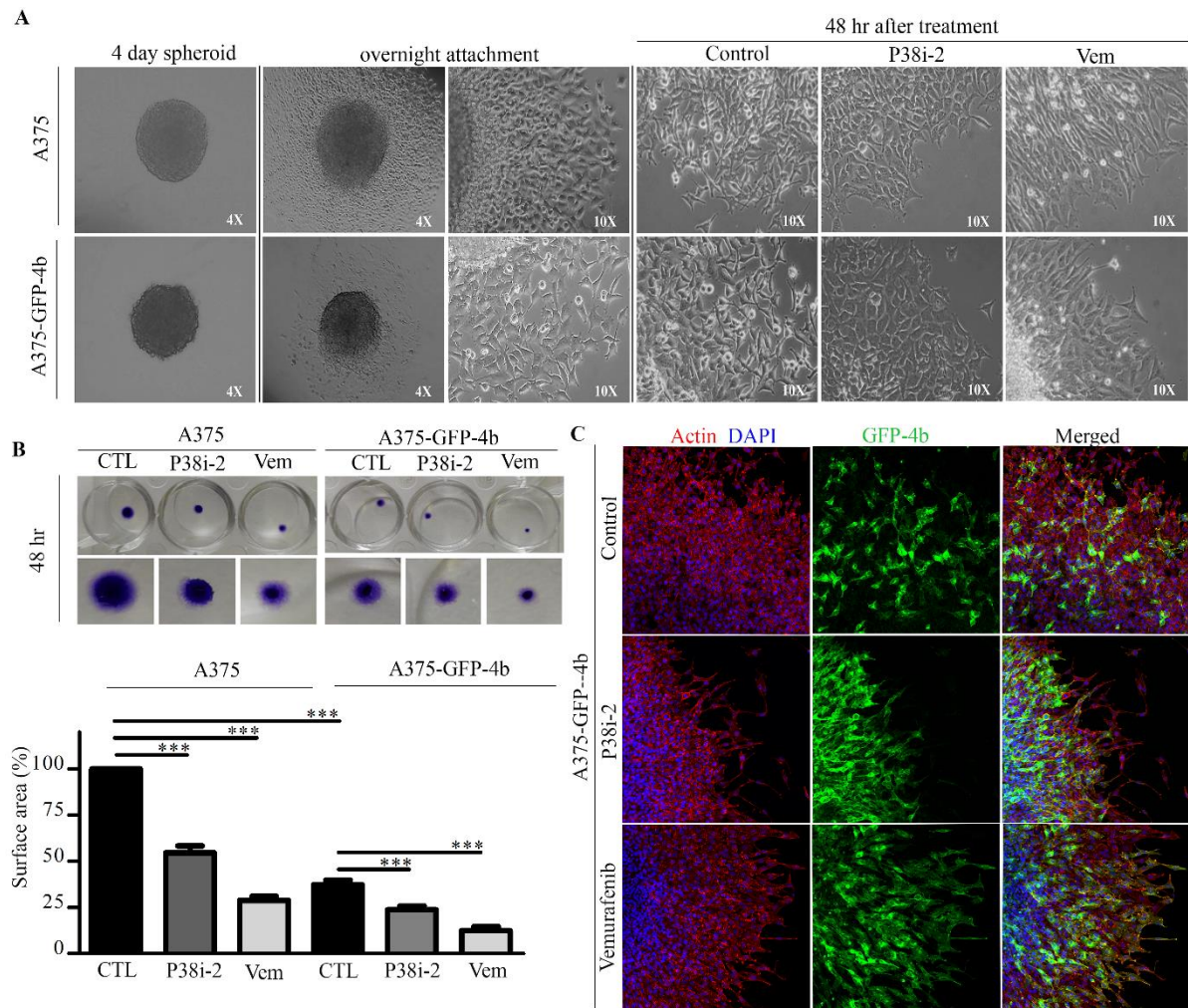
Figure 24. The metastatic activity of A375 spheroids is reduced with PMCA4b expression and/or treatment with p38 and BRAF inhibitors *in vitro*. (A+B) Three days formed spheroids were transferred to 24-well plates then 0.5 μM vemurafenib or 10 μM P38i-2 were added for 48 hours. Phase-contrast microscope images were acquired, 4x and 10x objectives. Cells then were fixed and stained with 0.5% crystal violet. The surface area was calculated using ImageJ software. Bars represent means % relative surface area to the control ± SD of three independent experiments. **(C)** Confocal microscope images of these spheroids were taken after fixation and staining with Phalloidin-TRITC and DAPI. Scale bar, 20 μm.

5.3. PMCA4b activity and trafficking are essential for migration and actin cytoskeleton reorganization of BRAF mutant melanoma cells.

5.3.1. The trafficking mutant PMCA4b-LA is not effective in changing A375 cell culture morphology and motility.

Earlier we showed that the shape of A375 cells is markedly affected by PMCA4b over-expression [82]. Several studies on a variety of different cell types have reported that endocytic

protein trafficking can regulate cell motility [205–207]. Previously, we identified an internalization signal (di-leucine like [1167] LLL) near the C-terminus of PMCA4b. Changing these leucines to alanines resulted in a mutant pump PMCA4b-LA with impaired endocytosis and enhanced plasma membrane expression [104]. To investigate if proper trafficking was essential in changing cell morphology and migration of A375 melanoma cells we used cell lines stably expressing GFP, GFP-PMCA4b or the trafficking mutant GFP-PMCA4b-LA (Figure 25 and 26). Phase contrast microscopy images of single cells show that A375 cells expressing the trafficking mutant GFP-PMCA4b-LA showed spindle-shaped mesenchymal character with protrusions with no significant change in area and circularity parameters could be detected when compared to the control cells. In contrast, the A375 cells expressing GFP-PMCA4b showed polarized mesenchymal character with wide lamellipodium at the cell front (Figure 25A) and significant change in morphology parameters (Figure 25A and B). Cell cultures at the sub-confluent level showed more clustered arrangements of A375-GFP-PMCA4b cells and closer contacts between cells compared to the random distribution and greater distances between cells in the trafficking mutant A375-GFP-PMCA4b-LA cells and the control GFP-A375 cell cultures (Figure 25C and D).

Changes in cell shape are a prerequisite for changes in cell motility and migration. As the trafficking mutant expressing cells retained the parental cell shape we investigated if this affected cell motility and directional cell migration. To test this, we used a non-directional assay in which we tested random movement of the cells and a directional migration assay in which cells move through a filter toward an attractant (fibronectin) in the lower Boyden Chamber. As expected, only wild type PMCA4b expressing cells showed dramatic reduction in both random motility and directed migration (Figure 26 A and B, Video 1). Live cell imaging of A375-GFP-PMCA4b cells showed slow-moving polarized cells with intense membrane ruffling at the front and short net displacement over time. However, both control and A375-GFP-PMCA4b-LA cells remained highly motile with highly dynamic changes of directionality as a result of dynamic protrusion and retractions activities (Figure 26C, Video 2).

All these data suggest that both PMCA4b abundance and proper trafficking are essential for the distinct morphology and migratory character of the PMCA4b expressing BRAF mutant melanoma cells.
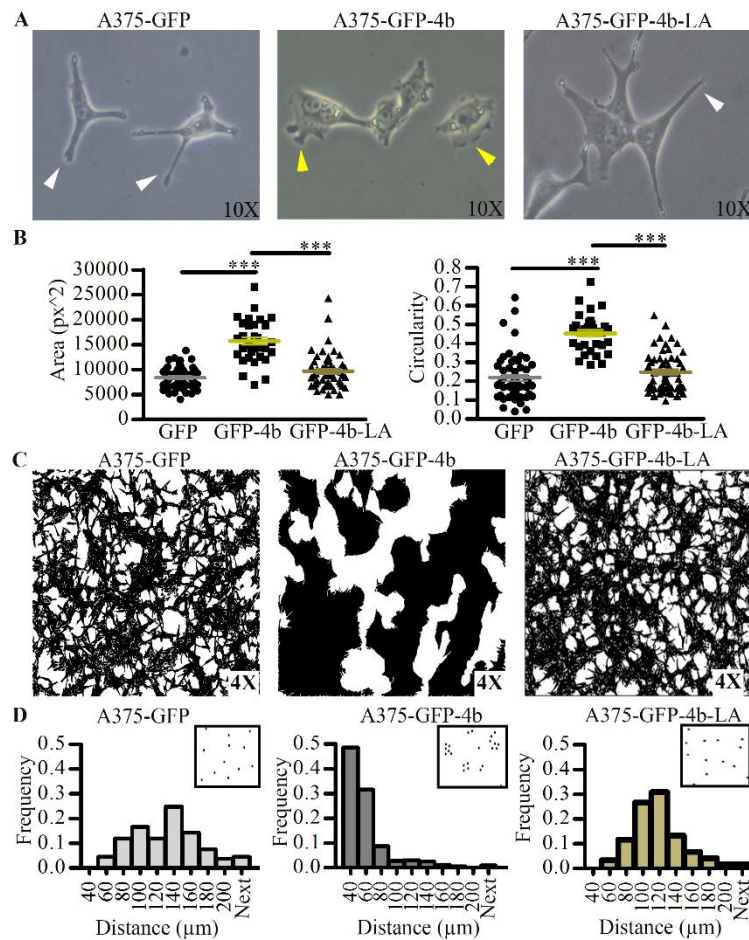
Figure 25. Changes in area, circularity and culture morphology are observed upon GFP-PMCA4b but not GFP-PMCA4b-LA expression in A375 melanoma cells. (A+C) Phase contrast microscope images for A375-GFP, A375-GFP-PMCA4b and A375-GFP-PMCA4b-LA cells after overnight culture (A) or after 80%confluency (C) at indicated magnification. For morphology analysis, a black mask was applied on cells to define the contour of the cells using ImageJ software. Protrusions and lamellipodia were indicated by white and yellow arrowheads, respectively. Scale bar, (A) 10 μm and (C) 50 μm **(B)** Area and Circularity parameters for A375-GFP (n= 56), A375-GFP-PMCA4b (n= 32) and A375-GFP-PMCA4b-LA cells (n= 54) were analyzed by ImageJ software. **(D)** To determine nearest neighbor distances, cell centers of the same cells in (C) were identified and distances calculated using ImageJ software. Insets show dots that represent cell centers.
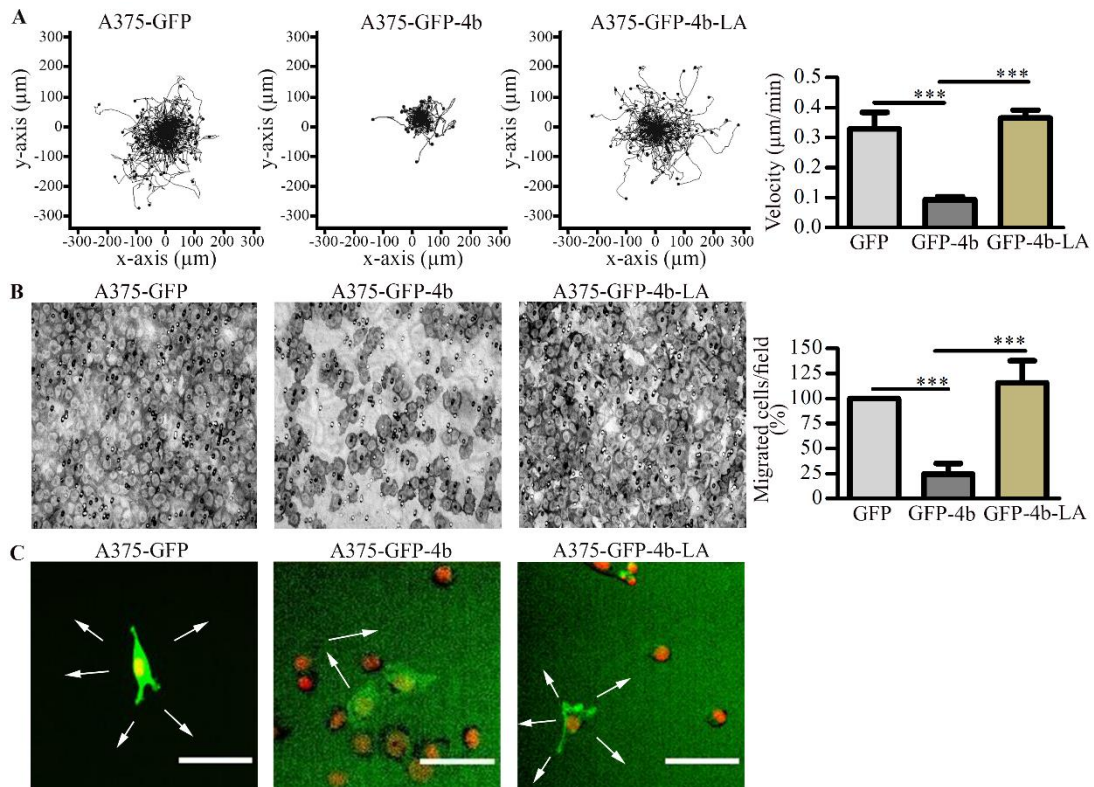
Figure 26. GFP-PMC4b but not the trafficking mutant GFP-PMCA4b-LA expression changed motility, migration and polarity of A375 melanoma cells. (A) Cells were cultured and their migration was followed for 24 hours by recording GFP and Hoechst 33342 signal. The images were taken using automated fluorescence microscopy. The plot shows the starting position of each cell trajectory and its migration. Bars represent mean velocity ± S.D. A 4-5 independent measurements were used from A375-GFP (n= 645), A375-PMCA4b (n= 941) and A375-PMCA4b-LA (n= 990) cells. **(B)** Boyden chamber assay was performed to assess directional cell migratory. Cells migrated toward fibronectin were fixed on the bottom of the membrane and stained with Toluidine blue. Images were taken and the number of cells migrated from 6 fields of view was counted. Data represent means % relative to control. **(C)** A movie was created from single cell images taken from (A) using ImageJ software.

5.3.2. Cell-cell connections, stress fibers and lamellipodia formation are characteristic features of the PMCA4b expressing melanoma cells.

5.3.2.1. PMCA4b trafficking is essential for the formation of cell connections, stress fiber and lamellipodia.

Cell shape and migration are largely affected by actin cytoskeleton remodeling [180]. Many studies have reported the role of Ca^{2+} in regulating actin dynamics through their effect on Ca^{2+} dependent actin-binding proteins and regulatory mechanisms [37,185]. PMCA4b is a

well-known regulator of cytosolic Ca^{2+}, therefore, to follow the changes of F-actin organization upon PMCA4b expression we stained the cells with Phalloidin-TRITC. A significant increase in cell-cell connections was detected in case of the wild type GFP-PMCA4b expressing cells when compared to the control GFP-A375 cells or the cells expressing the trafficking mutant GFP-PMCA4b-LA (Figure 27A). Live cell imaging of A375 cells co-expressing mCherry-PMCA4b and GFP-actin showed the mCherry-PMCA4b signal preceding the GFP-actin signal as cells start to form new connections. (Figure 27B, Video 3).
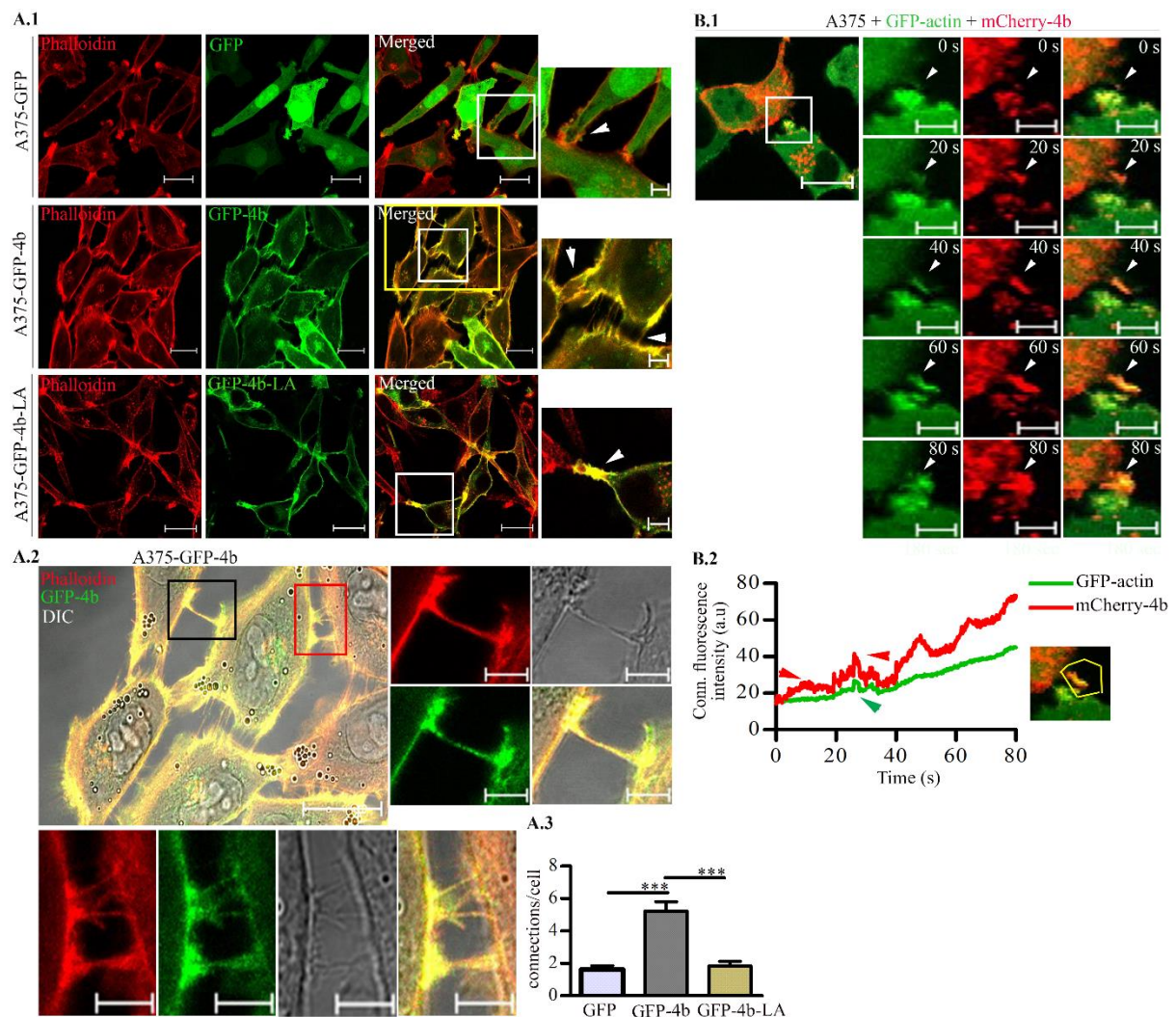
Figure 27. Increased formation of cell-cell connections between A375 melanoma cells after GFP-PMCA4b but not PMCA4b-LA expression. (A.1) Cells were fixed and then stained with Phalloidin-TRITC for F-actin labeling using a confocal laser microscope. Scale bar, 20 μm. Insets represent the cell-cell connections magnified indicated by arrowheads. **(A.2)** A magnified part of the image shown in A.1 marked with a yellow rectangle. Both DIC and fluorescent images are shown. Scale bar, 20 μm. Insets represent magnified intercellular connections, Scale bar, 5 μm. **(A.3)** Bars indicate the mean number of inter-connections per

cell for 12-13 cells **(B.1)** A375 cells were co-transfected with GFP-actin and mCherry-PMCA4b for 48 hours. Images shown are taken from live-cell recording every 0.2 s for 180 seconds at 37 ℃ by spinning-disc confocal microscope. Scale bar, 20 μm. Insets represent images for new cell connection formation between two neighboring cells at different times. Scale bar, 5 μm. **(B.2)** The graph shows the time course for both GFP and mCherry signals in the ROI (yellow polygon) drawn around the newly formed connection. Increased signals were indicated by arrowheads.

Another pronounced change observed upon the expression of the wild type PMCA4b pump is in the formation of stress fibers at the bottom of the cells and the wide lamellipodia at the cell front (Figure 28). In A375-GFP-PMCA4b cells, a significant increase (by 80%) in the number of cells with stress fibers was observed compared to the parental and trafficking mutant expressing cells. The number of cells with stress fibers was significantly reduced when PMCA4b was knocked down in the A375-PMCA4b cells by siRNA indicating the contribution of the pump in stress fiber formation (Figure 28).
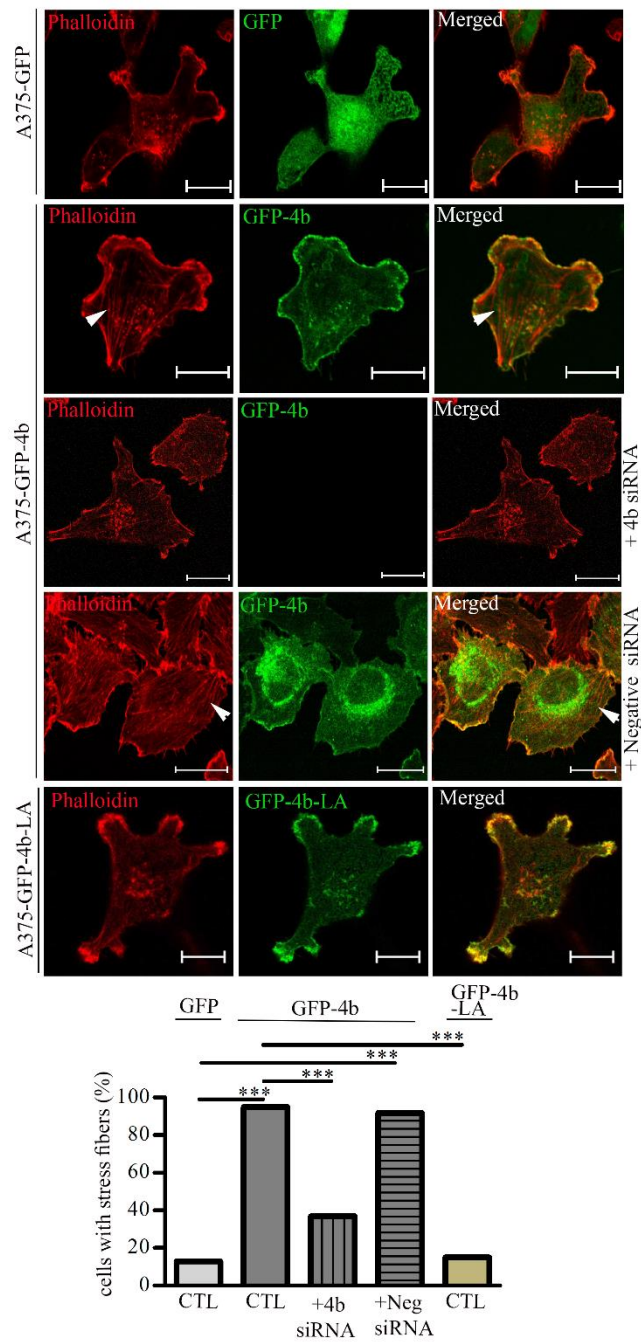
Figure 28. Increased formation of stress fibers and lamellipodia in A375 melanoma cells in PMCA4b but not in PMCA4b-LA expressing cells. Cells with or without siRNA transfections were immunostained with Phalloidin-TRITC, as indicated, and images were taken by a confocal laser microscope. Stress fibers were labeled with arrowheads. Scale bar, 20 μm. Bars represent the mean number of cells with stress fibers. Number of cells analyzed was A375-GFP (n=55), A375-GFP-PMCA4b-LA (72), A375-GFP-PMCA4b (n=60) -/+ PMCA4b siRNA (n=68) and negative siRNA (n=49).

5.3.2.2. PMCA4b activity is essential for the formation of stress fibers and lamellipodia.

To investigate if PMCA4b activity is required for the actin-related changes, we transiently co-transfected A375 melanoma cells with GFP-actin and mCherry-PMCA4b-DE, a non-functional PMCA4b mutant in which an aspartate is changed to glutamate at position 672 ($D^{672}E$)) [81]. Previous publications demonstrated that the N-terminal tags did not affect PMCA4b activity or localization [81,208]. As shown in Figure 29A, A375 cells transfected with wild type mCherry-PMCA4b showed lamellipodia and stress fiber formation, as expected with most of the GFP-actin at the cell front. In contrast, the A375 cells transfected with the non-functional mCherry-PMCA4b-DE mutant showed significantly less lamellipodia and stress fiber formation with more evenly distributed GFP-actin across the entire cell, similarly to that seen in the parental cells (Figure 29A,B and Figure 30). Kymograph analysis of the lamellipodia formed by the mCherry-PMCA4b expressing cells showed concentrated polymerized GFP-actin with intense ruffling and retraction activity at the cell front (Figure 29C). Interestingly, live-cell imaging of the same cell showed positive mCherry-PMCA4b vesicles moving towards the lamellipodia and back with GFP-actin retrograde flow (Figure 29D, Video 4). All these results indicate the role of PMCA4b activity and hence the contribution of Ca^{2+} in the formation of stress fibers, lamellipodia and actin remodeling.
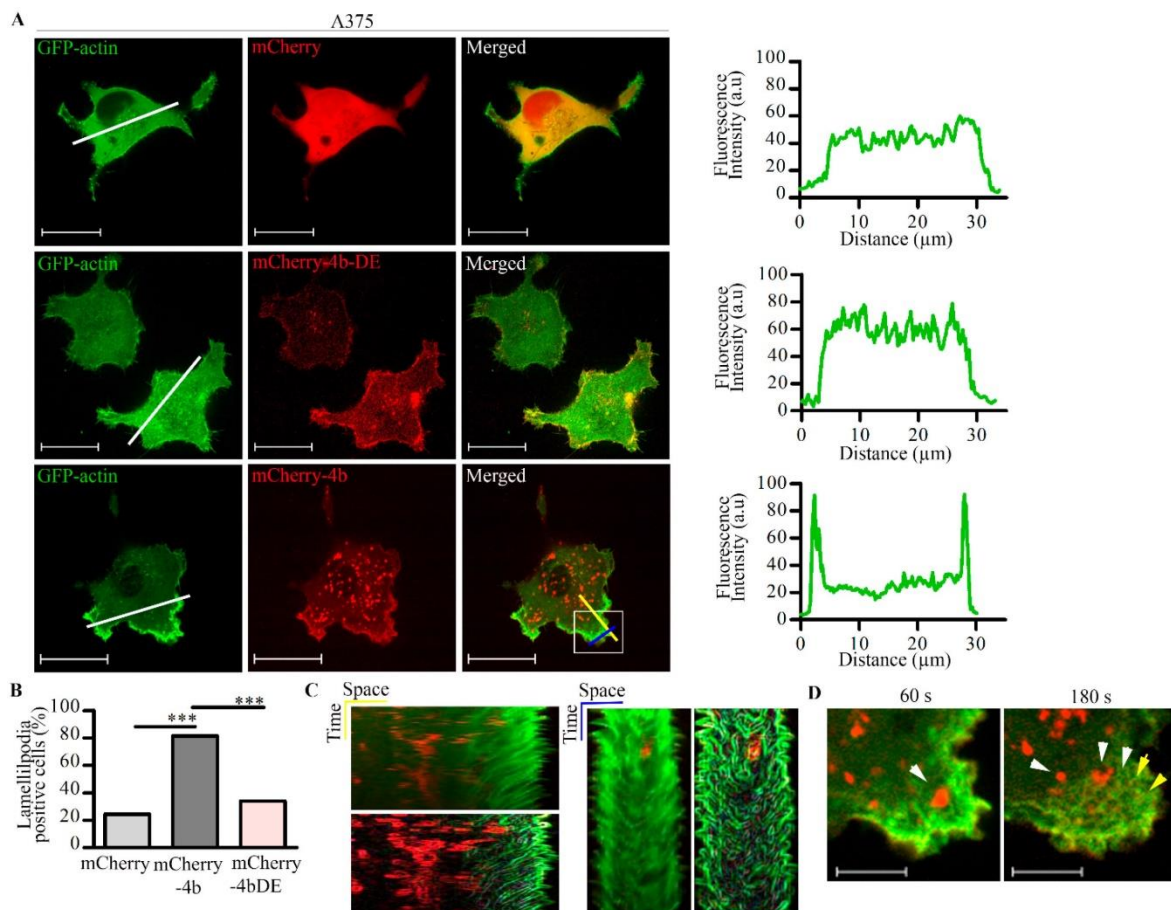
Figure 29. PMCA4b activity is essential for lamellipodia formation in A375 melanoma cells. (A) Confocal microscopy images of A375 transfected with GFP-actin + one of mCherry constructs (pmCherry-C1, mCherry-PMCA4b and mCherry-PMCA4b-DE). Scale bar, 20 μm. Line plots were analyzed by ImageJ software. **(B)** Bars represent the mean number of cells with lamellipodia for mCherry (41), mCherry-PMCA4b (65) and mCherry-PMCA4b-DE (59) together with GFP-actin expressed constructs. **(C+D)** Z-stack images were taken for the A375 cells expressing GFP-actin and mCherry-PMCA4b shown in (A.1) and were recorded every 5 seconds for 5 minutes by spinning-disc confocal microscope. **(C)** Lines drawn across the lamellipodia (yellow and blue) were analyzed and a kymograph was generated by ImageJ software. **(D)** Insets represent an enlarged part of Lamellipodia. Positive mCherry-PMCA4b vesicles were indicated with white arrowheads. Yellow arrowheads show GFP-actin retrograde flow. Scale bar, 5 μm.
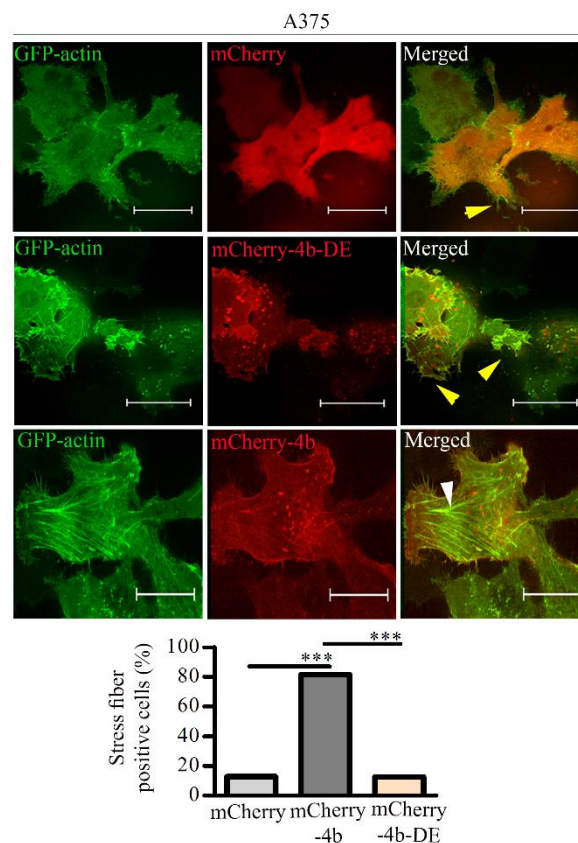
Figure 30. PMCA4b activity is essential for stress fiber formation in A375 melanoma cells. (A) Confocal microscopy images from the bottom of A375 cells transfected as in Figure 29. Yellow and white arrowheads represent spikes and stress fibers, respectively. Scale bar, 20 μm. Bars represent the number of cells with stress fibers. For analysis, GFP-actin and mCherry (31), mCherry-PMCA4b (43) and mCherry-PMCA4b-DE (48) transfected cells were counted.

5.3.2.3. PMCA4b loss in MCF-7 breast cancer cells causes loss of stress fibers associated with changes in cell culture morphology.

Further, we used an estrogen receptor positive (ER+) breast cancer cell line MCF-7 to confirm that the effects of PMCA4b on actin re-arrangements were not melanoma cell-type specific. MCF-7 cells were stably transfected with GFP-PMCA4b or Sh-PMCA4b to specifically silence PMCA4b expression (Figure 31A and B). Over-expression of GFP-PMCA4b showed changes in cell culture morphology with cells located closer to each other as indicated by the nearest neighbour distance when compared to the PMCA4b silenced and parental cells (Figure 31C). In addition, a dramatic loss of stress fibers (> 60%) and a significant increase in single cell area (1.75x) were observed in MCF-7 cells after PMCA4b silencing. These data confirm the role of PMCA4b in actin cytoskeleton reorganization.
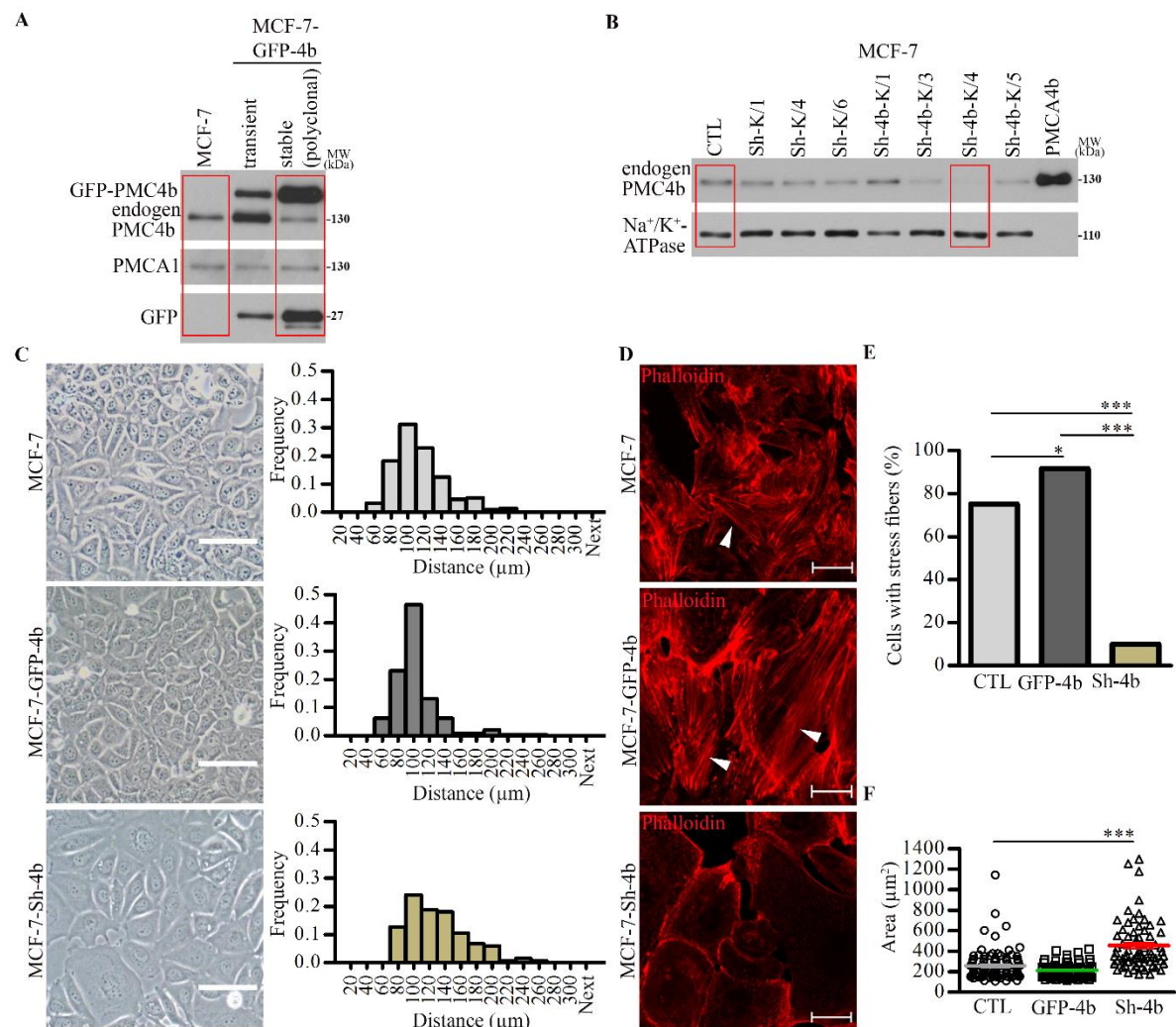
Figure 31. PMCA4b silencing induced increased cell area and loss of stress fibers in MCF-7 cells. (A+B) Cells were cultured and protein expression level of PMCA4b and GFP was

analyzed by Western blot. PMCA1 or NA$^+$/K$^+$ ATPase was used as loading controls as indicated. Cells used in **(C+D)** were from those prepared and indicated in red boxes. **(C)** Phase contrast microscopy images of cells grown for 48 hours, 10x objectives. The nearest neighbour distances of cell centers were determined using ImageJ software. **(D)** Confocal microscopy images of cells stained with Phalloidin-TRITC. Stress fibers are indicated by arrowheads. Scale bar, 20 μm. **(E)** Bars show the mean number of cells with stress fibers. For analysis, MCF-GFP (n= 48), MCF7-GFP-PMCA4b (n= 83) and MCF7-Sh-4b (n= 100) cells were counted. **(F)** The graph represents the area of single cells from phase contrast images shown in (C) (*n* = 100, 88, and 70, respectively) calculated using ImageJ software.

5.3.2.4. Effect of PMCA4b on focal adhesion assembly.

Focal adhesion turnover is important for cancer cell migration and changes in free intracellular Ca^{2+} level were found to have a role [209,210]. Therefore, we stained A375 and A375-GFP-PMCA4b cells for F-actin and one of the focal adhesion components vinculin. As shown in figure 32A, A375-GFP-PMCA4b cells have a punctate pattern of vinculin pointing to the ends of stress fibers while in A375 cells vinculin showed clustered dots positioned at the cell periphery towards the protrusions. In addition, vinculin expression was significantly reduced by GFP-PMCA4b expression as determined by Western blotting (Figure 32B). The accumulation of vinculin at stress fiber ends at focal adhesion sites may indicate that A375-GFP-PMCA4b cells have stronger adhesion to the ECM than the parental cells.
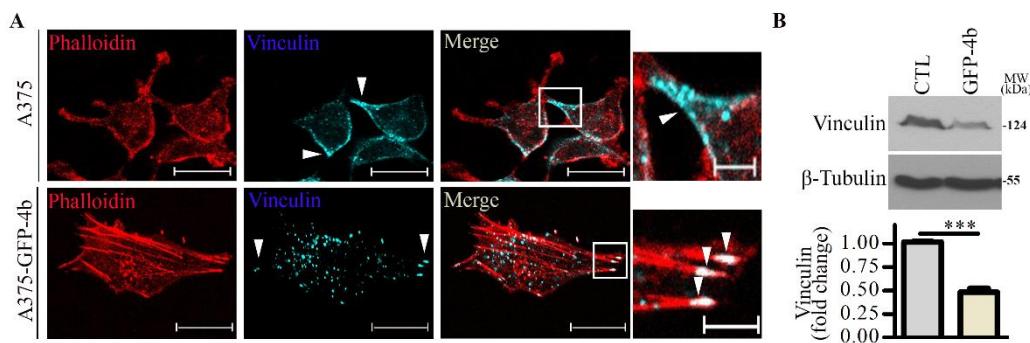
Figure 32. PMCA4b expression results in vinculin re-location and changes in expression in melanoma cells. (A) Cells were stained for vinculin and F-actin and images were taken by a confocal laser microscope. Scale bar, 20 μm. Insets represent part of the cell magnified and arrowheads indicate the position of vinculin. **(B)** Cells were cultured and the protein expression level of vinculin was analyzed by Western blot. β-tubulin was used as a loading control. Bars represent the mean ± SE of three independent experiments.

5.4. PMCA4b activity does not affect F-actin recovery after photobleaching.

F-actin dynamics are influenced by many factors and fluorescence recovery after photobleaching (FRAP) is often used to determine the mobile fraction and the turnover rate of F-actin ($t_{1/2}$) [211]. In this study, we used A375 cells co-transfected with GFP-actin together with one of the following plasmids: mCherry, mCherry-PMCA4b or mCherry-PMCA4b-DE, and photobleached GFP-actin at three different positions including ruffles (lamellipodia) (Figure 33A), cell-free edges and cell-cell connections. Neither the mobile fraction nor the recovery rate of F-actin was affected by mCherry-PMCA4b expression. Although, in mCherry-PMCA4b expressing A375 cells photobleaching of GFP-actin at the lamellipodia showed a somewhat faster recovery rate (lower $t_{1/2}$) compared to the control mCherry expressing cells, the difference was not significant (Figure 33B). These data suggest that F-actin assembly is not affected by mCherry-PMCA4b expression.

C

	Cell-lamellipodia			Free cell edge			Cell-cell connections	
	$t_{1/2}$ (s) ± SE	Mobile phase % ± SE		$t_{1/2}$ (s) ± SE	Mobile phase % ± SE		$t_{1/2}$ (s) ± SE	Mobile phase % ± SE
a	35.55 ± 9.49	66.51 ± 10.5	a	11.14 ± 3.59	45.95 ± 6.46	a	17.89 ±11.65	57.23 ± 5.15
b	24.85 ± 6.54	66.84 ± 6.74	b	17.19 ± 1.53	61.75 ± 6.21	b	22.69 ± 7.12	73.88 ± 6.53
c	17.09 ± 2.93	61.28 ± 4.52	c	15.75 ± 2.69	61.01 ± 3.61	c	15.71 ± 2.95	56.65 ± 3.27
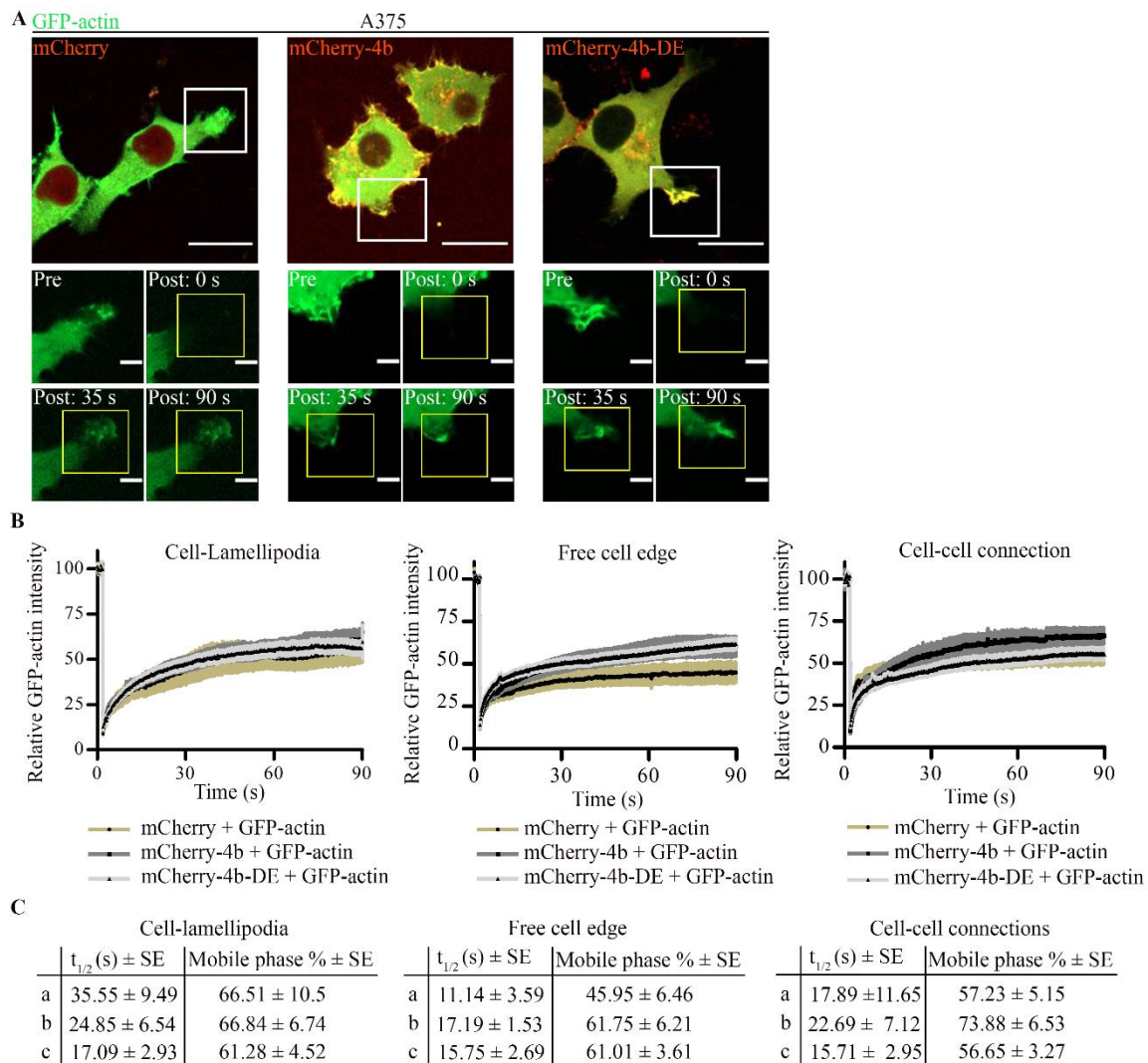
Figure 33. PMCA4b expression does not affect F-actin turnover. (A+B) Confocal microscopy images of A375 cells co-transfected with GFP-actin and one of the constructs for

48 hours as indicated. All FRAP experiments were done in phenol-free DMEM at 37 ºC using spinning-disc confocal microscope. **(A).** FRAP experiment was initiated by photobleaching of GFP-actin at three cell positions (ruffling lamellipodia, cell-cell connections and free cell edge) and GFP signals were recorded every 0.2 s for 90 seconds. Scale bar, 20 μm. Insets in (A) represent magnified part of ruffling lamellipodia at different time intervals from pre and post photobleached GFP-actin. Scale bar, 2 μm. **(B).** Graphs represent mean relative GFP-actin fluorescent intensity ± SEM of three independent experiments. The number of photobleached areas for mCherry, mCherry-PMCA4b and mCherry-PMCA4b-DE are as follow: ruffling lamellipodia (n = 8, n = 13, n = 23), cell-free edge (n=9, n=12, n=15) and cell connections (n=5, n=8, n=12). **(C)** From data in (B), $T_{1/2}$ and mobile phase ± SEM were calculated using GraphPad Prism software.

5.5. PMCA4b activity protects cells from Ca^{2+} induced actin depolymerization.

High free intracellular Ca^{2+} level was reported to induce F-actin depolymerization [183,212–214]. To test if PMCA4b can reverse the Ca^{2+} induced depolymerization of F-actin, we transiently co-transfected A375 cells with actin tagged with the Ca^{2+} indicator GCaMP2 (GCaMP2-actin) or GFP (GFP-actin) with one of the following constructs: mCherry, mCherry-PMCA4b or the non-functional mutant mCherry-PMCA4b-DE and applied the Ca^{2+} ionophore A23187 to initiate Ca^{2+} influx. As shown in Figure 34, once A23187 was added a sustained increase in near-actin Ca^{2+} concentration was detected as monitored by changes in GCAMP2-actin fluorescence in cells expressing the non-functional mCherry-PMCA4b-DE while GCAMP2 fluorescence returned to the baseline relatively quickly in the wild type mCherry-PMCA4b expressing cells. In parallel with the A23187 induced increase in intracellular Ca^{2+} concentration, we observed a dramatic change in cell shape indicated by the loss of protrusions, membrane blebbing and cell shrinkage of the cells expressing mCherry-PMCA4b-DE or mCherry. No such changes were observed in cells expressing the functional mCherry-PMCA4b that responded to the A23187 induced incoming Ca^{2+} signal quickly (Figure 35A, Video 5). Further analysis of cell shape changes showed an increase in circularity (1.64x and 1.83x) and a decrease in the area (28.4% and 42.7%) of the control mCherry or the non-functional mCherry-PMCA4b-DE mutant expressing cells, respectively. No significant change in morphology parameters or stress fibers could be observed when wild type mCherry-PMCA4b was expressed in A375 cells. Cytochalasin D - a potent inhibitor of actin polymerization - showed cell shape loss in all cell types with or without PMCA4b. When A23178 was applied in the absence of extracellular Ca^{2+} (Ca^{2+} free HBSS buffer containing EGTA) no change in

cell shape could be detected, ensuring that the observed effects were indeed induced by Ca^{2+} over-load (Figure 35B, Video 6).
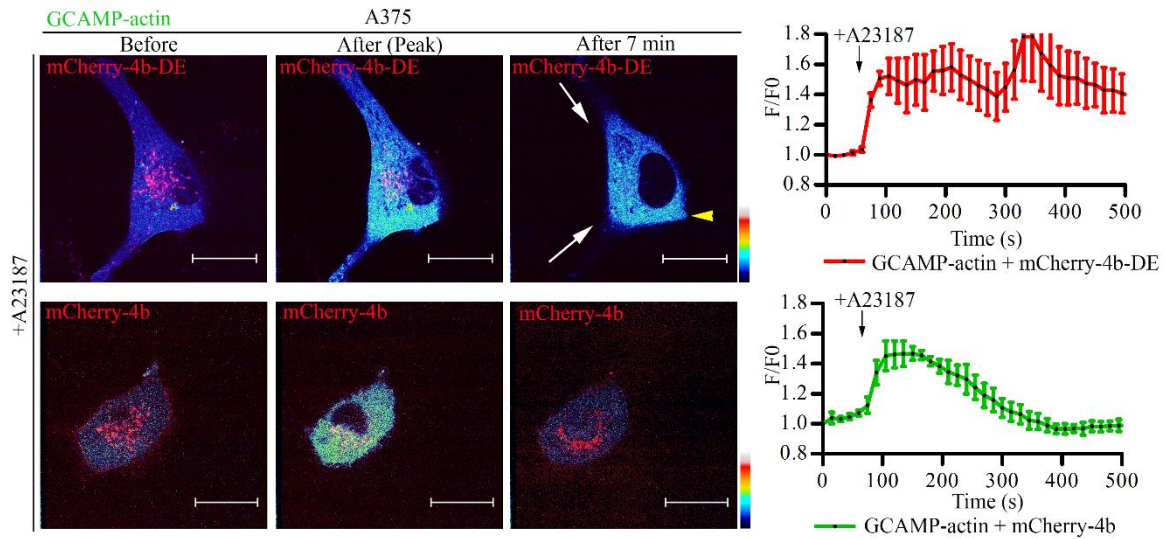
Figure 34. PMCA4b activity is essential for F-actin integrity. Live cell imaging of A375 cells transfected with GCAMP2-actin and either mCherry-PMCA4b or mCherry-PMCA4b-DE. After addition of 2 µM A23187, near actin signals were recorded every 15 seconds for 10 minutes by a spinning-disc confocal microscope, 100x oil immersion objective. Images at different timing were represented as indicated. GCAMP-actin signal retraction is indicated by arrowheads. Scale bar, 20 µm. Graph shows mean relative fluorescent intensity values (F/F0) ± SEM from two cells (two ROIs/cell) of two independent experiments. The addition of A23187 was indicated by arrows.
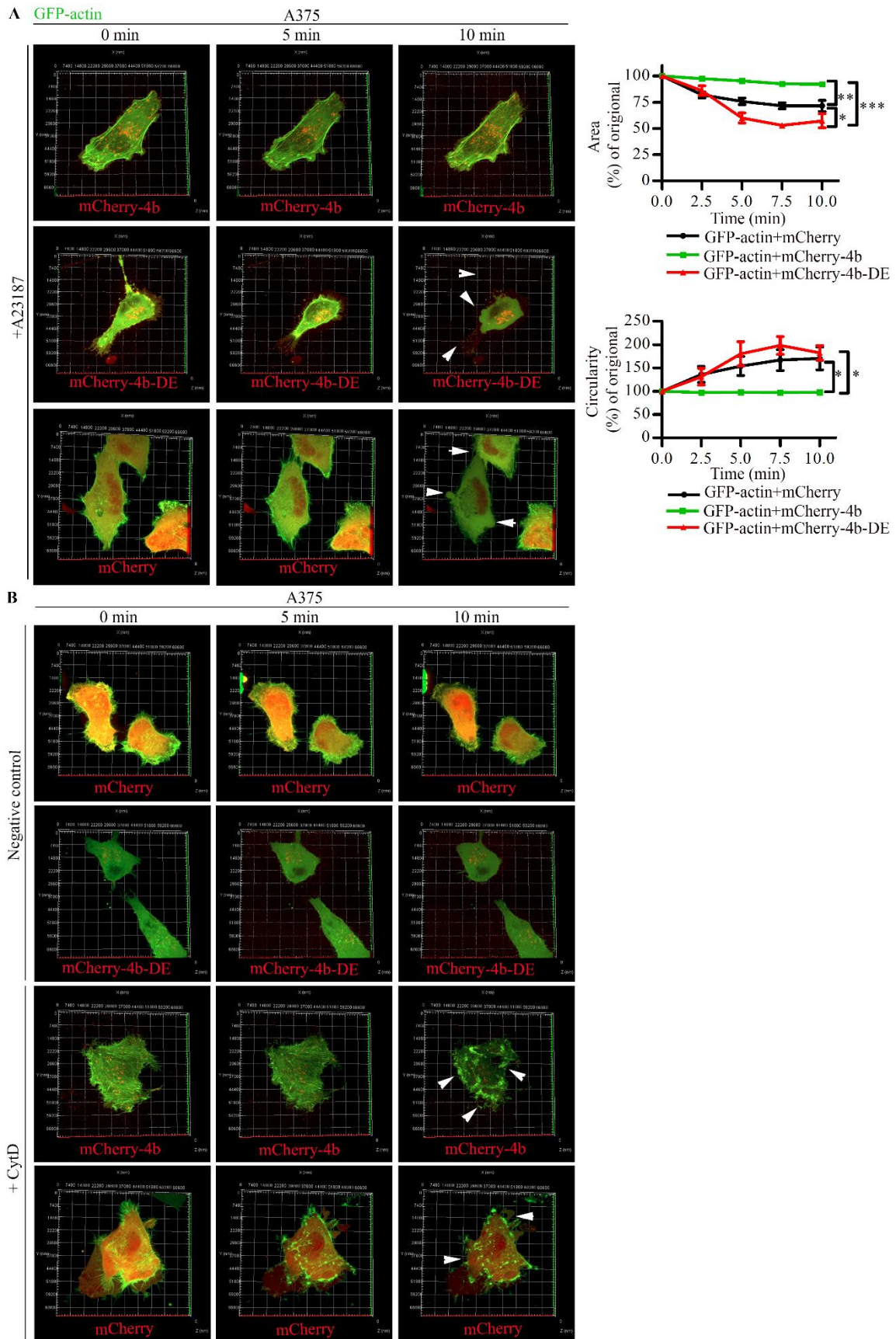
Figure 35. PMCA4b protects cells from F-actin depolymerization and collapse upon cytosolic Ca²⁺ overload. (A+B) A 3D confocal microscopy images of A375 cells expressing

GFP-actin + one the mCherry constructs (pmCherry-C1, mCherry-PMCA4b, or mCherry-PMCA4b-DE) after addition of (A) 2 µM A23187 or (B) 2.5 µM cytD, or 2 µM A23187 in a HBSS buffer without Ca^{2+} containing 100 µM EGTA, as indicated. Live microscope image recording was done every 15 seconds for 10 minutes using a spinning-disc confocal microscope, 100x oil immersion objective. Images shown are presented at 0, 5 and 10 minutes intervals. Changes in cell shape were indicated by arrowheads. Morphology analysis (area and circularity) of 2-3 cells in (A) were analyzed by ImageJ software. Data show mean ± SEM and significance is calculated for the end time points.

Endogenous F-actin staining with Phalloidin-TRITC confirmed the above findings (Figure 36). Cells expressing mCherry-PMCA4b-DE or mCherry started to shrink, form membrane blebs and rounding in response to A23187 (Figure 36A) resulting in circularity and area changes while cells expressing the wild type pump remained mostly intact, as shown in the graphs of Figure 36B. All these data indicate that the Ca^{2+} removal capacity of PMCA4b could sufficiently prevent Ca^{2+} induced actin depolymerization in A375 cells.
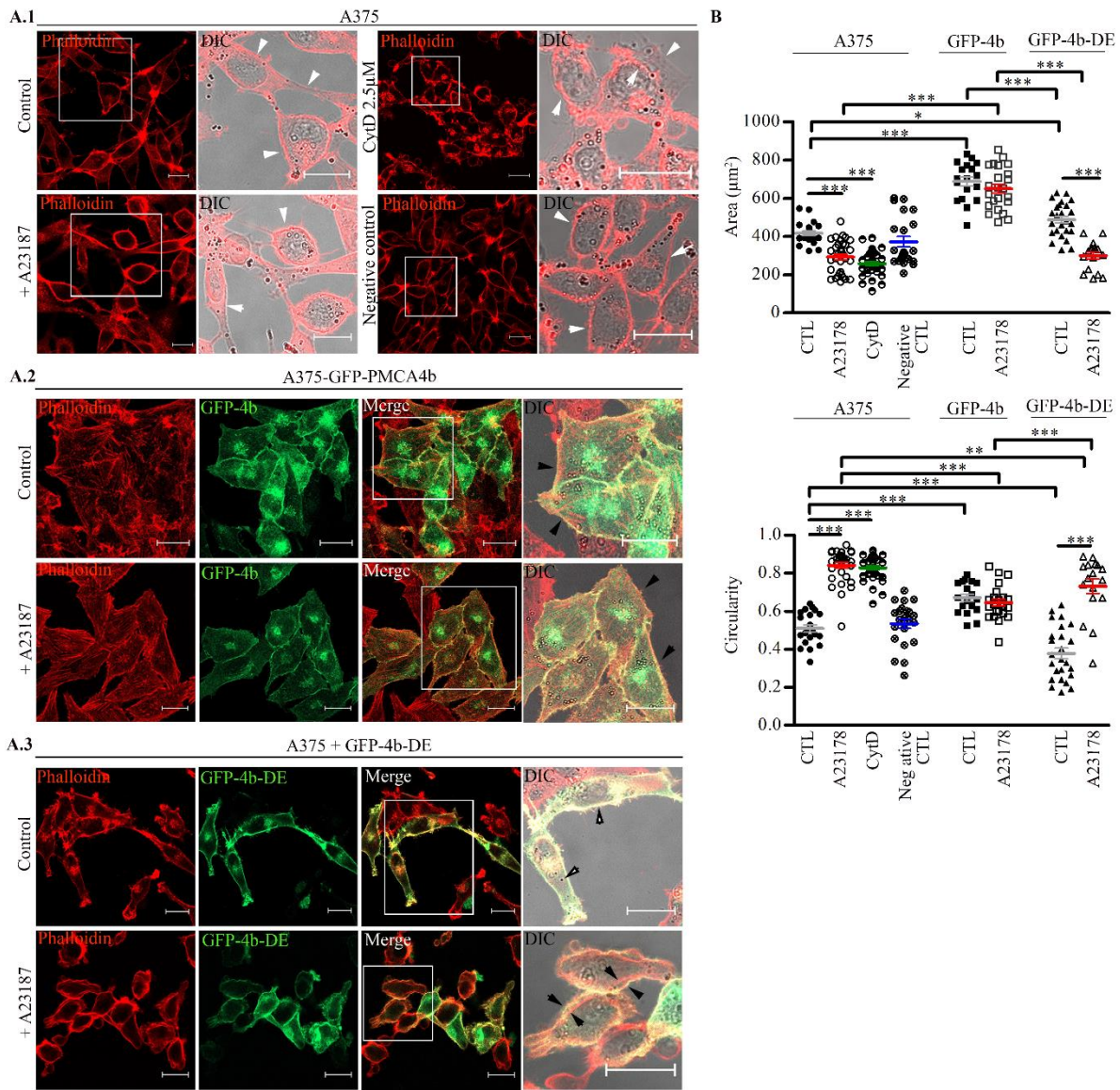
Figure 36. PMCA4b protects cells from Ca²⁺ overload induced cell shape changes. (A.1+A.2+A.3) Confocal microscopy images of cells stained with Phalloidin-TRITC after the following treatments: 2 μM A23187 in HBSS buffer with Ca²⁺, 2 μM A23187 in absence of Ca²⁺ + EGTA (negative control), or 2.5 μM cytD (positive control). Treatments were kept for 10 minutes at 37 ºC. Scale bar, 20 μm. DIC images were acquired to show cell boundaries. Position of actin to cell periphery is indicated by arrowheads. **(B)** A scatter plot for area and circularity parameters was analyzed for each cell type (n= 17-33) by ImageJ software. Data represents mean ± SEM.

5.6 PMCA4b induces F-actin re-arrangement by cofilin re-localization and formation of a front-to-rear Ca²⁺ concentration gradient in A375 melanoma cells.

It was reported that cytosolic Ca^{2+} can affect the actin cytoskeleton by inducing dephosphorylation and activation of the actin severing protein cofilin [192]. Therefore, we investigated the effect of PMCA4b on cofilin localization and activity. As shown in Figure 37A, cofilin is concentrated to the lamellipodia in A375-GFP-PMCA4b cells while positioned to the protrusions of the control and mutant GFP-PMCA4b-DE expressing A375 cells. Cofilin activity is controlled by its phosphorylation status at serine 3. Therefore, we tested the phosphorylation of cofilin by Western blotting that revealed no significant differences in p-cofilin protein levels between A375-GFP-PMCA4b and A375 melanoma cells (Figure 37B). Altogether, these data suggest that cofilin re-localization to the leading edge rather than changing its overall activity was responsible for actin re-arrangements in PMCA4b expressing A375 cells.
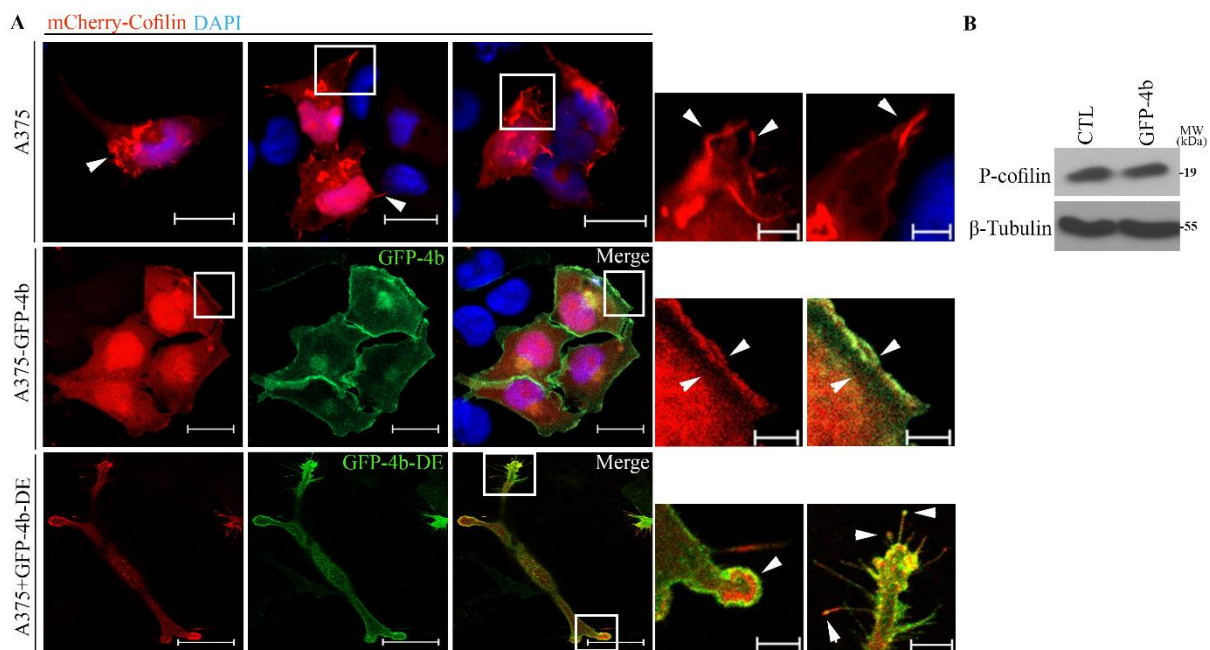
Figure 37. PMCA4b at the leading edge induces cofilin re-location. (A) Confocal microscopy images of A375 and A375-GFP-PMCA4b cells transfected with Cofilin-pmCherryC1 or co-transfected with GFP-PMCA4bDE in A375 cells after DAPI nuclear staining. Scale bar, 20 μm. Insets represent a magnified part of cells. Cofilin position is indicated with arrowheads. Scale bar, 5 μm. **(B)** A375 and A375-GFP-PMCA4b were cultured and the protein level of P-cofilin was measured by Western blot. β-tubulin was used as a loading control.

Several previous studies demonstrated that a Ca^{2+} concentration gradient across the cell affected cell polarization and migration [184,215,216]. Recent experiments demonstrated that

PMCA4b has a role in the formation of a front-to-rear increasing Ca2+ concentration gradient in migrating HUVEC cells [126]. Therefore, to evaluate the effect of PMCA4b and its trafficking mutant on the distribution of cytosolic free Ca^{2+} concentration, we transiently expressed the Ca^{2+} indicator R-GECO. As shown in Figure 38, analysis of the lines drawn across the cells for the recorded GFP and RGECO fluorescent signals showed that GFP-PMCA4b localized to the leading edge that coincided with a front-to-rear increasing Ca^{2+} concentration gradient, as indicated by the increasing RGECO signal. However, in both parental and trafficking mutant GFP-PMCA4b-LA expressing cells an even distribution of the fluorescence signal was observed. These data indicate that PMCA4b expression and localization at the leading edge was essential to induce front-to-rear increasing Ca^{2+} concentration gradient in A375 melanoma cells.
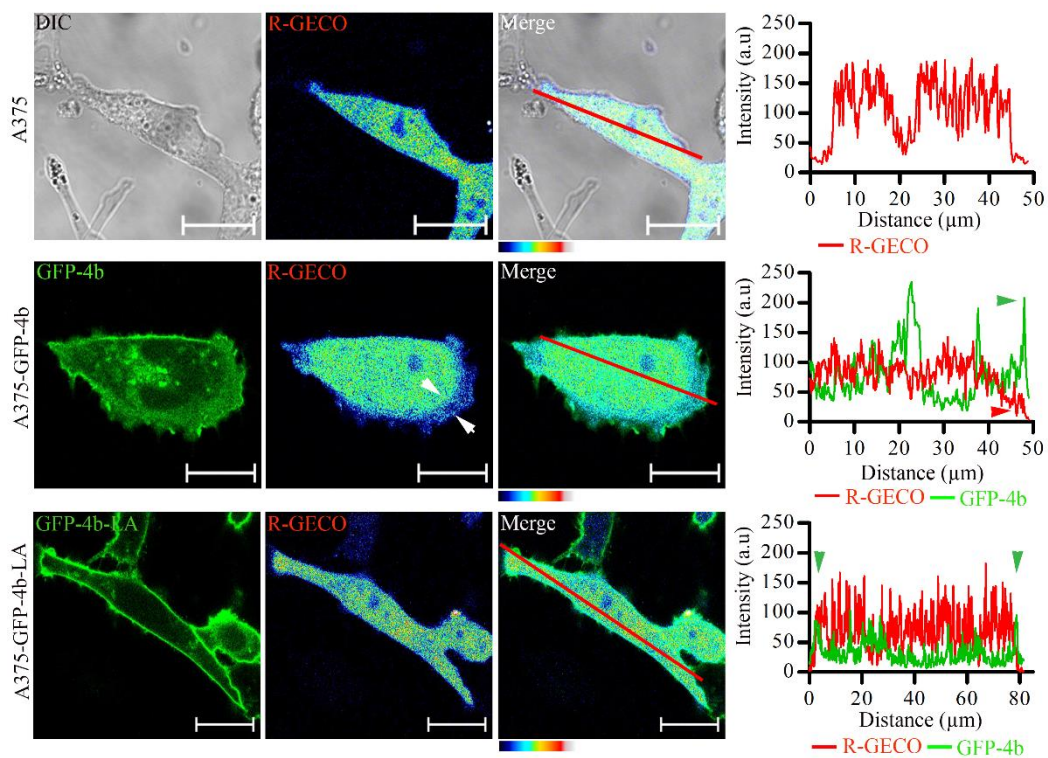
Figure 38. Proper trafficking of PMCA4b is essential for inducing front-to-rear increasing Ca^{2+} concentration gradient in A375 cells. Confocal microscopy images of cells transfected with CMV-R-GECO1 plasmid. While arrowheads indicate the position of low Ca^{2+} level. Scale bar, 20 µm. Line plot was obtained from analysis of the lines (red) drawn across the cells using ImageJ software. The GFP signals at the cell periphery are indicated by arrowheads.

6. Discussion

Ca^{2+} homeostasis is critical for normal cell physiology and any imbalance in its intracellular concentration is associated with a variety of diseases. Therefore, cells use a molecular toolkit that includes channels, pumps and exchangers to maintain free cytosolic Ca^{2+} level [41]. Alterations in the expression, activity, regulation and stability of these molecules are shown to affect cellular proliferation, survival, migration and metastasis [217]. Melanoma, a type of skin cancer, results from abnormal growth of pigment-containing cell named melanocyte. Metastasis is the main cause of death in patients with melanoma. Several studies showed changes in the expression of Ca^{2+} channels and their contribution to melanoma progression and metastasis [218].

PMCA4b is a plasma membrane Ca^{2+} transporter essential for lowering cytosolic Ca^{2+} concentration. Our laboratory has reported that PMCA4b expression is downregulated in BRAF mutant melanoma cells and its overexpression resulted in reduced melanoma cell migration and metastasis. In addition, we found that inhibition of the main constitutive pathway in melanoma cells (BRAF/MEK/ERK MAPK pathway) via BRAF or MEK inhibitors increased PMCA4b expression at both the mRNA and protein levels, and decreased melanoma cell migration and metastasis [82]. Therefore, in this study we investigated other regulators/pathways already reported to be active in melanoma for their role in PMCA4b regulation and melanoma metastasis. We found that p38 MAPK pathway inhibition enhanced PMCA4b protein level by increasing its stability at the plasma membrane and reducing its degradation through the endolysosomal pathway. In addition, we showed that inhibition of p38 MAPK activity led to reduced migration and metastatic activity of BRAF mutant melanoma cells *in vitro* partially through restoring PMCA4b function.

Other changes observed with PMCA4b overexpression in BRAF mutant melanoma cells include changes in cell morphology and motility [82]. For cells to metastasize, actin remodeling is required to allow changes in cell shape, polarity and motility. Several studies showed involvement of cytosolic Ca^{2+} level on many actin-related processes and actin reorganization (Martin-Romero *et al*, 2017; Tsai *et al*, 2015). In this study, we found that proper PMCA4b activity and trafficking were essential to induce actin re-arrangements and morphological changes including increased lamellipodia formation, cell-cell contacts, stress fiber formation and reduced motility. In addition, we found that PMCA4b activity is important to maintain actin cytoskeleton integrity in case of Ca^{2+} overload. Changes observed with cell polarity and reduced motility were also explained by the activity of PMCA4b and its proper

trafficking to the leading edge to generate front to rear increasing Ca^{2+} concentration gradient across the cell and by its ability to induce cofilin re-localization.

6.1. Inhibition of the p38 MAPK pathway protected PMCA4b from degradation and reduced migration BRAF mutant melanoma cells.

It was found that BRAF and MEK inhibitors upregulated PMCA4b at both the mRNA and protein levels in BRAF mutant melanoma cells and reduced melanoma cell migration and metastasis [82]. In the present study, other active pathways - p38 MAPK, JNK and NF-κB - implicated in melanoma progression and metastasis were tested for their effects on PMCA4b levels. P38 MAPK activity affects many downstream substrates such as transcription factors and protein kinases that are involved in cytoskeleton remodeling, protein degradation and localization, chromatin remodeling, cell differentiation, proliferation and cell migration [147]. We found that the p38 MAPK pathway acts as a novel modulator of PMCA4b expression. Similar to a previous study, we demonstrated that p38 MAPK is already active in BRAF mutant melanoma cells as shown by the high phosphorylation level of its substrate HSP27 and significant reduction of p-HSP27 upon p38 inhibitor treatment. [200]. Western blot analysis and fluorescence imaging showed that inhibition of p38 MAPK activity greatly enhanced PMCA4b in BRAF mutant cells while no change in PMCA4b level was observed in BRAF wild-type cells. In parallel, we observed reduced P-ERK in these cells after p38 inhibitor treatment that can be explained by the loss of the negative feedback loop between ERK and p38 in melanoma cells, as reported by Estrada *et al.*, 2009 [18].

P38 MAPK inhibition enhanced PMCA4b protein level but did not affect its mRNA expression, therefore, we assumed post-translational regulation. PMCA4b localization to the plasma membrane is critical for its proper function [104]. In BRAF mutant melanoma cells PMCA4b expression is downregulated. Moreover, when over-expressed it is localized more to the intracellular vesicles than to the plasma membrane. Using confocal microscopy, we showed that p38 MAPK inhibition enhanced plasma membrane localization of the pump. This accumulation of PMCA4b at the plasma membrane enhanced the Ca^{2+} clearance capacity of the cells indicating that the pump was active. Vemurafenib upregulated PMCA4b at both the mRNA and protein levels, however, interestingly our results show that part of its effect could also be contributed to its increased plasma membrane stability.

Proteins vary in their half-lives, some can be degraded in minutes and others in several days. Protein degradation is under tight control and is an important part of cell regulation. For example, many regulatory proteins such as transcription factors need to be degraded rapidly to allow their level to change properly in response to stimuli [219]. A study in rat brain showed

that PMCA is highly stable and has a long half-life with slow turnover rates [220]. The main pathways for protein degradation include ubiquitin-proteasomes, endolysosomes and autophagy [221]. These pathways are found de-regulated in melanoma to drive tumor progression [222]. Several studies reported that protein kinases including p38 MAPK are involved in protein internalization and hence degradation [201,223]. Our results showed for the first time that p38 MAPK activity regulates PMCA4b internalization in BRAF mutant melanoma cells, and its inhibition prevents downstream degradation through the endolysosomal system. In addition, we showed similar results in two other cell line models, HeLa cells and the non-tumorigenic doxycycline-inducible HEK cell lines. Previously, we identified a di-leucine-like motif near the C-terminus of PMCA4b that controls its endocytosis [104]. Further study is needed to identify if the same motif is involved in p38 MAPK induced PMCA4b internalization.

In contrast to vemurafenib, p38 inhibitor treatment decreased cell proliferation with no significant toxic effect. In addition, p38 inhibitor treatment showed reduced colony formation similar to that seen in colorectal and ovarian cancers [224,225]. Interestingly, while the parental cells formed compact cell aggregates/colonies, the PMCA4b expressing cells displayed flat monolayer in culture. P38 inhibitor treatment of the parental cells resulted in a similar monolayer appearance with reduced colony formation suggesting that the enhanced PMCA4b abundance played a role. This indicates that an increase in PMCA4b expression may result in reduced tumor-forming capacity of melanoma cells.

P38 MAPK activity was also correlated to cell migration. A study by Rousseau *et al.*, 1997 [165] reported for the first time the involvement of p38 MAPK activity in endothelial cell migration upon stimulation with VEGF. This was explained by the effect of one of the p38 MAPK substrates HSP27 on cytoskeleton re-arrangements. In this study, p38 MAPK inhibition significantly reduced migration of BRAF mutant melanoma cells and we found that this was partially PMCA4b dependent. Interestingly, a study on purified PMCA4b protein showed that there is a functional interaction between PMCA4b and actin cytoskeleton [189]. Therefore, we studied further the role of PMCA4b in actin cytoskeleton reorganization and cell motility, as discussed in the next section.

Besides 2D cell cultures, 3D cell cultures have been utilized more extensively as an *in vitro* tool to evaluate tumor growth and to screen for new anticancer drugs since they mimic solid tumors in their real environment in terms of spatial architecture, gene expression, physiological responses and drug resistance mechanisms [202]. P38 inhibitor has been tested using 3D spheroids in head and neck squamous cell carcinoma and glioma where it resulted in

reduced spheroid growth. Similarly, p38 inhibitor decreased growth of melanoma spheroids, however, much less effectively than the BRAF inhibitor, vemurafenib. Interestingly, no spheroid formed in the case of BRAF wild type melanoma cells (MEWO), and a delay in spheroid formation was observed in the case of A375-GFP-PMCA4b cells where spheroids were grown significantly smaller. A possible factor for this delay could be differences in integrin expression as integrins are important elements of spheroid formation and tissue integrity. In metastatic melanoma, β1 and β3 integrins were reported to be upregulated [203]. β4 integrin is an integrin involved in hemidesmosome formation and its disruption is found to result in keratinocyte migration and carcinoma invasion [204]. In this study, we found that β4 integrin is upregulated in BRAF mutant A375 cells and significantly reduced upon PMCA4b overexpression or treatment with p38 inhibitor. β4 protein is lost completely in the BRAF wild-type MEWO cells. These data suggest that a decrease in β4 integrin expression could be responsible for the delay in spheroid formation and reduced metastatic activity of cells with high PMCA4b abundance.

The reversal of multicellular spheroids can be utilized as an *in vitro* metastatic model [199]. Using this method, A375-GFP-PMCA4b and A375 cells treated with p38 inhibitor showed significant inhibition of metastatic activity when compared to the control cells without treatment. This is in good accordance with our previous findings on PMCA4b as a putative metastatic suppressor [82].

In conclusion, we found that p38 MAPK acts as a promoter for melanoma metastasis and this partially could be through increased internalization and degradation of PMCA4b. The present study suggests that p38 MAPK is a potential new therapeutic target in BRAF mutant melanoma. Moreover, inhibition of this pathway may provide another tool to overcome drug resistance.

6.2. PMCA4b inhibits migration of BRAF mutant melanoma cells through actin cytoskeleton remodeling.

Cell migration is a multi-step process that starts with protrusion extensions at the leading edge such as lamellipodia or filopodia, adhesion formation and finally cell tail retraction. The driving force for all these steps includes changes in actin cytoskeleton organization in response to a migratory signal [226]. Changes in cytosolic calcium affect actin dynamics, relocation of focal adhesions, rear-end retraction and cell migration [116,185]. A molecular toolkit is utilized by cells to maintain Ca^{2+} homeostasis and PMCAs are a key regulator of maintaining low basal free cytosolic Ca^{2+} concentration. In melanoma, changes in the expression of these tools and their effect on migration have been reported [218]. Our laboratory showed that the PMCA4b

Ca^{2+} pump is downregulated in BRAF mutant melanoma and identified this pump as a metastatic suppressor [82], however, the exact mechanism has not been determined. As PMCA4b is a key regulator of cytosolic Ca^{2+} concentration and Ca^{2+} affects actin cytoskeleton remodeling we hypothesized that PMCA4b reduced migration of BRAF mutant melanoma cells by inducing actin cytoskeleton rearrangements.

The plasticity of cell migration is a prerequisite for the dissemination of tumor cells to distal parts of the body. A transition between the amoeboid and mesenchymal type of migration has been reported in melanoma cells to adapt to changes in extracellular matrix stiffness and surrounding microenvironment [227]. In the present study, in contrast to the fast-moving A375 cells with dynamic protrusions, we found that A375-GFP-PMCA4b cells migrate significantly slower with enhanced polarity. As our previous study showed that PMCA4b expression did not affect MET markers (E-cadherin, ZEB1, snail, and vimentin) [82], we suggest that it may induce a transition from fast-to-slow mesenchymal migration type rather than MET transition phenotype.

Other changes observed in this study with PMCA4b expression are morphological changes and Ca^{2+} ion through its effect on the actin cytoskeleton is reported to have a role [228,229]. A study showed that an increase in cytosolic Ca^{2+} concentration in pulmonary endothelial cells by activation of store-operated Ca^{2+} channels (SOCs) induced changes in cell shape in an actin-cytoskeleton-dependent way [230]. We found a dramatic effect on cells and culture morphology upon PMCA4b expression in melanoma cells including increased formation of lamellipodia, cell-cell contacts, stress fibers and cell roundness. Similar changes in cell culture morphology parameters of a breast cancer cell line (MCF-7) were observed and this suggests general role of PMCA4b in the determination of cell shape.

For cell motility, focal adhesions need to be assembled at the cell front and disassembled at its rear. Stress fibers connect to focal adhesion and help cells to adhere and migrate. It was reported that stress fibers in cells with high motility have fewer, thinner and less dynamic stress fibers than static cells, and that slow re-arrangement of actin stress fiber bundles and slow focal adhesion turnover may inhibit cell motility [231,232]. This could explain the slow motility observed in A375-GFP-PMCA4b cells that have thick and high number of stress fibers in comparison to the fast-moving parental cells where stress fibers are nearly absent. Similarly, silencing PMCA4b expression in MCF-7 cells resulted in a nearly complete absence of stress fibers. In addition, we observed different localization of vinculin, a component of focal adhesion, upon PMCA4b expression in A375 cells. In A375-GFP-PMCA4b cells, it was mostly connected to the ends of stress fibers while in the case of the parental cells it clustered at the

cell periphery facing towards the protrusions. Since high cytosolic Ca^{2+} concentration has been reported to enhance focal adhesion turnover [185] we surmise that PMCA4b reduces focal adhesion turnover by reducing nearby Ca^{2+} [233], resulting in reduced cell motility. A study on ovarian cancer cells showed that increased focal adhesion turnover rate and consequently cell migration was mediated by SOCE [234]. In addition, we found not only vinculin localization was changed but also expression. In A375-GFP-PMCA4b cells, vinculin expression was downregulated compared to the parental cells. A study on bone marrow-derived mesenchymal cells showed that the addition of a Ca^{2+} channel blocker after exposure to electromagnetic field reduced vinculin expression to its basal level and resulted in reduced cell migration [235]. Therefore, we suggest that the observed decrease in vinculin expression in A375-GFP-PMCA4b cells could be one factor that resulted in reduced migration activity of melanoma cells.

We found that not only PMCA4b activity was essential for changes in cell shape, motility, migration and F-actin distribution but also its proper trafficking. A trafficking mutant A375-GFP-PMCA4b-LA showed similar F-actin arrangements, morphology and migration activity as the parental cells. This is in agreement with other reported studies that indicated the effect of membrane protein trafficking on cell shape and motility [205,206]. In addition, we found that A375 cells expressing the non-functional PMCA4b-DE are similar to the parental cells and did not induce formation of stress fibers, lamellipodia or cell-cell connection. These data indicate the importance of Ca^{2+} concentration in morphology and actin dynamics changes. In good agreement with our findings, a study in HeLa and prostate cancer (PC)-3, showed that activation of Ca^{2+} channel transient receptor potential melastatin (TRPM2) after treatment with H_2O_2 caused loss of stress fibers, filopodia formation and focal adhesion disassembly, and all these changes led to increased cell migration [236].

Changes in F-actin dynamics and formation of lamellipodia at the leading edge direct cell migration and cell polarity [237]. We found that in A375 cells expressing the functional PMCA4b F-actin localized to the lamellipodia at the cell front occupying a large part of the cell front while in cells expressing the non-functional PMCA4b or in the parental cells polymerized actin was more abundant at cell protrusions. Co-localization of PMCA4b and F-actin at the lamellipodia and cell-cell connections may suggest close contact between the pump and actin, as reported previously [189,238]. We could not find any significant differences in the rate of actin recovery or the steady-state F-actin level after photobleaching (FRAP) between cells with or without PMCA4b indicating that PMCA4b did not affect actin polymerization.

Many studies have shown that an increase in cytosolic Ca^{2+} concentration can induce F-

actin depolymerization with cell shape deformation [212–214]. Using the Ca^{2+} sensor GCAMP2 fused to actin (GCAMP2-actin) we found that persistent increase in cytosolic Ca^{2+} resulted in collapse of the actin cytoskeleton that accompanied with a profound change in cell shape while the expression of the fully active PMCA4b maintained both F-actin and cell shape integrity. These data suggest that PMCA4b activity act as a negative modulator of high cytosolic Ca^{2+} induced F-actin depolymerization.

It has been suggested that high concentration of cytosolic Ca^{2+} can induce actin rearrangement through the actin severing protein cofilin. Cofilin does not only mediate actin depolymerization but also can affect actin polymerization through providing G-actin monomers for the formation of new barbed ends. Cofilin was also reported to be involved in invadopodia and lamellipodia formation [190]. A study showed that Ca^{2+} entry by the CRAC channel is important for the activity of cofilin and lamellipodia formation [182]. In the present study, we found that mCherry-cofilin is re-localized from the protrusions to the lamellipodia of the PMCA4b expressing cells while the non-functional pump was not effective. The low Ca^{2+} concentration environment provided by the pump at the cell front may result in low cofilin activity and subsequent reduction in actin turnover. Interestingly, several studies showed that inhibition or knocking out cofilin reduced cell polarity [191,239]. The effect of cofilin expression on PMCA4b localization and in turn formation of Ca^{2+} concentration gradient still needs further study.

A study on HUVEC cells showed that an increasing front-to-rear cytosolic Ca^{2+} concentration gradient was essential for directional movement and PMCA4b localization at the cell front was vital for the effect. Lowering the free Ca^{2+} concentration at the cell front by PMCA4b enables effective local Ca^{2+} signaling by the local activity of Ca^{2+} entry channel STIM1/ORAI [126]. In agreement with this finding, our results showed that localization of PMCA4b at the leading edge also generated a front-to-rear increasing Ca^{2+} concentration gradient across the melanoma cells. Interestingly, neither parental cells nor the trafficking mutant PMCA4b-LA expressing cells displayed such Ca^{2+} gradient. These results indicate that not only activity but also proper trafficking are essential for generating Ca^{2+} gradient across the cell. Changes in cytosolic Ca^{2+} concentration throughout the cell could be responsible for the local changes in actin dynamics, morphology and hence motility of BRAF mutant melanoma cells.

Many tumor suppressors disappear in cancerous cells as an advantage for the cell to grow, therefore, the possibility for direct targeting is not applicable. In the case of PMCA4b, we reported some inhibitors/drugs that can be used to rescue PMCA4b from degradation such as

the the videly used BRAF inhibitors (vemurafenib or dabrafenib), HDAC inhibitors (vorinostat or valproic acid) and p38 inhibitor (identified in the present study). Treatment of BRAF mutant melanoma cells with these inhibitors resulted in a dramatic decrease in cell migration [82,94,240]. Identifying the actin cytoskeleton as one of the targets affected by PMCA4b and its possible role in PMCA4b induced anti-migratory activity can provide new insights for finding new potential therapeutic options to overcome drug resistance reported with currently used anti-metastatic drugs.

In conclusion, our results show that PMCA4b expression and proper trafficking are essential to fulfil its anti-migratory function in BRAF mutant melanoma cells, and this function is mediated by its effect on actin cytoskeleton remodeling. The expression of a fully functional PMCA4b in these cells showed a dramatic change in cell shape and cell culture morphology, a reduced motility and polarized migratory character. Along with these changes, we observed an increase in the formation of cell-cell connections, stress fiber and lamellipodia formations and a decrease in vinculin expression. These effects could be a result of PMCA4b redistribution to the leading edge, and generation of front-to-rear increasing Ca^{2+} concentration gradient with re-localization of cofilin and polymerized actin from protrusions to the leading edge. The effect of PMCA4b expression on actin redistribution was also observed in MCF-7 cells suggesting that PMCA4b is a general modulator of the actin cytoskeleton.

7. Summary

The plasma membrane Ca^{2+} pump (PMCA4b) is a key regulator of maintaining low basal cytosolic calcium ion concentration, and its de-regulation results in imbalance of Ca^{2+} homeostasis that could contribute to tumor progression. Melanoma is a type of skin cancer with a high rate of deadly metastasis. Earlier we found downregulation of PMCA4b in BRAF mutant melanoma cells and suggested the possible contribution of PMCA4b loss in tumor metastasis. In the present study, we investigated the role of p38 MAPK in PMCA4b degradation using a BRAF mutant melanoma cell line. In addition, we investigated the way PMCA4b mediates actin cytoskeleton remodeling and cell migration.

Our main findings are as follows:

1. Inhibition of p38 MAPK increased PMCA4b abundance and plasma membrane stability by reducing its internalization and consequent degradation through the endolysosomal pathway.
2. Using HEK cells with a doxycycline-inducible system, we confirmed that p38 MAPK acts as a universal modulator of PMCA4b endocytosis.
3. Inhibition of p38 MAPK reduced spheroid formation, migration and metastatic activity of BRAF mutant melanoma cells, at least partly through the upregulation of PMCA4b. We suggest that the altered spheroid formation could be due to changes in β4 integrin expression.
4. Inhibition of p38 MAPK reduced colony formation with monolayer type of cell growth.
5. Expression of PMCA4b caused a dramatic change in cell culture morphology, increased cell-cell connections, lamellipodia and stress fiber formation. We found that proper trafficking of PMCA4b was essential for these changes.
6. PMCA4b activity is needed for maintaining the integrity of the actin cytoskeleton during Ca^{2+} overload.
7. Localization of PMCA4b at the cell front is essential for maintaining front-to-rear increasing Ca^{2+} concentration gradient and re-localization of the actin severing protein cofilin for proper actin cytoskeleton re-arrangement and reduced cell motility.

In conclusion, this study shows that protecting the putative tumor suppressor PMCA4b from p38 MAPK mediated degradation can result in a less aggressive melanoma cell phenotype with low migratory and metastatic potential. In addition, we found that activity and proper

trafficking of PMCA4b was required for actin cytoskeleton remodeling and consequent anti-migratory function.

8. List of Tables

Table 6. Antibodies for Western blot and immunostaining assays

Name	Source, Cat #	Type	Dilution
Anti-PMCA4b (JA3)	Sigma-Aldrich, MABN1801	Mouse monoclonal	1:1000
Anti-PMCA4 (JA9)	Sigma-Aldrich, P1494	Mouse monoclonal	1:1000
Anti-PMCA1	Affinity BioReagents, PA1-914	Rabbit polyclonal	1:1000
Anti-NA$^+$/K$^+$ ATPase	Enzo Life Sciences, BML-SA247	Mouse monoclonal	1:2000
Anti-HSP	Cell Signaling Technology, 2402	Mouse monoclonal	1:1000
Anti-PHSP27	Cell Signaling Technology, 9709	Rabbit monoclonal	1:1000
Anti-P38	Cell Signaling Technology, 9212	Rabbit monoclonal	1:1000
Anti-PP38	Cell Signaling Technology, 9216	Mouse monoclonal	1:1000
Anti-ERK1/2 (MK1)	Cell Signaling Technology, 9102	Rabbit monoclonal	1:1000
Anti-phospho-p44/42 MAPK (ERK1/2)	Cell Signaling Technology, 4370	Rabbit monoclonal	1:2000
Anti-β4-integrin (D8P6C)XP	Cell Signaling Technology, 14803	Rabbit monoclonal	1:1000
Anti-β-tubulin	Abcam, ab6046	Rabbit polyclonal	1:1000
Anti-GFP	Aves, GFP-1020	Chicken polyclonal	1:5000
Anti-vinculin	Thermo Fisher scientific, 700062	Rabbit monoclonal	1:100
Anti-P-cofilin (Ser3)	Cell Signaling Technology, 77G2	Rabbit monoclonal	1:1000
Anti-EEA1	Abcam, Ab2900	Rabbit polyclonal	1:250
Anti-Rab7 (D95F2) XP	Cell Signaling Technology, 9367	Rabbit monoclonal	1:100
Anti-Rab11	Cell Signaling Technology, 5589	Rabbit monoclonal	1:100
Anti-LAMP1 (D2D11) XP	Cell Signaling Technology, 9091	Rabbit monoclonal	1:200
Anti-LC3A/B	Cell Signaling Technology, 12741	Rabbit monoclonal	1:100

9. List of Figures

Figure 22. Spheroid growth is reduced with PMCA4b expression and/or p38i-2 treatment in A375 melanoma but not in MEWO cells.

Figure 23. P38 MAPK inhibition or knockdown strongly decreased A375 melanoma cell migration in a PMCA4b dependent manner.

Figure 24. The metastatic activity of A375 spheroids is reduced with PMCA4b expression and/or treatment with p38 and BRAF inhibitors *in vitro*.

Figure 25. Changes in area, circularity and culture morphology are observed upon GFP-PMCA4b but not GFP-PMCA4b-LA expression in A375 melanoma cells.

Figure 26. GFP-PMC4b but not the trafficking mutant GFP-PMCA4b-LA expression changed motility, migration and polarity of A375 melanoma cells.

Figure 27. Increased formation of cell-cell connections between A375 melanoma cells after GFP-PMCA4b but not PMCA4b-LA expression.

Figure 28. Increased formation of stress fibers and lamellipodia in A375 melanoma cells in PMCA4b but not in PMCA4b-LA expressing cells.

Figure 29. PMCA4b activity is essential for lamellipodia formation in A375 melanoma cells.

Figure 30. PMCA4b activity is essential for stress fiber formation in A375 melanoma cells.

Figure 31. PMCA4b silencing induced increased cell area and loss of stress fibers in MCF-7 cells.

Figure 32. PMCA4b expression results in vinculin re-location and changes in expression in melanoma cells.

Figure 33. PMCA4b expression does not affect F-actin turnover.

Figure 34. PMCA4b activity is essential for F-actin integrity.

Figure 35. PMCA4b protects cells from F-actin depolymerization and collapse upon cytosolic Ca^{2+} overload.

Figure 36. PMCA4b protects cells from Ca^{2+} overload induced cell shape changes.

Figure 37. PMCA4b at the leading edge induces cofilin re-location.

Figure 38. Proper trafficking of PMCA4b is essential for inducing front-to-rear increasing Ca^{2+} concentration gradient in A375 cells.

9.1. Contribution:

Figures 12 and 13. mRNA studies were performed in Michael Grusch's laboratory, Medical University of Vienna.

Figure 25. Rita Padányi and Randa Naffa equally contributed to the experiments and analysis.

Figure 31. Rita Padányi performed the experiments, and Randa Naffa did the calculations for the stress fiber and area graphs.

Figure 38. Rita Padányi performed the experiments and Randa Naffa did the analysis.

10. Abbreviations

ADF: actin-depolymerizing factor

ADP: adenosine diphosphate

AKT: serine/threonine kinase, protein kinase B

ALN: another-regulin

ANOVA: analysis of variance

AP1: activator protein 1

APC: antigen-presenting cells

ARC: arachidonic acid-regulated Ca^{2+} channel

Arp2/3: actin-related protein 2/3

Asp: aspartate

ATF1: activating transcription factor

ATP: adenosine triphosphate

BM: basement membrane

BMMC: bone marrow-derived mast cell

BSG: basigin

CAD: calcium release-activated calcium (CRAC)-activating domain

CaM: calmodulin

CaMKII: Ca^{2+}/calmodulin-dependent protein kinase II

CASK: calcium/calmodulin-dependent serine protein kinase

CCLA2: calcium-activated chloride channel regulator-2

CD147: cluster of differentiation 147

CDK: cyclin-dependent kinases

CDKN2A: Cyclin Dependent Kinase Inhibitor 2A

CICR: Ca^{2+} induced Ca^{2+} release

CIN: chronophin

c-KIT: tyrosine-protein kinase Kit

CNGCs: cyclic nucleotide-gated channels

CQ: chloroquine

CRAC: calcium release-activated calcium current

CREB: cAMP-responsive element binding

CTLA-4: cytotoxic T-lymphocyte associated antigen 4

CytD: cytochalasin D

DAG: diacylglycerol

DAPI: 4´,6-diamidino-2-fenilindol

DIC: differential interference contrast

DMEM: Dulbecco's modified Eagle's medium

Dox: doxycycline

DTIC: dacarbazine

DTT: dithiothreitol

DUSP6: dual-specificity phosphatase 6

ECM: extracellular matrix

EDTA: Ethylenediaminetetraacetic Acid

EEA1: early endosomal antigen 1

EGF: epidermal growth factor

EGTA: ethylene glycol tetraacetic acid

ELK-1: ETS Like-1 protein

ELN: endoregulin

EMMPRIN: extracellular matrix metalloproteinase inducer

EMT: epithelial-mesenchymal transition

ER: endoplasmic reticulum

ER-α: estrogen receptor-α

ERK: extracellular signal-regulated kinase

FA: focal adhesion

F-actin: fibrous-actin

FAK: focal adhesion kinase

FBS: fetal bovine serum

FDA: food and drug administration

FRAP: fluorescence recovery after photobleaching

G-actin: globular-actin

GAPDH: glyceraldehyde-3-phosphate dehydrogenase

GCaMP2: GFP-based Ca^{2+} probe

GFP: green fluorescent protein

GPCR: G-protein-coupled receptor

HBSS: Hanks´ Balanced Salt Solution

HDAC: histone deacetylase

HEK: human embryonic kidney

HGF: hepatocyte growth factor

HeLa: cervix adenocarcinoma cells

Hsp27: heat shock protein 27

HUVEC: human umbilical vein endothelial cell

IGF: insulin-like growth factor

IKK: IκB kinase

IL: interleukin

IP3: inositol 1,4,5-trisphosphate

IP3R: inositol 1,4,5-trisphosphate receptor

JNK: c-Jun N-terminal kinase

KO: knock out

LAMP1: lysosomal-associated membrane protein 1

LC3A/B: microtubule-associated protein 1A/1B-light chain 3

MAA: melanoma-associated antigens

MAGUK: membrane-associate guanylate kinase

MAPK: mitogen-activated protein kinase

MAP3K: MAP Kinase-kinase-kinase

MAP2K: MAP Kinase-Kinase

MAT: mesenchymal to amoeboid transition

MEF: myocyte enhancing factor

MEK: MAPK/ERK kinase

MCU: mitochondria uniporter

MCUR1: mitochondrial calcium uniporter regulator 1

MHC: major histocompatibility complex

MKs: MAPK-activated protein kinases

MLCK: myosin light chain kinase

MMP: matrix metalloprotease

MRLN: myoregulin

mTOR: mechanistic target of rapamycin

NF1: neurofibromatosis type 1

NFAT: nuclear factor of activated T-cell

NCX: Na^+/Ca^{2+} exchange

NF-κB: nuclear factor-kappa B

nNOS: neuronal nitric oxide synthase

NPTN: neuroplastin

NSCLC: non-small cell lung carcinoma

N-WASP: neural Wiskott-Aldrich syndrome protein

OMM: outer mitochondrial membrane

OPLs: oral premalignant lesions

ORAI: calcium release-activated calcium modulator

OS: overall survival

OSCC: oral squamous cell carcinoma

OSM: osmosensing scaffold for MEKK3

PBS: phosphate buffer saline

PC: prostate cancer

PD-1: programmed death 1

PD-L1: programmed death-ligand 1

PDGF: platelet-derived growth factor

PFA: paraformaldehyde

PI3K: phosphoinositide 3-kinase

PIP2: phosphatidylinositol 4,5-bisphosphate

PKA: protein kinase A

PKC: protein kinase C

PLC: phospholipase C

PLN: phospholamban

PMA: phorbol myristate acetate

PMCA: plasma membrane Ca^{2+} ATPase

Poly-HEMA: 2-Hydroxyethyl methacrylate

PP2C: protein phosphatase 2C

PTEN: phosphatase and tensin homolog

PTP: protein tyrosine phosphatase

PVDF: polyvinylidene fluoride

PyMT: polyoma middle T

Rab: Ras-related protein

RAF: rapidly accelerated fibrosarcoma

RAS: rat sarcoma

RASSF1: Ras-associated factor 1

Rack1: receptor for activated C kinase 1

Rac1: Ras-related C3 botulinum toxin substrate 1

RB: retinoblastoma

RhoA: Ras homolog family member A

ROC: receptor-operated channels

ROS: reactive oxygen species

ROI: regions of interests

R.T: room temperature

RTK: receptor tyrosine Kinase

RTKR: receptor tyrosine kinase-linked receptor

RYR: ryanodine receptor

SAP-1: serum response factor accessory protein

SAPK: stress-activated protein kinase

SDS: Sodium dodecyl sulfate

SERCA: sarco-endoplasmic reticular Ca^{2+} ATPase

SLC8: solute carrier 8

SLN: sarcolipin

SMOCs: second-messenger-operated channels

SOC: store-operated Ca^{2+} channel

SOCE: store-operated Ca^{2+} entry

SPCA: secretory pathway Ca^{2+} ATPase

SRB: sulforhodamine B

SSH: slingshot

STIM: stromal interacting molecule protein

TAB1: Transforming growth factor-β-activated protein 1 (TAK1)- binding protein 1

Taf-1: TATA-Box Binding Protein Associated Factor 1

TAK1: Transforming growth factor-β (TGF-β)-activated kinase-1

TCA: trichloroacetic acid

TCR: T-cell antigen receptor

TEM: Transmission Electron microscopy

TNF-α: tumor necrosis factor-α

TPC2: two-pore Ca^{2+} channels 2

TPCN2: Two pore segment channel 2

TRPC: transient receptor potential cation channel subfamily C ("C" for canonical)

TRPM: transient receptor potential cation channel subfamily M ("M" for melastatin)

TRPV: transient receptor potential cation channel subfamily V ("M" for vanilloid)

TTCCs: T-type calcium channels

UVR: ultraviolet radiation

VDAC: voltage-dependent anion channel

VEGF: vascular endothelial growth factor

VGCS1: voltage gated Ca^{2+} channel

VOC: Voltage operated channel

11. List of publications

1. Naffa, R.; Padányi, R.; Ignácz, A.; Hegyi, Z.; Jezsó, B.; Tóth, S.; Varga, K.; Homolya, L.; Hegedűs, L.; Schlett, K.; et al. The Plasma Membrane Ca2+ Pump PMCA4b Regulates Melanoma Cell Migration through Remodeling of the Actin Cytoskeleton. *Cancers (Basel)* **2021**, *13*, doi:10.3390/cancers13061354.

2. Naffa, R.; Vogel, L.; Hegedűs, L.; Pászty, K.; Tóth, S.; Kelemen, K.; Singh, N.; Reményi, A.; Kállay, E.; Cserepes, M.; et al. P38 MAPK Promotes Migration and Metastatic Activity of BRAF Mutant Melanoma Cells by Inducing Degradation of PMCA4b. *Cells* **2020**, *9*, doi:10.3390/cells9051209.

Publications unrelated to the thesis

1. Zihlif, M.; Mahafza, T.; Froukh, T.; Al-Akhras, F.M.; Alsalman, R.; Zuriekat, M.; **Naffa, R.** Association between Gasdermin A, Gasdermin B Polymorphisms and Allergic Rhinitis Amongst Jordanians. *Endocr Metab Immune Disord Drug Targets* **2021**, *21*, 472–477, doi:10.2174/1871530320666200604161656.

2. Odeh, F.; **Naffa, R**.; Azzam, H.; Mahmoud, I.S.; Alshaer, W.; Al Bawab, A.; Ismail, S. Co-Encapsulation of Thymoquinone with Docetaxel Enhances the Encapsulation Efficiency into PEGylated Liposomes and the Chemosensitivity of MCF7 Breast Cancer Cells to Docetaxel. *Heliyon* **2019**, *5*, e02919, doi:10.1016/j.heliyon.2019.e02919.

3. Alqaraleh, M.; Kasabri, V.; Farha, R.A.; **Naffa, R.G**.; Yousef, I.; Aljaafreh, A. Branched Amino Acids as Potential Biomarkers in Metabolic Syndrome Patients and as Hypolipidemic Compounds. *Eurasian Journal of Biosciences* **2019**, *13*, 2233–2241.

4. Al-khafaje, Z.; Kasabri, V.; Akour, A.; **Naffa, R**. Cross-Sectional Correlates of Increasing Vaspin and Asymmetrical Dimethylarginine Plasma Levels with Adiposity Indices and Atherogenic Index of Plasma in Metabolic Syndrome Subjects in Jordan. *Jordan Journal of Pharmaceutical Sciences* **2019**, *12*.

5. Abushahla, H.S.; Bulatova, N.; Kasabri, V.; **Naffa, R.** Correlates of Ghrelin and Visfatin in Metabolic Syndrome Patients with and without Prediabetes. *Int J Diabetes Dev Ctries* **2019**, *39*, 82–93, doi:10.1007/s13410-018-0654-x.

6. Kasabri, V.; Shawakri, E.; Akour, A.; **Naffa, R.**; Khawaja, N.; Al-Sarraf, I.; Bzour, J. Cross-Sectional Correlates of Increased IL-18 but Reduced Fetuin-A and Oxytocin with Adiposity and Blood Indices in Metabolic Syndrome Patients with and without Prediabetes. *Ther Adv Endocrinol Metab* **2018**, *9*, 329–338, doi:10.1177/2042018818788802.

7. Al Saudi, R.M.; Kasabri, V.; **Naffa, R.**; Bulatova, N.; Bustanji, Y. Glycated LDL-C and Glycated HDL-C in Association with Adiposity, Blood and Atherogenicity Indices in

Metabolic Syndrome Patients with and without Prediabetes. *Ther Adv Endocrinol Metab* **2018**, *9*, 311–323, doi:10.1177/2042018818788198.

8. Al-Heety, Q.Q.; Kasabri, V.; Akour, A.; **Naffa, R.**; Abu Rkhaya, S. Cross-Sectional Correlates of Paraoxonase 1 and Soluble Intercellular Adhesion Molecule-1 in Metabolic Syndrome Patients with and without Diabetes. *Ther Adv Endocrinol Metab* **2018**, *9*, 303–310, doi:10.1177/2042018818787396.

9. Alquoqa, R.S.; Kasabri, V.; **Naffa, R.**; Akour, A.; Bustanji, Y. Cross-Sectional Correlates of Myeloperoxidase and Alpha-1-Acid Glycoprotein with Adiposity, Atherogenic and Hematological Indices in Metabolic Syndrome Patients with or without Diabetes. *Ther Adv Endocrinol Metab* **2018**, *9*, 283–291, doi:10.1177/2042018818779742.

10. Al-Sarraf, I.A.K.; Kasabri, V.; Akour, A.; **Naffa, R.** Melatonin and Cryptochrome 2 in Metabolic Syndrome Patients with or without Diabetes: A Cross-Sectional Study. *Horm Mol Biol Clin Investig* **2018**, *35*, doi:10.1515/hmbci-2018-0016.

11. Rkhaya, S.A.; Bulatova, N.; Kasabri, V.; **Naffa, R.**; Alquoqa, R. Increased Malondialdehyde vs. Reduced Sirtuin 1 in Relation with Adiposity, Atherogenicity and Hematological Indices in Metabolic Syndrome Patients with and without Prediabetes. *Diabetes Metab Syndr* **2018**, *12*, 903–909, doi:10.1016/j.dsx.2018.05.013.

12. Al-Athami, T.F.; Kasabri, V.; **Naffa, R.**; Akour, A.; Hyasat, D.; Bustanji, Y. Oxytocin and Cholecystokinin Correlates with Metabolic Syndrome's Atherogenecity and Adiposity Indices. *Jordan Journal of Pharmaceutical Sciences* **2018**, *11*, 14.

13. Naserallah, R. 0; Kasabri, V. 0; Akour, A. 0; **Naffa, R.** 0; Bustanji, Y. 0; Khawaja, N. 0 The Levels of Oxytocin and Oxyntomodulin, Adiposity and Blood Indices in Pharmacotherapy Naive Diabetic and Non-Diabetic Patients with Metabolic Syndrome. *Jordan Journal of Pharmaceutical Sciences* **2018**, *11*.

14. Akour, A.; Kasabri, V.; Bulatova, N.; Al Muhaissen, S.; **Naffa, R.**; Fahmawi, H.; Momani, M.; Zayed, A.; Bustanji, Y. Association of Oxytocin with Glucose Intolerance and Inflammation Biomarkers in Metabolic Syndrome Patients with and without Prediabetes. *Rev Diabet Stud* **2018**, *14*, 364–371, doi:10.1900/RDS.2017.14.364.

15. Shafagoj, Y.A.; **Naffa, R.G.**; El-Khateeb, M.S.; Abdulla, Y.L.; Al-Qaddoumi, A.A.; Khatib, F.A.; Al-Motassem, Y.F.; Al-Khateeb, E.M. APOE Gene Polymorphism among Jordanian Alzheimer`s Patients with Relation to Lipid Profile. *Neurosciences (Riyadh)* **2018**, *23*, 29–34, doi:10.17712/nsj.2018.1.20170169.

16. Zihlif, M.; Afifi, F.; Abu-Dahab, R.; Majid, A.M.S.A.; Somrain, H.; Saleh, M.M.; Nassar, Z.D.; **Naffa, R.** Correction to: The Antiangiogenic Activities of Ethanolic Crude Extracts

of Four Salvia Species. *BMC Complement Altern Med* **2018**, *18*, 64, doi:10.1186/s12906-018-2126-8.

17. Amarin, J.Z.; **Naffa, R.G.**; Suradi, H.H.; Alsaket, Y.M.; Obeidat, N.M.; Mahafza, T.M.; Zihlif, M.A. An Intronic Single-Nucleotide Polymorphism (Rs13217795) in FOXO3 Is Associated with Asthma and Allergic Rhinitis: A Case-Case-Control Study. *BMC Med Genet* **2017**, *18*, 132, doi:10.1186/s12881-017-0494-4.

18. Akour, A.; Farha, R.A.; Alefishat, E.; Kasabri, V.; Bulatova, N.; **Naffa, R.** Insulin Resistance and Levels of Cardiovascular Biomarkers in Night-Shift Workers. *Sleep Biol. Rhythms* **2017**, *15*, 283–290, doi:10.1007/s41105-017-0109-7.

19. Akour, A.; Kasabri, V.; Boulatova, N.; Bustanji, Y.; **Naffa, R.**; Hyasat, D.; Khawaja, N.; Bustanji, H.; Zayed, A.; Momani, M. Levels of Metabolic Markers in Drug-Naive Prediabetic and Type 2 Diabetic Patients. *Acta Diabetol* **2017**, *54*, 163–170, doi:10.1007/s00592-016-0926-1.

12. References

1. Luo, J.; Solimini, N.L.; Elledge, S.J. Principles of Cancer Therapy: Oncogene and Non-Oncogene Addiction. *Cell* **2009**, *136*, 823–837, doi:10.1016/j.cell.2009.02.024.
2. Guan, X. Cancer Metastases: Challenges and Opportunities. *Acta Pharm Sin B* **2015**, *5*, 402–418, doi:10.1016/j.apsb.2015.07.005.
3. Gloster, H.M.; Neal, K. Skin Cancer in Skin of Color. *J Am Acad Dermatol* **2006**, *55*, 741–760; quiz 761–764, doi:10.1016/j.jaad.2005.08.063.
4. Narayanan, D.L.; Saladi, R.N.; Fox, J.L. Ultraviolet Radiation and Skin Cancer. *Int J Dermatol* **2010**, *49*, 978–986, doi:10.1111/j.1365-4632.2010.04474.x.
5. Wang, H.-Z.; Wang, F.; Chen, P.-F.; Zhang, M.; Yu, M.-X.; Wang, H.-L.; Zhao, Q.; Liu, J. Coexpression Network Analysis Identified That Plakophilin 1 Is Associated with the Metastasis in Human Melanoma. *Biomed Pharmacother* **2019**, *111*, 1234–1242, doi:10.1016/j.biopha.2018.12.135.
6. Siegel, R.L.; Miller, K.D.; Jemal, A. Cancer Statistics, 2020. *CA Cancer J Clin* **2020**, *70*, 7–30, doi:10.3322/caac.21590.
7. Winder, M.; Virós, A. Mechanisms of Drug Resistance in Melanoma. *Handb Exp Pharmacol* **2018**, *249*, 91–108, doi:10.1007/164_2017_17.
8. Balch, C.M.; Gershenwald, J.E.; Soong, S.-J.; Thompson, J.F.; Atkins, M.B.; Byrd, D.R.; Buzaid, A.C.; Cochran, A.J.; Coit, D.G.; Ding, S.; et al. Final Version of 2009 AJCC Melanoma Staging and Classification. *J Clin Oncol* **2009**, *27*, 6199–6206, doi:10.1200/JCO.2009.23.4799.
9. Hsu, M.-Y.; Meier, F.; Herlyn, M. Melanoma Development and Progression: A Conspiracy between Tumor and Host. *Differentiation* **2002**, *70*, 522–536, doi:10.1046/j.1432-0436.2002.700906.x.
10. Shih, I.M.; Elder, D.E.; Hsu, M.Y.; Herlyn, M. Regulation of Mel-CAM/MUC18 Expression on Melanocytes of Different Stages of Tumor Progression by Normal Keratinocytes. *Am J Pathol* **1994**, *145*, 837–845.
11. Urso, C. Are Growth Phases Exclusive to Cutaneous Melanoma? *J Clin Pathol* **2004**, *57*, 560, doi:10.1136/jcp.2003.014852.
12. Berger, M.F.; Hodis, E.; Heffernan, T.P.; Deribe, Y.L.; Lawrence, M.S.; Protopopov, A.; Ivanova, E.; Watson, I.R.; Nickerson, E.; Ghosh, P.; et al. Melanoma Genome Sequencing Reveals Frequent PREX2 Mutations. *Nature* **2012**, *485*, 502–506, doi:10.1038/nature11071.
13. Shtivelman, E.; Davies, M.Q.A.; Hwu, P.; Yang, J.; Lotem, M.; Oren, M.; Flaherty, K.T.; Fisher, D.E. Pathways and Therapeutic Targets in Melanoma. *Oncotarget* **2014**, *5*, 1701–1752, doi:10.18632/oncotarget.1892.
14. Maurer, G.; Tarkowski, B.; Baccarini, M. Raf Kinases in Cancer-Roles and Therapeutic Opportunities. *Oncogene* **2011**, *30*, 3477–3488, doi:10.1038/onc.2011.160.
15. Ascierto, P.A.; Kirkwood, J.M.; Grob, J.-J.; Simeone, E.; Grimaldi, A.M.; Maio, M.; Palmieri, G.; Testori, A.; Marincola, F.M.; Mozzillo, N. The Role of BRAF V600 Mutation in Melanoma. *J Transl Med* **2012**, *10*, 85, doi:10.1186/1479-5876-10-85.
16. Carvajal, R.D.; Antonescu, C.R.; Wolchok, J.D.; Chapman, P.B.; Roman, R.-A.; Teitcher, J.; Panageas, K.S.; Busam, K.J.; Chmielowski, B.; Lutzky, J.; et al. KIT as a Therapeutic Target in Metastatic Melanoma. *JAMA* **2011**, *305*, 2327–2334, doi:10.1001/jama.2011.746.
17. Decatur, C.L.; Ong, E.; Garg, N.; Anbunathan, H.; Bowcock, A.M.; Field, M.G.; Harbour, J.W. Driver Mutations in Uveal Melanoma: Associations With Gene Expression Profile and Patient Outcomes. *JAMA Ophthalmol* **2016**, *134*, 728–733, doi:10.1001/jamaophthalmol.2016.0903.

18. Estrada, Y.; Dong, J.; Ossowski, L. Positive Crosstalk between ERK and P38 in Melanoma Stimulates Migration and in Vivo Proliferation. *Pigment Cell Melanoma Res* **2009**, *22*, 66–76, doi:10.1111/j.1755-148X.2008.00520.x.

19. Lopez-Bergami, P.; Huang, C.; Goydos, J.S.; Yip, D.; Bar-Eli, M.; Herlyn, M.; Smalley, K.S.M.; Mahale, A.; Eroshkin, A.; Aaronson, S.; et al. Rewired ERK-JNK Signaling Pathways in Melanoma. *Cancer Cell* **2007**, *11*, 447–460, doi:10.1016/j.ccr.2007.03.009.

20. Huang, S.; DeGuzman, A.; Bucana, C.D.; Fidler, I.J. Nuclear Factor-KappaB Activity Correlates with Growth, Angiogenesis, and Metastasis of Human Melanoma Cells in Nude Mice. *Clin Cancer Res* **2000**, *6*, 2573–2581.

21. Niezgoda, A.; Niezgoda, P.; Czajkowski, R. Novel Approaches to Treatment of Advanced Melanoma: A Review on Targeted Therapy and Immunotherapy. *Biomed Res Int* **2015**, *2015*, doi:10.1155/2015/851387.

22. Moreira, A.; Heinzerling, L.; Bhardwaj, N.; Friedlander, P. Current Melanoma Treatments: Where Do We Stand? *Cancers (Basel)* **2021**, *13*, doi:10.3390/cancers13020221.

23. Ascierto, P.A.; Kirkwood, J.M.; Grob, J.-J.; Simeone, E.; Grimaldi, A.M.; Maio, M.; Palmieri, G.; Testori, A.; Marincola, F.M.; Mozzillo, N. The Role of BRAF V600 Mutation in Melanoma. *J Transl Med* **2012**, *10*, 85, doi:10.1186/1479-5876-10-85.

24. Sullivan, R.J.; Flaherty, K.T. Resistance to BRAF-Targeted Therapy in Melanoma. *Eur J Cancer* **2013**, *49*, 1297–1304, doi:10.1016/j.ejca.2012.11.019.

25. Hauschild, A.; Grob, J.-J.; Demidov, L.V.; Jouary, T.; Gutzmer, R.; Millward, M.; Rutkowski, P.; Blank, C.U.; Miller, W.H.; Kaempgen, E.; et al. Dabrafenib in BRAF-Mutated Metastatic Melanoma: A Multicentre, Open-Label, Phase 3 Randomised Controlled Trial. *Lancet* **2012**, *380*, 358–365, doi:10.1016/S0140-6736(12)60868-X.

26. Xing, F.; Persaud, Y.; Pratilas, C.A.; Taylor, B.S.; Janakiraman, M.; She, Q.-B.; Gallardo, H.; Liu, C.; Merghoub, T.; Hefter, B.; et al. Concurrent Loss of the PTEN and RB1 Tumor Suppressors Attenuates RAF Dependence in Melanomas Harboring (V600E)BRAF. *Oncogene* **2012**, *31*, 446–457, doi:10.1038/onc.2011.250.

27. Greger, J.G.; Eastman, S.D.; Zhang, V.; Bleam, M.R.; Hughes, A.M.; Smitheman, K.N.; Dickerson, S.H.; Laquerre, S.G.; Liu, L.; Gilmer, T.M. Combinations of BRAF, MEK, and PI3K/MTOR Inhibitors Overcome Acquired Resistance to the BRAF Inhibitor GSK2118436 Dabrafenib, Mediated by NRAS or MEK Mutations. *Mol Cancer Ther* **2012**, *11*, 909–920, doi:10.1158/1535-7163.MCT-11-0989.

28. Straussman, R.; Morikawa, T.; Shee, K.; Barzily-Rokni, M.; Qian, Z.R.; Du, J.; Davis, A.; Mongare, M.M.; Gould, J.; Frederick, D.T.; et al. Tumour Micro-Environment Elicits Innate Resistance to RAF Inhibitors through HGF Secretion. *Nature* **2012**, *487*, 500–504, doi:10.1038/nature11183.

29. Johnson, D.B.; Puzanov, I. Treatment of NRAS-Mutant Melanoma. *Curr Treat Options Oncol* **2015**, *16*, 15, doi:10.1007/s11864-015-0330-z.

30. Guo, J.; Si, L.; Kong, Y.; Flaherty, K.T.; Xu, X.; Zhu, Y.; Corless, C.L.; Li, L.; Li, H.; Sheng, X.; et al. Phase II, Open-Label, Single-Arm Trial of Imatinib Mesylate in Patients with Metastatic Melanoma Harboring c-Kit Mutation or Amplification. *J Clin Oncol* **2011**, *29*, 2904–2909, doi:10.1200/JCO.2010.33.9275.

31. Johnson, D.B.; Puzanov, I.; Kelley, M.C. Talimogene Laherparepvec (T-VEC) for the Treatment of Advanced Melanoma. *Immunotherapy* **2015**, *7*, 611–619, doi:10.2217/imt.15.35.

32. Pilla, L.; Alberti, A.; Di Mauro, P.; Gemelli, M.; Cogliati, V.; Cazzaniga, M.E.; Bidoli, P.; Maccalli, C. Molecular and Immune Biomarkers for Cutaneous Melanoma: Current Status and Future Prospects. *Cancers (Basel)* **2020**, *12*, doi:10.3390/cancers12113456.

33. Tanaka, Y.; Murata, M.; Shen, C.-H.; Furue, M.; Ito, T. NECTIN4: A Novel Therapeutic Target for Melanoma. *Int J Mol Sci* **2021**, *22*, doi:10.3390/ijms22020976.

34. Jaune, E.; Cavazza, E.; Ronco, C.; Grytsai, O.; Abbe, P.; Tekaya, N.; Zerhouni, M.; Beranger, G.; Kaminski, L.; Bost, F.; et al. Discovery of a New Molecule Inducing Melanoma Cell Death: Dual AMPK/MELK Targeting for Novel Melanoma Therapies. *Cell Death Dis* **2021**, *12*, 64, doi:10.1038/s41419-020-03344-6.

35. Buchbinder, E.I.; Desai, A. CTLA-4 and PD-1 Pathways: Similarities, Differences, and Implications of Their Inhibition. *Am J Clin Oncol* **2016**, *39*, 98–106, doi:10.1097/COC.0000000000000239.

36. Parry, R.V.; Chemnitz, J.M.; Frauwirth, K.A.; Lanfranco, A.R.; Braunstein, I.; Kobayashi, S.V.; Linsley, P.S.; Thompson, C.B.; Riley, J.L. CTLA-4 and PD-1 Receptors Inhibit T-Cell Activation by Distinct Mechanisms. *Mol Cell Biol* **2005**, *25*, 9543–9553, doi:10.1128/MCB.25.21.9543-9553.2005.

37. Tsai, F.-C.; Kuo, G.-H.; Chang, S.-W.; Tsai, P.-J. Ca2+ Signaling in Cytoskeletal Reorganization, Cell Migration, and Cancer Metastasis. *Biomed Res Int* **2015**, *2015*, 409245, doi:10.1155/2015/409245.

38. Clapham, D.E. Calcium Signaling. *Cell* **2007**, *131*, 1047–1058, doi:10.1016/j.cell.2007.11.028.

39. Harraz, O.F.; Altier, C. STIM1-Mediated Bidirectional Regulation of Ca(2+) Entry through Voltage-Gated Calcium Channels (VGCC) and Calcium-Release Activated Channels (CRAC). *Front Cell Neurosci* **2014**, *8*, 43, doi:10.3389/fncel.2014.00043.

40. Berridge, M.J.; Lipp, P.; Bootman, M.D. The Versatility and Universality of Calcium Signalling. *Nat Rev Mol Cell Biol* **2000**, *1*, 11–21, doi:10.1038/35036035.

41. Berridge, M.J.; Bootman, M.D.; Roderick, H.L. Calcium Signalling: Dynamics, Homeostasis and Remodelling. *Nat Rev Mol Cell Biol* **2003**, *4*, 517–529, doi:10.1038/nrm1155.

42. Uhlén, P.; Fritz, N. Biochemistry of Calcium Oscillations. *Biochem Biophys Res Commun* **2010**, *396*, 28–32, doi:10.1016/j.bbrc.2010.02.117.

43. Prevarskaya, N.; Skryma, R.; Shuba, Y. Ion Channels and the Hallmarks of Cancer. *Trends Mol Med* **2010**, *16*, 107–121, doi:10.1016/j.molmed.2010.01.005.

44. Francisco Javier Martin-Romero The Interplay between Cytoskeleton and Calcium Dynamics. In *Cytoskeleton*; Aida M. Lopez-Guerrero, Ed.; IntechOpen: Rijeka, 2017; p. Ch. 4 ISBN 978-953-51-3170-0.

45. Catterall, W.A.; Zheng, N. Deciphering Voltage-Gated Na(+) and Ca(2+) Channels by Studying Prokaryotic Ancestors. *Trends Biochem Sci* **2015**, *40*, 526–534, doi:10.1016/j.tibs.2015.07.002.

46. Neher, E. Receptor-Operated Ca Channels. *Nature* **1987**, *326*, 242–242, doi:10.1038/326242a0.

47. Vial, C.; Roberts, J.A.; Evans, R.J. Molecular Properties of ATP-Gated P2X Receptor Ion Channels. *Trends Pharmacol Sci* **2004**, *25*, 487–493, doi:10.1016/j.tips.2004.07.008.

48. Tsien, R.W.; Tsien, R.Y. Calcium Channels, Stores, and Oscillations. *Annu Rev Cell Biol* **1990**, *6*, 715–760, doi:10.1146/annurev.cb.06.110190.003435.

49. Smyth, J.T.; Hwang, S.-Y.; Tomita, T.; DeHaven, W.I.; Mercer, J.C.; Putney, J.W. Activation and Regulation of Store-Operated Calcium Entry. *J Cell Mol Med* **2010**, *14*, 2337–2349, doi:10.1111/j.1582-4934.2010.01168.x.

50. Ong, H.L.; Subedi, K.P.; Son, G.-Y.; Liu, X.; Ambudkar, I.S. Tuning Store-Operated Calcium Entry to Modulate Ca2+-Dependent Physiological Processes. *Biochim Biophys Acta Mol Cell Res* **2019**, *1866*, 1037–1045, doi:10.1016/j.bbamcr.2018.11.018.

51. Endo, M.; Tanaka, M.; Ogawa, Y. Calcium Induced Release of Calcium from the Sarcoplasmic Reticulum of Skinned Skeletal Muscle Fibres. *Nature* **1970**, *228*, 34–36, doi:10.1038/228034a0.

52. Luongo, T.S.; Lambert, J.P.; Gross, P.; Nwokedi, M.; Lombardi, A.A.; Shanmughapriya, S.; Carpenter, A.C.; Kolmetzky, D.; Gao, E.; van Berlo, J.H.; et al. The Mitochondrial Na+/Ca2+ Exchanger Is Essential for Ca2+ Homeostasis and Viability. *Nature* **2017**, *545*, 93–97, doi:10.1038/nature22082.

53. Bononi, A.; Missiroli, S.; Poletti, F.; Suski, J.M.; Agnoletto, C.; Bonora, M.; De Marchi, E.; Giorgi, C.; Marchi, S.; Patergnani, S.; et al. Mitochondria-Associated Membranes (MAMs) as Hotspot Ca(2+) Signaling Units. *Adv Exp Med Biol* **2012**, *740*, 411–437, doi:10.1007/978-94-007-2888-2_17.

54. Dolman, N.J.; Tepikin, A.V. Calcium Gradients and the Golgi. *Cell Calcium* **2006**, *40*, 505–512, doi:10.1016/j.ceca.2006.08.012.

55. Marchi, S.; Giorgi, C.; Galluzzi, L.; Pinton, P. Ca2+ Fluxes and Cancer. *Mol Cell* **2020**, *78*, 1055–1069, doi:10.1016/j.molcel.2020.04.017.

56. Brini, M.; Carafoli, E. The Plasma Membrane Ca2+ ATPase and the Plasma Membrane Sodium Calcium Exchanger Cooperate in the Regulation of Cell Calcium. *Cold Spring Harb Perspect Biol* **2011**, *3*, doi:10.1101/cshperspect.a004168.

57. Lytton, J. Na+/Ca2+ Exchangers: Three Mammalian Gene Families Control Ca2+ Transport. *Biochem J* **2007**, *406*, 365–382, doi:10.1042/BJ20070619.

58. Antony, A.N.; Paillard, M.; Moffat, C.; Juskeviciute, E.; Correnti, J.; Bolon, B.; Rubin, E.; Csordás, G.; Seifert, E.L.; Hoek, J.B.; et al. MICU1 Regulation of Mitochondrial Ca(2+) Uptake Dictates Survival and Tissue Regeneration. *Nat Commun* **2016**, *7*, 10955, doi:10.1038/ncomms10955.

59. Prins, D.; Michalak, M. Organellar Calcium Buffers. *Cold Spring Harb Perspect Biol* **2011**, *3*, doi:10.1101/cshperspect.a004069.

60. Michalak, M.; Opas, M. Endoplasmic and Sarcoplasmic Reticulum in the Heart. *Trends Cell Biol* **2009**, *19*, 253–259, doi:10.1016/j.tcb.2009.03.006.

61. Wei, L.; Hanna, A.D.; Beard, N.A.; Dulhunty, A.F. Unique Isoform-Specific Properties of Calsequestrin in the Heart and Skeletal Muscle. *Cell Calcium* **2009**, *45*, 474–484, doi:10.1016/j.ceca.2009.03.006.

62. Rizzuto, R.; Marchi, S.; Bonora, M.; Aguiari, P.; Bononi, A.; De Stefani, D.; Giorgi, C.; Leo, S.; Rimessi, A.; Siviero, R.; et al. Ca(2+) Transfer from the ER to Mitochondria: When, How and Why. *Biochim Biophys Acta* **2009**, *1787*, 1342–1351, doi:10.1016/j.bbabio.2009.03.015.

63. Schwaller, B. Cytosolic Ca2+ Buffers. *Cold Spring Harb Perspect Biol* **2010**, *2*, a004051, doi:10.1101/cshperspect.a004051.

64. Palmgren, M.G.; Nissen, P. P-Type ATPases. *Annu Rev Biophys* **2011**, *40*, 243–266, doi:10.1146/annurev.biophys.093008.131331.

65. Wuytack, F.; Raeymaekers, L.; Missiaen, L. PMR1/SPCA Ca2+ Pumps and the Role of the Golgi Apparatus as a Ca2+ Store. *Pflugers Arch* **2003**, *446*, 148–153, doi:10.1007/s00424-003-1011-5.

66. Van Baelen, K.; Dode, L.; Vanoevelen, J.; Callewaert, G.; De Smedt, H.; Missiaen, L.; Parys, J.B.; Raeymaekers, L.; Wuytack, F. The Ca2+/Mn2+ Pumps in the Golgi Apparatus. *Biochim Biophys Acta* **2004**, *1742*, 103–112, doi:10.1016/j.bbamcr.2004.08.018.

67. Primeau, J.O.; Armanious, G.P.; Fisher, M.E.; Young, H.S. The SarcoEndoplasmic Reticulum Calcium ATPase. In *Membrane Protein Complexes: Structure and Function*; Harris, J.R., Boekema, E.J., Eds.; Subcellular Biochemistry; Springer: Singapore, 2018; pp. 229–258 ISBN 978-981-10-7757-9.

68. Wuytack, F.; Raeymaekers, L.; Missiaen, L. Molecular Physiology of the SERCA and SPCA Pumps. *Cell Calcium* **2002**, *32*, 279–305, doi:10.1016/s0143416002001847.
69. Peterková, L.; Kmoníčková, E.; Ruml, T.; Rimpelová, S. Sarco/Endoplasmic Reticulum Calcium ATPase Inhibitors: Beyond Anticancer Perspective. *J Med Chem* **2020**, *63*, 1937–1963, doi:10.1021/acs.jmedchem.9b01509.
70. Schatzmann, H.J. ATP-Dependent Ca++-Extrusion from Human Red Cells. *Experientia* **1966**, *22*, 364–365, doi:10.1007/BF01901136.
71. Wolf, H.U.; Dieckvoss, G.; Lichtner, R. Purification and Properties of High-Affinity Ca2+-ATPase of Human Erythrocyte Membranes. *Acta Biol Med Ger* **1977**, *36*, 847–858.
72. Strehler, E.E. Plasma Membrane Calcium ATPases as Novel Candidates for Therapeutic Agent Development. *J Pharm Pharm Sci* **2013**, *16*, 190–206, doi:10.18433/j3z011.
73. Carafoli, E.; Brini, M. Calcium Pumps: Structural Basis for and Mechanism of Calcium Transmembrane Transport. *Curr Opin Chem Biol* **2000**, *4*, 152–161, doi:10.1016/s1367-5931(99)00069-1.
74. Brini, M. Plasma Membrane Ca(2+)-ATPase: From a Housekeeping Function to a Versatile Signaling Role. *Pflugers Arch* **2009**, *457*, 657–664, doi:10.1007/s00424-008-0505-6.
75. Prasad, V.; Okunade, G.; Liu, L.; Paul, R.J.; Shull, G.E. Distinct Phenotypes among Plasma Membrane Ca2+-ATPase Knockout Mice. *Ann N Y Acad Sci* **2007**, *1099*, 276–286, doi:10.1196/annals.1387.029.
76. Holton, M.L.; Wang, W.; Emerson, M.; Neyses, L.; Armesilla, A.L. Plasma Membrane Calcium ATPase Proteins as Novel Regulators of Signal Transduction Pathways. *World J Biol Chem* **2010**, *1*, 201–208, doi:10.4331/wjbc.v1.i6.201.
77. Supper, V.; Schiller, H.B.; Paster, W.; Forster, F.; Boulègue, C.; Mitulovic, G.; Leksa, V.; Ohradanova-Repic, A.; Machacek, C.; Schatzlmaier, P.; et al. Association of CD147 and Calcium Exporter PMCA4 Uncouples IL-2 Expression from Early TCR Signaling. *J Immunol* **2016**, *196*, 1387–1399, doi:10.4049/jimmunol.1501889.
78. Holton, M.; Yang, D.; Wang, W.; Mohamed, T.M.A.; Neyses, L.; Armesilla, A.L. The Interaction between Endogenous Calcineurin and the Plasma Membrane Calcium-Dependent ATPase Is Isoform Specific in Breast Cancer Cells. *FEBS Lett* **2007**, *581*, 4115–4119, doi:10.1016/j.febslet.2007.07.054.
79. Armesilla, A.L.; Williams, J.C.; Buch, M.H.; Pickard, A.; Emerson, M.; Cartwright, E.J.; Oceandy, D.; Vos, M.D.; Gillies, S.; Clark, G.J.; et al. Novel Functional Interaction between the Plasma Membrane Ca2+ Pump 4b and the Proapoptotic Tumor Suppressor Ras-Associated Factor 1 (RASSF1). *J Biol Chem* **2004**, *279*, 31318–31328, doi:10.1074/jbc.M307557200.
80. Schuh, K.; Uldrijan, S.; Gambaryan, S.; Roethlein, N.; Neyses, L. Interaction of the Plasma Membrane Ca2+ Pump 4b/CI with the Ca2+/Calmodulin-Dependent Membrane-Associated Kinase CASK. *J Biol Chem* **2003**, *278*, 9778–9783, doi:10.1074/jbc.M212507200.
81. Penniston, J.T.; Padányi, R.; Pászty, K.; Varga, K.; Hegedus, L.; Enyedi, A. Apart from Its Known Function, the Plasma Membrane Ca^{2+}ATPase Can Regulate Ca^{2+} Signaling by Controlling Phosphatidylinositol 4,5-Bisphosphate Levels. *J Cell Sci* **2014**, *127*, 72–84, doi:10.1242/jcs.132548.
82. Hegedũs, L.; Garay, T.; Molnár, E.; Varga, K.; Bilecz, Á.; Török, S.; Padányi, R.; Pászty, K.; Wolf, M.; Grusch, M.; et al. The Plasma Membrane Ca2+ Pump PMCA4b Inhibits the Migratory and Metastatic Activity of BRAF Mutant Melanoma Cells. *Int J Cancer* **2017**, *140*, 2758–2770, doi:10.1002/ijc.30503.

83. Lee, W.J.; Roberts-Thomson, S.J.; Holman, N.A.; May, F.J.; Lehrbach, G.M.; Monteith, G.R. Expression of Plasma Membrane Calcium Pump Isoform MRNAs in Breast Cancer Cell Lines. *Cell Signal* **2002**, *14*, 1015–1022, doi:10.1016/s0898-6568(02)00049-9.

84. Lee, W.J.; Roberts-Thomson, S.J.; Monteith, G.R. Plasma Membrane Calcium-ATPase 2 and 4 in Human Breast Cancer Cell Lines. *Biochem Biophys Res Commun* **2005**, *337*, 779–783, doi:10.1016/j.bbrc.2005.09.119.

85. Varga, K.; Pászty, K.; Padányi, R.; Hegedűs, L.; Brouland, J.-P.; Papp, B.; Enyedi, A. Histone Deacetylase Inhibitor- and PMA-Induced Upregulation of PMCA4b Enhances Ca2+ Clearance from MCF-7 Breast Cancer Cells. *Cell Calcium* **2014**, *55*, 78–92, doi:10.1016/j.ceca.2013.12.003.

86. Varga, K.; Hollósi, A.; Pászty, K.; Hegedűs, L.; Szakács, G.; Tímár, J.; Papp, B.; Enyedi, Á.; Padányi, R. Expression of Calcium Pumps Is Differentially Regulated by Histone Deacetylase Inhibitors and Estrogen Receptor Alpha in Breast Cancer Cells. *BMC Cancer* **2018**, *18*, 1029, doi:10.1186/s12885-018-4945-x.

87. Rüschoff, J.H.; Brandenburger, T.; Strehler, E.E.; Filoteo, A.G.; Heinmöller, E.; Aumüller, G.; Wilhelm, B. Plasma Membrane Calcium ATPase Expression in Human Colon Multistep Carcinogenesis. *Cancer Invest* **2012**, *30*, 251–257, doi:10.3109/07357907.2012.657817.

88. Aung, C.S.; Ye, W.; Plowman, G.; Peters, A.A.; Monteith, G.R.; Roberts-Thomson, S.J. Plasma Membrane Calcium ATPase 4 and the Remodeling of Calcium Homeostasis in Human Colon Cancer Cells. *Carcinogenesis* **2009**, *30*, 1962–1969, doi:10.1093/carcin/bgp223.

89. Saito, K.; Uzawa, K.; Endo, Y.; Kato, Y.; Nakashima, D.; Ogawara, K.; Shiba, M.; Bukawa, H.; Yokoe, H.; Tanzawa, H. Plasma Membrane Ca2+ ATPase Isoform 1 Down-Regulated in Human Oral Cancer. *Oncol Rep* **2006**, *15*, 49–55.

90. Hegedűs, L.; Zámbó, B.; Pászty, K.; Padányi, R.; Varga, K.; Penniston, J.T.; Enyedi, Á. Molecular Diversity of Plasma Membrane Ca2+ Transporting ATPases: Their Function Under Normal and Pathological Conditions. *Adv Exp Med Biol* **2020**, *1131*, 93–129, doi:10.1007/978-3-030-12457-1_5.

91. Silverstein, R.S.; Tempel, B.L. Atp2b2, Encoding Plasma Membrane Ca2+-ATPase Type 2, (PMCA2) Exhibits Tissue-Specific First Exon Usage in Hair Cells, Neurons, and Mammary Glands of Mice. *Neuroscience* **2006**, *141*, 245–257, doi:10.1016/j.neuroscience.2006.03.036.

92. Habib, T.; Park, H.; Tsang, M.; de Alborán, I.M.; Nicks, A.; Wilson, L.; Knoepfler, P.S.; Andrews, S.; Rawlings, D.J.; Eisenman, R.N.; et al. Myc Stimulates B Lymphocyte Differentiation and Amplifies Calcium Signaling. *J Cell Biol* **2007**, *179*, 717–731, doi:10.1083/jcb.200704173.

93. Lessard, S.; Gatof, E.S.; Beaudoin, M.; Schupp, P.G.; Sher, F.; Ali, A.; Prehar, S.; Kurita, R.; Nakamura, Y.; Baena, E.; et al. An Erythroid-Specific ATP2B4 Enhancer Mediates Red Blood Cell Hydration and Malaria Susceptibility. *J Clin Invest* **2017**, *127*, 3065–3074, doi:10.1172/JCI94378.

94. Hegedüs, L.; Padányi, R.; Molnár, J.; Pászty, K.; Varga, K.; Kenessey, I.; Sárközy, E.; Wolf, M.; Grusch, M.; Hegyi, Z.; et al. Histone Deacetylase Inhibitor Treatment Increases the Expression of the Plasma Membrane Ca2+ Pump PMCA4b and Inhibits the Migration of Melanoma Cells Independent of ERK. *Front. Oncol.* **2017**, *7*, 95, doi:10.3389/fonc.2017.00095.

95. Strehler, E.E. Plasma Membrane Calcium ATPases: From Generic Ca(2+) Sump Pumps to Versatile Systems for Fine-Tuning Cellular Ca(2.). *Biochem Biophys Res Commun* **2015**, *460*, 26–33, doi:10.1016/j.bbrc.2015.01.121.

96.   Caride, A.J.; Filoteo, A.G.; Penniston, J.T.; Strehler, E.E. The Plasma Membrane Ca2+ Pump Isoform 4a Differs from Isoform 4b in the Mechanism of Calmodulin Binding and Activation Kinetics: Implications for Ca2+ Signaling. *J Biol Chem* **2007**, *282*, 25640–25648, doi:10.1074/jbc.M701129200.

97.   Dumont, R.A.; Lins, U.; Filoteo, A.G.; Penniston, J.T.; Kachar, B.; Gillespie, P.G. Plasma Membrane Ca2+-ATPase Isoform 2a Is the PMCA of Hair Bundles. *J Neurosci* **2001**, *21*, 5066–5078.

98.   Enyedi, A.; Verma, A.K.; Filoteo, A.G.; Penniston, J.T. Protein Kinase C Activates the Plasma Membrane Ca2+ Pump Isoform 4b by Phosphorylation of an Inhibitory Region Downstream of the Calmodulin-Binding Domain. *J Biol Chem* **1996**, *271*, 32461–32467, doi:10.1074/jbc.271.50.32461.

99.   Enyedi, A.; Elwess, N.L.; Filoteo, A.G.; Verma, A.K.; Paszty, K.; Penniston, J.T. Protein Kinase C Phosphorylates the "a" Forms of Plasma Membrane Ca2+ Pump Isoforms 2 and 3 and Prevents Binding of Calmodulin. *J Biol Chem* **1997**, *272*, 27525–27528, doi:10.1074/jbc.272.44.27525.

100.   Mangialavori, I.; Villamil-Giraldo, A.M.; Pignataro, M.F.; Ferreira-Gomes, M.; Caride, A.J.; Rossi, J.P.F.C. Plasma Membrane Calcium Pump (PMCA) Differential Exposure of Hydrophobic Domains after Calmodulin and Phosphatidic Acid Activation. *J Biol Chem* **2011**, *286*, 18397–18404, doi:10.1074/jbc.M110.210088.

101.   Zaidi, A.; Adewale, M.; McLean, L.; Ramlow, P. The Plasma Membrane Calcium Pumps-The Old and the New. *Neurosci Lett* **2018**, *663*, 12–17, doi:10.1016/j.neulet.2017.09.066.

102.   Padányi, R.; Pászty, K.; Penheiter, A.R.; Filoteo, A.G.; Penniston, J.T.; Enyedi, A. Intramolecular Interactions of the Regulatory Region with the Catalytic Core in the Plasma Membrane Calcium Pump. *J Biol Chem* **2003**, *278*, 35798–35804, doi:10.1074/jbc.M305794200.

103.   Pászty, K.; Verma, A.K.; Padányi, R.; Filoteo, A.G.; Penniston, J.T.; Enyedi, A. Plasma Membrane Ca2+ATPase Isoform 4b Is Cleaved and Activated by Caspase-3 during the Early Phase of Apoptosis. *J Biol Chem* **2002**, *277*, 6822–6829, doi:10.1074/jbc.M109548200.

104.   Antalffy, G.; Pászty, K.; Varga, K.; Hegedűs, L.; Enyedi, Á.; Padányi, R. A C-Terminal Di-Leucine Motif Controls Plasma Membrane Expression of PMCA4b. *Biochim Biophys Acta* **2013**, *1833*, 2561–2572, doi:10.1016/j.bbamcr.2013.06.021.

105.   Linde, C.I.; Di Leva, F.; Domi, T.; Tosatto, S.C.E.; Brini, M.; Carafoli, E. Inhibitory Interaction of the 14-3-3 Proteins with Ubiquitous (PMCA1) and Tissue-Specific (PMCA3) Isoforms of the Plasma Membrane Ca2+ Pump. *Cell Calcium* **2008**, *43*, 550–561, doi:10.1016/j.ceca.2007.09.003.

106.   Rimessi, A.; Coletto, L.; Pinton, P.; Rizzuto, R.; Brini, M.; Carafoli, E. Inhibitory Interaction of the 14-3-3{epsilon} Protein with Isoform 4 of the Plasma Membrane Ca(2+)-ATPase Pump. *J Biol Chem* **2005**, *280*, 37195–37203, doi:10.1074/jbc.M504921200.

107.   Antalffy, G.; Mauer, A.S.; Pászty, K.; Hegedus, L.; Padányi, R.; Enyedi, A.; Strehler, E.E. Plasma Membrane Calcium Pump (PMCA) Isoform 4 Is Targeted to the Apical Membrane by the w-Splice Insert from PMCA2. *Cell Calcium* **2012**, *51*, 171–178, doi:10.1016/j.ceca.2011.12.010.

108.   DeMarco, S.J.; Chicka, M.C.; Strehler, E.E. Plasma Membrane Ca2+ ATPase Isoform 2b Interacts Preferentially with Na+/H+ Exchanger Regulatory Factor 2 in Apical Plasma Membranes. *J Biol Chem* **2002**, *277*, 10506–10511, doi:10.1074/jbc.M111616200.

109. Kim, E.; DeMarco, S.J.; Marfatia, S.M.; Chishti, A.H.; Sheng, M.; Strehler, E.E. Plasma Membrane Ca2+ ATPase Isoform 4b Binds to Membrane-Associated Guanylate Kinase (MAGUK) Proteins via Their PDZ (PSD-95/Dlg/ZO-1) Domains. *J Biol Chem* **1998**, *273*, 1591–1595, doi:10.1074/jbc.273.3.1591.

110. Aravindan, R.G.; Fomin, V.P.; Naik, U.P.; Modelski, M.J.; Naik, M.U.; Galileo, D.S.; Duncan, R.L.; Martin-Deleon, P.A. CASK Interacts with PMCA4b and JAM-A on the Mouse Sperm Flagellum to Regulate Ca2+ Homeostasis and Motility. *J Cell Physiol* **2012**, *227*, 3138–3150, doi:10.1002/jcp.24000.

111. Schmidt, N.; Kollewe, A.; Constantin, C.E.; Henrich, S.; Ritzau-Jost, A.; Bildl, W.; Saalbach, A.; Hallermann, S.; Kulik, A.; Fakler, B.; et al. Neuroplastin and Basigin Are Essential Auxiliary Subunits of Plasma Membrane Ca2+-ATPases and Key Regulators of Ca2+ Clearance. *Neuron* **2017**, *96*, 827-838.e9, doi:10.1016/j.neuron.2017.09.038.

112. Dean, W.L.; Whiteheart, S.W. Plasma Membrane Ca(2+)-ATPase (PMCA) Translocates to Filopodia during Platelet Activation. *Thromb Haemost* **2004**, *91*, 325–333, doi:10.1160/TH03-07-0425.

113. Dalghi, M.G.; Ferreira-Gomes, M.; Montalbetti, N.; Simonin, A.; Strehler, E.E.; Hediger, M.A.; Rossi, J.P. Cortical Cytoskeleton Dynamics Regulates Plasma Membrane Calcium ATPase Isoform-2 (PMCA2) Activity. *Biochim Biophys Acta Mol Cell Res* **2017**, *1864*, 1413–1424, doi:10.1016/j.bbamcr.2017.05.014.

114. Stewart, T.A.; Yapa, K.T.D.S.; Monteith, G.R. Altered Calcium Signaling in Cancer Cells. *Biochim Biophys Acta* **2015**, *1848*, 2502–2511, doi:10.1016/j.bbamem.2014.08.016.

115. Hanahan, D.; Weinberg, R.A. Hallmarks of Cancer: The next Generation. *Cell* **2011**, *144*, 646–674, doi:10.1016/j.cell.2011.02.013.

116. Déliot, N.; Constantin, B. Plasma Membrane Calcium Channels in Cancer: Alterations and Consequences for Cell Proliferation and Migration. *Biochim Biophys Acta* **2015**, *1848*, 2512–2522, doi:10.1016/j.bbamem.2015.06.009.

117. Monteith, G.R.; Davis, F.M.; Roberts-Thomson, S.J. Calcium Channels and Pumps in Cancer: Changes and Consequences. *J Biol Chem* **2012**, *287*, 31666–31673, doi:10.1074/jbc.R112.343061.

118. Cui, C.; Merritt, R.; Fu, L.; Pan, Z. Targeting Calcium Signaling in Cancer Therapy. *Acta Pharm Sin B* **2017**, *7*, 3–17, doi:10.1016/j.apsb.2016.11.001.

119. Roderick, H.L.; Cook, S.J. Ca2+ Signalling Checkpoints in Cancer: Remodelling Ca2+ for Cancer Cell Proliferation and Survival. *Nat Rev Cancer* **2008**, *8*, 361–375, doi:10.1038/nrc2374.

120. Fixemer, T.; Wissenbach, U.; Flockerzi, V.; Bonkhoff, H. Expression of the Ca2+-Selective Cation Channel TRPV6 in Human Prostate Cancer: A Novel Prognostic Marker for Tumor Progression. *Oncogene* **2003**, *22*, 7858–7861, doi:10.1038/sj.onc.1206895.

121. Dhennin-Duthille, I.; Gautier, M.; Faouzi, M.; Guilbert, A.; Brevet, M.; Vaudry, D.; Ahidouch, A.; Sevestre, H.; Ouadid-Ahidouch, H. High Expression of Transient Receptor Potential Channels in Human Breast Cancer Epithelial Cells and Tissues: Correlation with Pathological Parameters. *Cell Physiol Biochem* **2011**, *28*, 813–822, doi:10.1159/000335795.

122. Feng, M.; Grice, D.M.; Faddy, H.M.; Nguyen, N.; Leitch, S.; Wang, Y.; Muend, S.; Kenny, P.A.; Sukumar, S.; Roberts-Thomson, S.J.; et al. Store-Independent Activation of Orai1 by SPCA2 in Mammary Tumors. *Cell* **2010**, *143*, 84–98, doi:10.1016/j.cell.2010.08.040.

123. Ay, A.-S.; Benzerdjeb, N.; Benzerdjerb, N.; Sevestre, H.; Ahidouch, A.; Ouadid-Ahidouch, H. Orai3 Constitutes a Native Store-Operated Calcium Entry That Regulates

Non Small Cell Lung Adenocarcinoma Cell Proliferation. *PLoS One* **2013**, *8*, e72889, doi:10.1371/journal.pone.0072889.

124. Benzerdjeb, N.; Sevestre, H.; Ahidouch, A.; Ouadid-Ahidouch, H. Orai3 Is a Predictive Marker of Metastasis and Survival in Resectable Lung Adenocarcinoma. *Oncotarget* **2016**, *7*, 81588–81597, doi:10.18632/oncotarget.13149.

125. Wei, C.; Wang, X.; Chen, M.; Ouyang, K.; Zheng, M.; Cheng, H. Flickering Calcium Microdomains Signal Turning of Migrating Cells. *Can J Physiol Pharmacol* **2010**, *88*, 105–110, doi:10.1139/Y09-118.

126. Tsai, F.-C.; Seki, A.; Yang, H.W.; Hayer, A.; Carrasco, S.; Malmersjö, S.; Meyer, T. A Polarized Ca2+, Diacylglycerol and STIM1 Signalling System Regulates Directed Cell Migration. *Nat Cell Biol* **2014**, *16*, 133–144, doi:10.1038/ncb2906.

127. Wei, C.; Wang, X.; Chen, M.; Ouyang, K.; Song, L.-S.; Cheng, H. Calcium Flickers Steer Cell Migration. *Nature* **2009**, *457*, 901–905, doi:10.1038/nature07577.

128. Derouiche, S.; Warnier, M.; Mariot, P.; Gosset, P.; Mauroy, B.; Bonnal, J.-L.; Slomianny, C.; Delcourt, P.; Prevarskaya, N.; Roudbaraki, M. Bisphenol A Stimulates Human Prostate Cancer Cell Migration via Remodelling of Calcium Signalling. *Springerplus* **2013**, *2*, 54, doi:10.1186/2193-1801-2-54.

129. Sun, Y.; Sukumaran, P.; Varma, A.; Derry, S.; Sahmoun, A.E.; Singh, B.B. Cholesterol-Induced Activation of TRPM7 Regulates Cell Proliferation, Migration, and Viability of Human Prostate Cells. *Biochim Biophys Acta* **2014**, *1843*, 1839–1850, doi:10.1016/j.bbamcr.2014.04.019.

130. Gao, H.; Chen, X.; Du, X.; Guan, B.; Liu, Y.; Zhang, H. EGF Enhances the Migration of Cancer Cells by Up-Regulation of TRPM7. *Cell Calcium* **2011**, *50*, 559–568, doi:10.1016/j.ceca.2011.09.003.

131. Kang, S.S.; Han, K.-S.; Ku, B.M.; Lee, Y.K.; Hong, J.; Shin, H.Y.; Almonte, A.G.; Woo, D.H.; Brat, D.J.; Hwang, E.M.; et al. Caffeine-Mediated Inhibition of Calcium Release Channel Inositol 1,4,5-Trisphosphate Receptor Subtype 3 Blocks Glioblastoma Invasion and Extends Survival. *Cancer Res* **2010**, *70*, 1173–1183, doi:10.1158/0008-5472.CAN-09-2886.

132. Böhme, I.; Schönherr, R.; Eberle, J.; Bosserhoff, A.K. Membrane Transporters and Channels in Melanoma. *Rev Physiol Biochem Pharmacol* **2020**, doi:10.1007/112_2020_17.

133. Guo, H.; Carlson, J.A.; Slominski, A. Role of TRPM in Melanocytes and Melanoma. *Exp Dermatol* **2012**, *21*, 650–654, doi:10.1111/j.1600-0625.2012.01565.x.

134. Barceló, C.; Sisó, P.; Maiques, O.; de la Rosa, I.; Martí, R.M.; Macià, A. T-Type Calcium Channels: A Potential Novel Target in Melanoma. *Cancers (Basel)* **2020**, *12*, doi:10.3390/cancers12020391.

135. Das, A.; Pushparaj, C.; Bahí, N.; Sorolla, A.; Herreros, J.; Pamplona, R.; Vilella, R.; Matias-Guiu, X.; Martí, R.M.; Cantí, C. Functional Expression of Voltage-Gated Calcium Channels in Human Melanoma. *Pigment Cell Melanoma Res* **2012**, *25*, 200–212, doi:10.1111/j.1755-148X.2012.00978.x.

136. Umemura, M.; Baljinnyam, E.; Feske, S.; De Lorenzo, M.S.; Xie, L.-H.; Feng, X.; Oda, K.; Makino, A.; Fujita, T.; Yokoyama, U.; et al. Store-Operated Ca2+ Entry (SOCE) Regulates Melanoma Proliferation and Cell Migration. *PLoS One* **2014**, *9*, e89292, doi:10.1371/journal.pone.0089292.

137. Sun, J.; Lu, F.; He, H.; Shen, J.; Messina, J.; Mathew, R.; Wang, D.; Sarnaik, A.A.; Chang, W.-C.; Kim, M.; et al. STIM1- and Orai1-Mediated Ca(2+) Oscillation Orchestrates Invadopodium Formation and Melanoma Invasion. *J Cell Biol* **2014**, *207*, 535–548, doi:10.1083/jcb.201407082.

138. Abdel-Ghany, M.; Cheng, H.-C.; Elble, R.C.; Lin, H.; DiBiasio, J.; Pauli, B.U. The Interacting Binding Domains of the Beta(4) Integrin and Calcium-Activated Chloride Channels (CLCAs) in Metastasis. *J Biol Chem* **2003**, *278*, 49406–49416, doi:10.1074/jbc.M309086200.

139. Deli, T.; Varga, N.; Ádám, A.; Kenessey, I.; Rásó, E.; Puskás, L.G.; Tóvári, J.; Fodor, J.; Fehér, M.; Szigeti, G.P.; et al. Functional Genomics of Calcium Channels in Human Melanoma Cells. *Int J Cancer* **2007**, *121*, 55–65, doi:10.1002/ijc.22621.

140. Beck, D.; Niessner, H.; Smalley, K.S.M.; Flaherty, K.; Paraiso, K.H.T.; Busch, C.; Sinnberg, T.; Vasseur, S.; Iovanna, J.L.; Drießen, S.; et al. Vemurafenib Potently Induces Endoplasmic Reticulum Stress-Mediated Apoptosis in BRAFV600E Melanoma Cells. *Sci Signal* **2013**, *6*, ra7, doi:10.1126/scisignal.2003057.

141. Roux, P.P.; Blenis, J. ERK and P38 MAPK-Activated Protein Kinases: A Family of Protein Kinases with Diverse Biological Functions. *Microbiol Mol Biol Rev* **2004**, *68*, 320–344, doi:10.1128/MMBR.68.2.320-344.2004.

142. Han, J.; Lee, J.D.; Bibbs, L.; Ulevitch, R.J. A MAP Kinase Targeted by Endotoxin and Hyperosmolarity in Mammalian Cells. *Science* **1994**, *265*, 808–811, doi:10.1126/science.7914033.

143. Zarubin, T.; Han, J. Activation and Signaling of the P38 MAP Kinase Pathway. *Cell Res* **2005**, *15*, 11–18, doi:10.1038/sj.cr.7290257.

144. Cuadrado, A.; Nebreda, A.R. Mechanisms and Functions of P38 MAPK Signalling. *Biochem J* **2010**, *429*, 403–417, doi:10.1042/BJ20100323.

145. Bellon, S.; Fitzgibbon, M.J.; Fox, T.; Hsiao, H.M.; Wilson, K.P. The Structure of Phosphorylated P38gamma Is Monomeric and Reveals a Conserved Activation-Loop Conformation. *Structure* **1999**, *7*, 1057–1065, doi:10.1016/s0969-2126(99)80173-7.

146. Brancho, D.; Tanaka, N.; Jaeschke, A.; Ventura, J.-J.; Kelkar, N.; Tanaka, Y.; Kyuuma, M.; Takeshita, T.; Flavell, R.A.; Davis, R.J. Mechanism of P38 MAP Kinase Activation in Vivo. *Genes Dev* **2003**, *17*, 1969–1978, doi:10.1101/gad.1107303.

147. Cuenda, A.; Rousseau, S. P38 MAP-Kinases Pathway Regulation, Function and Role in Human Diseases. *Biochim Biophys Acta* **2007**, *1773*, 1358–1375, doi:10.1016/j.bbamcr.2007.03.010.

148. Salvador, J.M.; Mittelstadt, P.R.; Guszczynski, T.; Copeland, T.D.; Yamaguchi, H.; Appella, E.; Fornace, A.J.; Ashwell, J.D. Alternative P38 Activation Pathway Mediated by T Cell Receptor-Proximal Tyrosine Kinases. *Nat Immunol* **2005**, *6*, 390–395, doi:10.1038/ni1177.

149. Uhlik, M.T.; Abell, A.N.; Johnson, N.L.; Sun, W.; Cuevas, B.D.; Lobel-Rice, K.E.; Horne, E.A.; Dell'Acqua, M.L.; Johnson, G.L. Rac-MEKK3-MKK3 Scaffolding for P38 MAPK Activation during Hyperosmotic Shock. *Nat Cell Biol* **2003**, *5*, 1104–1110, doi:10.1038/ncb1071.

150. Cheung, P.C.F.; Campbell, D.G.; Nebreda, A.R.; Cohen, P. Feedback Control of the Protein Kinase TAK1 by SAPK2a/P38alpha. *EMBO J* **2003**, *22*, 5793–5805, doi:10.1093/emboj/cdg552.

151. Keyse, S.M. Protein Phosphatases and the Regulation of Mitogen-Activated Protein Kinase Signalling. *Curr Opin Cell Biol* **2000**, *12*, 186–192, doi:10.1016/s0955-0674(99)00075-7.

152. Canovas, B.; Nebreda, A.R. Diversity and Versatility of P38 Kinase Signalling in Health and Disease. *Nat Rev Mol Cell Biol* **2021**, doi:10.1038/s41580-020-00322-w.

153. Kuma, Y.; Sabio, G.; Bain, J.; Shpiro, N.; Márquez, R.; Cuenda, A. BIRB796 Inhibits All P38 MAPK Isoforms in Vitro and in Vivo. *J Biol Chem* **2005**, *280*, 19472–19479, doi:10.1074/jbc.M414221200.

154. Cuenda, A.; Cohen, P.; Buée-Scherrer, V.; Goedert, M. Activation of Stress-Activated Protein Kinase-3 (SAPK3) by Cytokines and Cellular Stresses Is Mediated via SAPKK3 (MKK6); Comparison of the Specificities of SAPK3 and SAPK2 (RK/P38). *EMBO J* **1997**, *16*, 295–305, doi:10.1093/emboj/16.2.295.

155. Igea, A.; Nebreda, A.R. The Stress Kinase P38α as a Target for Cancer Therapy. *Cancer Res* **2015**, *75*, 3997–4002, doi:10.1158/0008-5472.CAN-15-0173.

156. Brancho, D.; Tanaka, N.; Jaeschke, A.; Ventura, J.-J.; Kelkar, N.; Tanaka, Y.; Kyuuma, M.; Takeshita, T.; Flavell, R.A.; Davis, R.J. Mechanism of P38 MAP Kinase Activation in Vivo. *Genes Dev* **2003**, *17*, 1969–1978, doi:10.1101/gad.1107303.

157. Bulavin, D.V.; Phillips, C.; Nannenga, B.; Timofeev, O.; Donehower, L.A.; Anderson, C.W.; Appella, E.; Fornace, A.J. Inactivation of the Wip1 Phosphatase Inhibits Mammary Tumorigenesis through P38 MAPK-Mediated Activation of the P16(Ink4a)-P19(Arf) Pathway. *Nat Genet* **2004**, *36*, 343–350, doi:10.1038/ng1317.

158. Pereira, L.; Igea, A.; Canovas, B.; Dolado, I.; Nebreda, A.R. Inhibition of P38 MAPK Sensitizes Tumour Cells to Cisplatin-Induced Apoptosis Mediated by Reactive Oxygen Species and JNK. *EMBO Mol Med* **2013**, *5*, 1759–1774, doi:10.1002/emmm.201302732.

159. Wagner, E.F.; Nebreda, A.R. Signal Integration by JNK and P38 MAPK Pathways in Cancer Development. *Nat Rev Cancer* **2009**, *9*, 537–549, doi:10.1038/nrc2694.

160. Gupta, J.; del Barco Barrantes, I.; Igea, A.; Sakellariou, S.; Pateras, I.S.; Gorgoulis, V.G.; Nebreda, A.R. Dual Function of P38α MAPK in Colon Cancer: Suppression of Colitis-Associated Tumor Initiation but Requirement for Cancer Cell Survival. *Cancer Cell* **2014**, *25*, 484–500, doi:10.1016/j.ccr.2014.02.019.

161. Chiacchiera, F.; Matrone, A.; Ferrari, E.; Ingravallo, G.; Lo Sasso, G.; Murzilli, S.; Petruzzelli, M.; Salvatore, L.; Moschetta, A.; Simone, C. P38alpha Blockade Inhibits Colorectal Cancer Growth in Vivo by Inducing a Switch from HIF1alpha- to FoxO-Dependent Transcription. *Cell Death Differ* **2009**, *16*, 1203–1214, doi:10.1038/cdd.2009.36.

162. Campbell, R.M.; Anderson, B.D.; Brooks, N.A.; Brooks, H.B.; Chan, E.M.; De Dios, A.; Gilmour, R.; Graff, J.R.; Jambrina, E.; Mader, M.; et al. Characterization of LY2228820 Dimesylate, a Potent and Selective Inhibitor of P38 MAPK with Antitumor Activity. *Mol Cancer Ther* **2014**, *13*, 364–374, doi:10.1158/1535-7163.MCT-13-0513.

163. Ambrosino, C.; Nebreda, A.R. Cell Cycle Regulation by P38 MAP Kinases. *Biol Cell* **2001**, *93*, 47–51, doi:10.1016/s0248-4900(01)01124-8.

164. Molnár, A.; Theodoras, A.M.; Zon, L.I.; Kyriakis, J.M. Cdc42Hs, but Not Rac1, Inhibits Serum-Stimulated Cell Cycle Progression at G1/S through a Mechanism Requiring P38/RK. *J Biol Chem* **1997**, *272*, 13229–13235, doi:10.1074/jbc.272.20.13229.

165. Rousseau, S.; Houle, F.; Landry, J.; Huot, J. P38 MAP Kinase Activation by Vascular Endothelial Growth Factor Mediates Actin Reorganization and Cell Migration in Human Endothelial Cells. *Oncogene* **1997**, *15*, 2169–2177, doi:10.1038/sj.onc.1201380.

166. Kim, M.-S.; Lee, E.-J.; Kim, H.-R.C.; Moon, A. P38 Kinase Is a Key Signaling Molecule for H-Ras-Induced Cell Motility and Invasive Phenotype in Human Breast Epithelial Cells. *Cancer Res* **2003**, *63*, 5454–5461.

167. Rousseau, S.; Dolado, I.; Beardmore, V.; Shpiro, N.; Marquez, R.; Nebreda, A.R.; Arthur, J.S.C.; Case, L.M.; Tessier-Lavigne, M.; Gaestel, M.; et al. CXCL12 and C5a Trigger Cell Migration via a PAK1/2-P38alpha MAPK-MAPKAP-K2-HSP27 Pathway. *Cell Signal* **2006**, *18*, 1897–1905, doi:10.1016/j.cellsig.2006.02.006.

168. Benndorf, R.; Hayess, K.; Ryazantsev, S.; Wieske, M.; Behlke, J.; Lutsch, G. Phosphorylation and Supramolecular Organization of Murine Small Heat Shock Protein

HSP25 Abolish Its Actin Polymerization-Inhibiting Activity. *J Biol Chem* **1994**, *269*, 20780–20784.

169. Piotrowicz, R.S.; Hickey, E.; Levin, E.G. Heat Shock Protein 27 KDa Expression and Phosphorylation Regulates Endothelial Cell Migration. *FASEB J* **1998**, *12*, 1481–1490, doi:10.1096/fasebj.12.14.1481.

170. Simon, C.; Goepfert, H.; Boyd, D. Inhibition of the P38 Mitogen-Activated Protein Kinase by SB 203580 Blocks PMA-Induced Mr 92,000 Type IV Collagenase Secretion and in Vitro Invasion. *Cancer Res* **1998**, *58*, 1135–1139.

171. Davis, R.J. Signal Transduction by the JNK Group of MAP Kinases. *Cell* **2000**, *103*, 239–252, doi:10.1016/s0092-8674(00)00116-1.

172. Gilmore, T.D. Introduction to NF-KappaB: Players, Pathways, Perspectives. *Oncogene* **2006**, *25*, 6680–6684, doi:10.1038/sj.onc.1209954.

173. Ridley, A.J.; Schwartz, M.A.; Burridge, K.; Firtel, R.A.; Ginsberg, M.H.; Borisy, G.; Parsons, J.T.; Horwitz, A.R. Cell Migration: Integrating Signals from Front to Back. *Science* **2003**, *302*, 1704–1709, doi:10.1126/science.1092053.

174. Yamazaki, D.; Kurisu, S.; Takenawa, T. Regulation of Cancer Cell Motility through Actin Reorganization. *Cancer Sci* **2005**, *96*, 379–386, doi:10.1111/j.1349-7006.2005.00062.x.

175. Friedl, P.; Wolf, K. Tumour-Cell Invasion and Migration: Diversity and Escape Mechanisms. *Nat Rev Cancer* **2003**, *3*, 362–374, doi:10.1038/nrc1075.

176. Friedl, P.; Hegerfeldt, Y.; Tusch, M. Collective Cell Migration in Morphogenesis and Cancer. *Int J Dev Biol* **2004**, *48*, 441–449, doi:10.1387/ijdb.041821pf.

177. Friedl, P. Prespecification and Plasticity: Shifting Mechanisms of Cell Migration. *Curr Opin Cell Biol* **2004**, *16*, 14–23, doi:10.1016/j.ceb.2003.11.001.

178. Tamariz, E.; Grinnell, F. Modulation of Fibroblast Morphology and Adhesion during Collagen Matrix Remodeling. *Mol Biol Cell* **2002**, *13*, 3915–3929, doi:10.1091/mbc.e02-05-0291.

179. Wolf, K.; Mazo, I.; Leung, H.; Engelke, K.; von Andrian, U.H.; Deryugina, E.I.; Strongin, A.Y.; Bröcker, E.-B.; Friedl, P. Compensation Mechanism in Tumor Cell Migration: Mesenchymal-Amoeboid Transition after Blocking of Pericellular Proteolysis. *J Cell Biol* **2003**, *160*, 267–277, doi:10.1083/jcb.200209006.

180. Svitkina, T. The Actin Cytoskeleton and Actin-Based Motility. *Cold Spring Harb Perspect Biol* **2018**, *10*, doi:10.1101/cshperspect.a018267.

181. Tunduguru, R.; Thurmond, D.C. Promoting Glucose Transporter-4 Vesicle Trafficking along Cytoskeletal Tracks: PAK-Ing Them Out. *Front Endocrinol (Lausanne)* **2017**, *8*, 329, doi:10.3389/fendo.2017.00329.

182. Maus, M.; Medgyesi, D.; Kiss, E.; Schneider, A.E.; Enyedi, A.; Szilágyi, N.; Matkó, J.; Sármay, G. B Cell Receptor-Induced Ca2+ Mobilization Mediates F-Actin Rearrangements and Is Indispensable for Adhesion and Spreading of B Lymphocytes. *J Leukoc Biol* **2013**, *93*, 537–547, doi:10.1189/jlb.0312169.

183. Lee, J.; Ishihara, A.; Oxford, G.; Johnson, B.; Jacobson, K. Regulation of Cell Movement Is Mediated by Stretch-Activated Calcium Channels. *Nature* **1999**, *400*, 382–386, doi:10.1038/22578.

184. Brundage, R.A.; Fogarty, K.E.; Tuft, R.A.; Fay, F.S. Calcium Gradients Underlying Polarization and Chemotaxis of Eosinophils. *Science* **1991**, *254*, 703–706, doi:10.1126/science.1948048.

185. Martin-Romero, F.J.; Lopez-Guerrero, A.M.; Pascual-Caro, C.; Pozo-Guisado, E. The Interplay between Cytoskeleton and Calcium Dynamics. In *Cytoskeleton - Structure, Dynamics, Function and Disease*; Jimenez-Lopez, J.C., Ed.; InTech, 2017 ISBN 978-953-51-3169-4.

186. Shimizu, T.; Owsianik, G.; Freichel, M.; Flockerzi, V.; Nilius, B.; Vennekens, R. TRPM4 Regulates Migration of Mast Cells in Mice. *Cell Calcium* **2009**, *45*, 226–232, doi:10.1016/j.ceca.2008.10.005.

187. Lee, W.H.; Choong, L.Y.; Mon, N.N.; Lu, S.; Lin, Q.; Pang, B.; Yan, B.; Krishna, V.S.R.; Singh, H.; Tan, T.Z.; et al. TRPV4 Regulates Breast Cancer Cell Extravasation, Stiffness and Actin Cortex. *Sci Rep* **2016**, *6*, 27903, doi:10.1038/srep27903.

188. Bozulic, L.D.; Malik, M.T.; Powell, D.W.; Nanez, A.; Link, A.J.; Ramos, K.S.; Dean, W.L. Plasma Membrane Ca(2+) -ATPase Associates with CLP36, Alpha-Actinin and Actin in Human Platelets. *Thromb Haemost* **2007**, *97*, 587–597.

189. Dalghi, M.G.; Ferreira-Gomes, M.; Rossi, J.P. Regulation of the Plasma Membrane Calcium ATPases by the Actin Cytoskeleton. *Biochem Biophys Res Commun* **2018**, *506*, 347–354, doi:10.1016/j.bbrc.2017.11.151.

190. Oser, M.; Condeelis, J. The Cofilin Activity Cycle in Lamellipodia and Invadopodia. *J Cell Biochem* **2009**, *108*, 1252–1262, doi:10.1002/jcb.22372.

191. Bravo-Cordero, J.J.; Magalhaes, M.A.O.; Eddy, R.J.; Hodgson, L.; Condeelis, J. Functions of Cofilin in Cell Locomotion and Invasion. *Nat Rev Mol Cell Biol* **2013**, *14*, 405–415, doi:10.1038/nrm3609.

192. Wang, Y.; Shibasaki, F.; Mizuno, K. Calcium Signal-Induced Cofilin Dephosphorylation Is Mediated by Slingshot via Calcineurin. *J Biol Chem* **2005**, *280*, 12683–12689, doi:10.1074/jbc.M411494200.

193. Mao, T.; O'Connor, D.H.; Scheuss, V.; Nakai, J.; Svoboda, K. Characterization and Subcellular Targeting of GCaMP-Type Genetically-Encoded Calcium Indicators. *PLoS One* **2008**, *3*, e1796, doi:10.1371/journal.pone.0001796.

194. Taylor, M.J.; Perrais, D.; Merrifield, C.J. A High Precision Survey of the Molecular Dynamics of Mammalian Clathrin-Mediated Endocytosis. *PLoS Biol* **2011**, *9*, e1000604, doi:10.1371/journal.pbio.1000604.

195. Zhao, Y.; Araki, S.; Wu, J.; Teramoto, T.; Chang, Y.-F.; Nakano, M.; Abdelfattah, A.S.; Fujiwara, M.; Ishihara, T.; Nagai, T.; et al. An Expanded Palette of Genetically Encoded Ca^{2+} Indicators. *Science* **2011**, *333*, 1888–1891, doi:10.1126/science.1208592.

196. Vőfély, G.; Berecz, T.; Szabó, E.; Szebényi, K.; Hathy, E.; Orbán, T.I.; Sarkadi, B.; Homolya, L.; Marchetto, M.C.; Réthelyi, J.M.; et al. Characterization of Calcium Signals in Human Induced Pluripotent Stem Cell-Derived Dentate Gyrus Neuronal Progenitors and Mature Neurons, Stably Expressing an Advanced Calcium Indicator Protein. *Mol Cell Neurosci* **2018**, *88*, 222–230, doi:10.1016/j.mcn.2018.02.003.

197. Bach, M.; Grigat, S.; Pawlik, B.; Fork, C.; Utermöhlen, O.; Pal, S.; Banczyk, D.; Lazar, A.; Schömig, E.; Gründemann, D. Fast Set-up of Doxycycline-Inducible Protein Expression in Human Cell Lines with a Single Plasmid Based on Epstein-Barr Virus Replication and the Simple Tetracycline Repressor. *FEBS J* **2007**, *274*, 783–790, doi:10.1111/j.1742-4658.2006.05623.x.

198. Ivanov, D.P.; Parker, T.L.; Walker, D.A.; Alexander, C.; Ashford, M.B.; Gellert, P.R.; Garnett, M.C. Multiplexing Spheroid Volume, Resazurin and Acid Phosphatase Viability Assays for High-Throughput Screening of Tumour Spheroids and Stem Cell Neurospheres. *PLoS One* **2014**, *9*, e103817, doi:10.1371/journal.pone.0103817.

199. Kunjithapatham, R.; Karthikeyan, S.; Geschwind, J.-F.; Kieserman, E.; Lin, M.; Fu, D.-X.; Ganapathy-Kanniappan, S. Reversal of Anchorage-Independent Multicellular Spheroid into a Monolayer Mimics a Metastatic Model. *Sci Rep* **2014**, *4*, 6816, doi:10.1038/srep06816.

200. Corazzari, M.; Rapino, F.; Ciccosanti, F.; Giglio, P.; Antonioli, M.; Conti, B.; Fimia, G.M.; Lovat, P.E.; Piacentini, M. Oncogenic BRAF Induces Chronic ER Stress

Condition Resulting in Increased Basal Autophagy and Apoptotic Resistance of Cutaneous Melanoma. *Cell Death Differ* **2015**, *22*, 946–958, doi:10.1038/cdd.2014.183.

201. Vergarajauregui, S.; San Miguel, A.; Puertollano, R. Activation of P38 Mitogen-Activated Protein Kinase Promotes Epidermal Growth Factor Receptor Internalization. *Traffic* **2006**, *7*, 686–698, doi:10.1111/j.1600-0854.2006.00420.x.

202. Costa, E.C.; Moreira, A.F.; de Melo-Diogo, D.; Gaspar, V.M.; Carvalho, M.P.; Correia, I.J. 3D Tumor Spheroids: An Overview on the Tools and Techniques Used for Their Analysis. *Biotechnol Adv* **2016**, *34*, 1427–1441, doi:10.1016/j.biotechadv.2016.11.002.

203. Huang, R.; Rofstad, E.K. Integrins as Therapeutic Targets in the Organ-Specific Metastasis of Human Malignant Melanoma. *J Exp Clin Cancer Res* **2018**, *37*, 92, doi:10.1186/s13046-018-0763-x.

204. Mariotti, A.; Kedeshian, P.A.; Dans, M.; Curatola, A.M.; Gagnoux-Palacios, L.; Giancotti, F.G. EGF-R Signaling through Fyn Kinase Disrupts the Function of Integrin Alpha6beta4 at Hemidesmosomes: Role in Epithelial Cell Migration and Carcinoma Invasion. *J Cell Biol* **2001**, *155*, 447–458, doi:10.1083/jcb.200105017.

205. Traynor, D.; Kay, R.R. Possible Roles of the Endocytic Cycle in Cell Motility. *J Cell Sci* **2007**, *120*, 2318–2327, doi:10.1242/jcs.007732.

206. Wilson, B.J.; Allen, J.L.; Caswell, P.T. Vesicle Trafficking Pathways That Direct Cell Migration in 3D Matrices and in Vivo. *Traffic* **2018**, *19*, 899–909, doi:10.1111/tra.12605.

207. Sigismund, S.; Confalonieri, S.; Ciliberto, A.; Polo, S.; Scita, G.; Di Fiore, P.P. Endocytosis and Signaling: Cell Logistics Shape the Eukaryotic Cell Plan. *Physiol Rev* **2012**, *92*, 273–366, doi:10.1152/physrev.00005.2011.

208. Pászty, K.; Caride, A.J.; Bajzer, Ž.; Offord, C.P.; Padányi, R.; Hegedűs, L.; Varga, K.; Strehler, E.E.; Enyedi, A. Plasma Membrane Ca^{2+}-ATPases Can Shape the Pattern of Ca^{2+} Transients Induced by Store-Operated Ca^{2+} Entry. *Sci Signal* **2015**, *8*, ra19, doi:10.1126/scisignal.2005672.

209. Franco, S.J.; Rodgers, M.A.; Perrin, B.J.; Han, J.; Bennin, D.A.; Critchley, D.R.; Huttenlocher, A. Calpain-Mediated Proteolysis of Talin Regulates Adhesion Dynamics. *Nat Cell Biol* **2004**, *6*, 977–983, doi:10.1038/ncb1175.

210. Giannone, G.; Rondé, P.; Gaire, M.; Beaudouin, J.; Haiech, J.; Ellenberg, J.; Takeda, K. Calcium Rises Locally Trigger Focal Adhesion Disassembly and Enhance Residency of Focal Adhesion Kinase at Focal Adhesions. *J Biol Chem* **2004**, *279*, 28715–28723, doi:10.1074/jbc.M404054200.

211. Koskinen, M.; Hotulainen, P. Measuring F-Actin Properties in Dendritic Spines. *Front Neuroanat* **2014**, *8*, 74, doi:10.3389/fnana.2014.00074.

212. Hartzell, C.A.; Jankowska, K.I.; Burkhardt, J.K.; Lewis, R.S. Calcium Influx through CRAC Channels Controls Actin Organization and Dynamics at the Immune Synapse. *Elife* **2016**, *5*, doi:10.7554/eLife.14850.

213. Yoneda, M.; Nishizaki, T.; Tasaka, K.; Kurachi, H.; Miyake, A.; Murata, Y. Changes in Actin Network during Calcium-Induced Exocytosis in Permeabilized GH3 Cells: Calcium Directly Regulates F-Actin Disassembly. *J Endocrinol* **2000**, *166*, 677–687, doi:10.1677/joe.0.1660677.

214. Wales, P.; Schuberth, C.E.; Aufschnaiter, R.; Fels, J.; García-Aguilar, I.; Janning, A.; Dlugos, C.P.; Schäfer-Herte, M.; Klingner, C.; Wälte, M.; et al. Calcium-Mediated Actin Reset (CaAR) Mediates Acute Cell Adaptations. *Elife* **2016**, *5*, doi:10.7554/eLife.19850.

215. Schwab, A.; Fabian, A.; Hanley, P.J.; Stock, C. Role of Ion Channels and Transporters in Cell Migration. *Physiol Rev* **2012**, *92*, 1865–1913, doi:10.1152/physrev.00018.2011.

216. Schwab, A.; Finsterwalder, F.; Kersting, U.; Danker, T.; Oberleithner, H. Intracellular Ca2+ Distribution in Migrating Transformed Epithelial Cells. *Pflugers Arch* **1997**, *434*, 70–76, doi:10.1007/s004240050364.

217. Bong, A.H.L.; Monteith, G.R. Calcium Signaling and the Therapeutic Targeting of Cancer Cells. *Biochim Biophys Acta Mol Cell Res* **2018**, *1865*, 1786–1794, doi:10.1016/j.bbamcr.2018.05.015.

218. Macià, A.; Herreros, J.; Martí, R.M.; Cantí, C. Calcium Channel Expression and Applicability as Targeted Therapies in Melanoma. *Biomed Res Int* **2015**, *2015*, 587135, doi:10.1155/2015/587135.

219. Cooper, G.M.; Cooper, G.M. *The Cell*; 2nd ed.; Sinauer Associates, 2000; ISBN 978-0-87893-106-4.

220. Ferrington, D.A.; Chen, X.; Krainev, A.G.; Michaelis, E.K.; Bigelow, D.J. Protein Half-Lives of Calmodulin and the Plasma Membrane Ca-ATPase in Rat Brain. *Biochem Biophys Res Commun* **1997**, *237*, 163–165, doi:10.1006/bbrc.1997.7105.

221. Jin, E.J.; Kiral, F.R.; Hiesinger, P.R. The Where, What, and When of Membrane Protein Degradation in Neurons. *Dev Neurobiol* **2018**, *78*, 283–297, doi:10.1002/dneu.22534.

222. Li, S.; Song, Y.; Quach, C.; Guo, H.; Jang, G.-B.; Maazi, H.; Zhao, S.; Sands, N.A.; Liu, Q.; In, G.K.; et al. Transcriptional Regulation of Autophagy-Lysosomal Function in BRAF-Driven Melanoma Progression and Chemoresistance. *Nat Commun* **2019**, *10*, 1693, doi:10.1038/s41467-019-09634-8.

223. Pelkmans, L.; Fava, E.; Grabner, H.; Hannus, M.; Habermann, B.; Krausz, E.; Zerial, M. Genome-Wide Analysis of Human Kinases in Clathrin- and Caveolae/Raft-Mediated Endocytosis. *Nature* **2005**, *436*, 78–86, doi:10.1038/nature03571.

224. Matrone, A.; Grossi, V.; Chiacchiera, F.; Fina, E.; Cappellari, M.; Caringella, A.M.; Di Naro, E.; Loverro, G.; Simone, C. P38alpha Is Required for Ovarian Cancer Cell Metabolism and Survival. *Int J Gynecol Cancer* **2010**, *20*, 203–211, doi:10.1111/igc.0b013e3181c8ca12.

225. Grossi, V.; Liuzzi, M.; Murzilli, S.; Martelli, N.; Napoli, A.; Ingravallo, G.; Del Rio, A.; Simone, C. Sorafenib Inhibits P38α Activity in Colorectal Cancer Cells and Synergizes with the DFG-in Inhibitor SB202190 to Increase Apoptotic Response. *Cancer Biol Ther* **2012**, *13*, 1471–1481, doi:10.4161/cbt.22254.

226. Yamaguchi, H.; Condeelis, J. Regulation of the Actin Cytoskeleton in Cancer Cell Migration and Invasion. *Biochim Biophys Acta* **2007**, *1773*, 642–652, doi:10.1016/j.bbamcr.2006.07.001.

227. Taddei, M.L.; Giannoni, E.; Morandi, A.; Ippolito, L.; Ramazzotti, M.; Callari, M.; Gandellini, P.; Chiarugi, P. Mesenchymal to Amoeboid Transition Is Associated with Stem-like Features of Melanoma Cells. *Cell Commun Signal* **2014**, *12*, 24, doi:10.1186/1478-811X-12-24.

228. Anand, P.; Harper, A.G.S. Human Platelets Use a Cytosolic Ca2+ Nanodomain to Activate Ca2+-Dependent Shape Change Independently of Platelet Aggregation. *Cell Calcium* **2020**, *90*, 102248, doi:10.1016/j.ceca.2020.102248.

229. Mermelstein, C.S.; Rebello, M.I.L.; Amaral, L.M.; Costa, M.L. Changes in Cell Shape, Cytoskeletal Proteins and Adhesion Sites of Cultured Cells after Extracellular Ca2+ Chelation. *Braz J Med Biol Res* **2003**, *36*, 1111–1116, doi:10.1590/s0100-879x2003000800018.

230. Moore, T.M.; Brough, G.H.; Babal, P.; Kelly, J.J.; Li, M.; Stevens, T. Store-Operated Calcium Entry Promotes Shape Change in Pulmonary Endothelial Cells Expressing Trp1. *Am J Physiol* **1998**, *275*, L574-582, doi:10.1152/ajplung.1998.275.3.L574.

231. Tojkander, S.; Gateva, G.; Lappalainen, P. Actin Stress Fibers--Assembly, Dynamics and Biological Roles. *J Cell Sci* **2012**, *125*, 1855–1864, doi:10.1242/jcs.098087.

232. Pellegrin, S.; Mellor, H. Actin Stress Fibres. *J Cell Sci* **2007**, *120*, 3491–3499, doi:10.1242/jcs.018473.

233. Go, C.K.; Hooper, R.; Aronson, M.R.; Schultz, B.; Cangoz, T.; Nemani, N.; Zhang, Y.; Madesh, M.; Soboloff, J. The Ca2+ Export Pump PMCA Clears Near-Membrane Ca2+ to Facilitate Store-Operated Ca2+ Entry and NFAT Activation. *Sci Signal* **2019**, *12*, doi:10.1126/scisignal.aaw2627.

234. Huang, H.-K.; Lin, Y.-H.; Chang, H.-A.; Lai, Y.-S.; Chen, Y.-C.; Huang, S.-C.; Chou, C.-Y.; Chiu, W.-T. Chemoresistant Ovarian Cancer Enhances Its Migration Abilities by Increasing Store-Operated Ca2+ Entry-Mediated Turnover of Focal Adhesions. *J Biomed Sci* **2020**, *27*, 36, doi:10.1186/s12929-020-00630-5.

235. Zhang, Y.; Yan, J.; Xu, H.; Yang, Y.; Li, W.; Wu, H.; Liu, C. Extremely Low Frequency Electromagnetic Fields Promote Mesenchymal Stem Cell Migration by Increasing Intracellular Ca2+ and Activating the FAK/Rho GTPases Signaling Pathways in Vitro. *Stem Cell Res Ther* **2018**, *9*, 143, doi:10.1186/s13287-018-0883-4.

236. Li, F.; Abuarab, N.; Sivaprasadarao, A. Reciprocal Regulation of Actin Cytoskeleton Remodelling and Cell Migration by Ca2+ and Zn2+: Role of TRPM2 Channels. *J Cell Sci* **2016**, *129*, 2016–2029, doi:10.1242/jcs.179796.

237. Ballestrem, C.; Wehrle-Haller, B.; Hinz, B.; Imhof, B.A. Actin-Dependent Lamellipodia Formation and Microtubule-Dependent Tail Retraction Control-Directed Cell Migration. *Mol Biol Cell* **2000**, *11*, 2999–3012, doi:10.1091/mbc.11.9.2999.

238. Zabe, M.; Dean, W.L. Plasma Membrane Ca(2+)-ATPase Associates with the Cytoskeleton in Activated Platelets through a PDZ-Binding Domain. *J Biol Chem* **2001**, *276*, 14704–14709, doi:10.1074/jbc.M009850200.

239. Lee, S.; Kumar, S. Cofilin Is Required for Polarization of Tension in Stress Fiber Networks during Migration. *J Cell Sci* **2020**, *133*, doi:10.1242/jcs.243873.

240. Naffa, R.; Vogel, L.; Hegedűs, L.; Pászty, K.; Tóth, S.; Kelemen, K.; Singh, N.; Reményi, A.; Kállay, E.; Cserepes, M.; et al. P38 MAPK Promotes Migration and Metastatic Activity of BRAF Mutant Melanoma Cells by Inducing Degradation of PMCA4b. *Cells* **2020**, *9*, doi:10.3390/cells9051209.